Analysis of a novel allosteric inhibitor of the AAA+ ATPase p97 and its mechanism

Inaugural-Dissertation

zur

Erlangung des Doktorgrades

Dr. rer. nat.

der Fakultät für

Biologie

an der

Universität Duisburg-Essen

vorgelegt von

Robert Pöhler

aus Frankfurt am Main

Juni 2017

Die der vorliegenden Arbeit zugrunde liegenden Experimente wurden in der Abteilung für Molekularbiologie I am Zentrum für Medizinische Biotechnologie der Universität Duisburg-Essen durchgeführt.

1. Gutachter: Prof. Dr. Hemmo Meyer

2. Gutachter: Prof. Dr. Markus Kaiser

Vorsitzender des Prüfungsausschusses: Prof. Dr. Michael Ehrmann

Tag der mündlichen Prüfung: 22.08.2017

Table of contents

List of figures

List of tables

Summary

The hexameric AAA+ ATPase p97/VCP is an abundant enzyme found in the cytoplasm and the nucleus and an essential part of protein homeostasis. In concert with the proteasome, p97 is involved in the degradation of ubiquitinated proteins. These substrate proteins can be unfolded by p97 using the energy provided by ATP hydrolysis. The enzyme harbors two ATPase domains, D1 and D2, that regulate the activity and conformation of p97. To understand the mechanism and function of p97 on the molecular and cellular level, inhibitors of p97 emerged as invaluable research tools that facilitated numerous experiments. Furthermore, a p97 inhibitor is currently in clinical trials to treat cancer types like multiple myeloma that rely on an effective ubiquitin proteasome system to deal with stress caused by aberrant or excessively synthetized proteins.

Our goal was to evaluate a new compound as an inhibitor of p97 that emerged from a high throughput screen. We confirmed that the compound called I8 inhibits purified p97 reversibly with an IC_{50} of 7 µM. To test the selectivity of I8, we used the AAA+ ATPases NSF and VPS4B. NSF is essential for trafficking and secretion and VPS4B is a key factor for reverse topology abscission events at membranes. We found that I8 has weak activity against NSF, whereas VPS4B is inhibited with an IC_{50} of 0.7 µM. Subsequently, we showed that I8 inhibits both ATPases p97 and VPS4B via an allosteric mechanism. Moreover, our study implicated a non-competitive inhibition, which is binding between I8 and p97 independently of ATP binding. Structure activity relationship studies revealed that the fluorinated bisphenyl and tetrahydrocarbazole group are important structural features of I8. We investigated effects of I8 on the structure of p97 and found that it does not influence the hexamerization but increases the stability of the D2 domain against degradation. Via mass spectrometry analysis and comparison of I8 with known p97 inhibitors, we found potential homologous binding sites of I8 in the p97 D1 and D2 domains and in VPS4B. The comparison revealed a possible shared inhibitory pathway in p97 between a diverse set of inhibitors that disrupts the inter-domain communication in the D2 domains.

In summary, our characterization of a novel ATPase inhibitor identified a possible general mechanism of action common to different classes of inhibitors.

Zusammenfassung

Die AAA+ ATPase p97/VCP ist ein hexameres Enzym, das in hoher Anzahl im Zytoplasma und Zellkern vorkommt und einen essentiellen Beitrag zur Proteinhomöostase leistet. Zusammen mit dem Proteasom ist p97 am Abbau von ubiquitinierten Proteinen beteiligt, die von p97 unter ATP Verbrauch entfaltet werden können. Das Enzym besitzt zwei ATPase-Domänen, D1 und D2, die die Aktivität und Konformation von p97 regulieren. Um den Mechanismus und die Funktion von p97 auf der molekularen und zellulären Ebene zu verstehen, dienen p97 Inhibitoren als wertvolle Forschungsinstrumente, die zahlreiche Experimente ermöglicht und erleichtert haben. Einer dieser Inhibitoren wird außerdem in klinischen Tests gegen Krebstypen wie das Multiple Myelom eingesetzten, die ein effektives Ubiquitin Proteasome System benötigen um mit Stress umzugehen, der von falsch gefalteten oder überzähligen Proteinen verursacht wird.

In dieser Studie untersuchten wir eine neue Substanz, die als p97 Inhibitor in einem Hochdurchsatz-Screening gefunden wurde. Wir konnten bestätigen, dass die I8 genannte Substanz aufgereinigtes p97 reversibel mit einem IC_{50} Wert von 7 µM inhibiert. Um die Selektivität zu überprüfen, nutzten wir die mit p97 verwandten AAA+ ATPasen NSF und VPS4B. NSF ist ein essentieller Bestandteil des Transport- und Sekretionssytems, VPS4B ist ein Schlüsselelement in Abschnürungsvorgängen reverser Topologie von Membranen. Wir fanden heraus, dass I8 nur eine schwache Aktivität gegen NSF hat, VPS4B jedoch mit eine IC_{50} von 0,7 µM inhibiert. Daran anschließend zeigten wir, dass die ATPasen p97 und VPS4B durch einen allosterischen Mechanismus inhibiert werden. Außerdem deutete unsere Studie eine nicht-kompetitive Inhibition an, das heißt eine Bindung zwischen I8 und p97 unabhängig von der ATP Bindung. Untersuchungen zur Struktur-Wirkbeziehung zeigten, dass die fluorierte Bisphenyl- und Tetrahydrocarbazolgruppe wichtige Teile des I8 Moleküls darstellen. Wir untersuchten den Einfluss von I8 auf die Struktur von p97 und fanden heraus, dass es nicht die Hexamerisierung beeinträchtigt aber die D2 Domäne gegen Verdau schützt. Durch eine massenspektrometrische Analyse und dem Vergleich von I8 mit anderen p97 Inhibitoren fanden wir eine mögliche homologe Bindestelle in den beiden p97 ATPase Domänen und in VPS4B. Dieser Vergleich zeigte auch einen möglichen Signalweg auf, der von unterschiedlichen Inhibitoren genutzt wird, um die Kommunikation zwischen den D2 Domänen zu stören.

Zusammengefasst zeigt unsere Charakterisierung des neuen ATPase Inhibitors I8 einen möglichen generellen Mechanismus auf, über den verschiedene Klassen von Inhibitoren wirken.

1 Introduction

1.1 The ubiquitin proteasome system

Cellular protein homeostasis is maintained by sustained and highly regulated protein expression that is balanced by controlled protein degradation. Proteins are usually degraded in one of two major pathways. First, degradation can happen in the lysosome, a vesicular structure with acidic lumen that contains proteases. For example, multivesicular bodies formed after endocytosis fuse with the lysosome for the turnover of membrane proteins (see 1.3). Furthermore, autophagosomes can fuse with the lysosome for degradation of organelles or parts of the cytosol. Second, proteins can be degraded in the proteasome (see 1.1.2) (Clague, Urbe 2010). A common signal in both pathways is ubiquitination.

1.1.1 Ubiquitin

The turnover of proteins needs to be tightly regulated to maintain a fully functional cell. An important regulatory step is ubiquitination, a posttranslational modification. Ubiquitin is a small protein (76 amino acids, 8.6 kDa) that is covalently linked via its C-terminus to lysine residues, forming an isopeptide bond and thus resulting in monoubiquitination. Ubiquitin itself can be ubiquitinated at eight different positions and form chains, resulting in polyubiquitination. This happens either at the N-terminus (M1) or at seven different lysines: K6, K11, K27, K29, K33, K48, and K63. All eight linkages are present in the cell (Komander, Rape 2012).

Ubiquitination depends on an enzyme cascade of E1 ubiquitin-activating enzymes, E2 ubiquitin-conjugating enzymes and E3 ubiquitin-ligating enzymes (Figure 1.1). With each level in the cascade, the number of the different enzymes rises: There are only two E1s, 40 E2s, and over 600 E3s. First, ubiquitin is loaded to the E1. To activate the C-terminus of ubiquitin, ATP and therefore energy is consumed. Second, the activated ubiquitin is transferred to an E2. Ubiquitin is attached to the E1 and E2 via a cysteine, intermediately forming thioester bonds. Third, a complex of E2 and E3 attaches the ubiquitin to the substrate. Depending on the E3, the ubiquitin is either directly transferred from the E2 to the substrate or first transferred to the E3 and then to the substrate. The largest group of E3s, the RING (really interesting new gene) or U-box containing ligases, act without receiving the ubiquitin themselves. HECT (Homologous to E6-AP carboxyl terminus) and RBR (RING between RING) ligases

have an active site cysteine and are charged with ubiquitin before it is linked to a substrate (Kleiger, Mayor 2014).

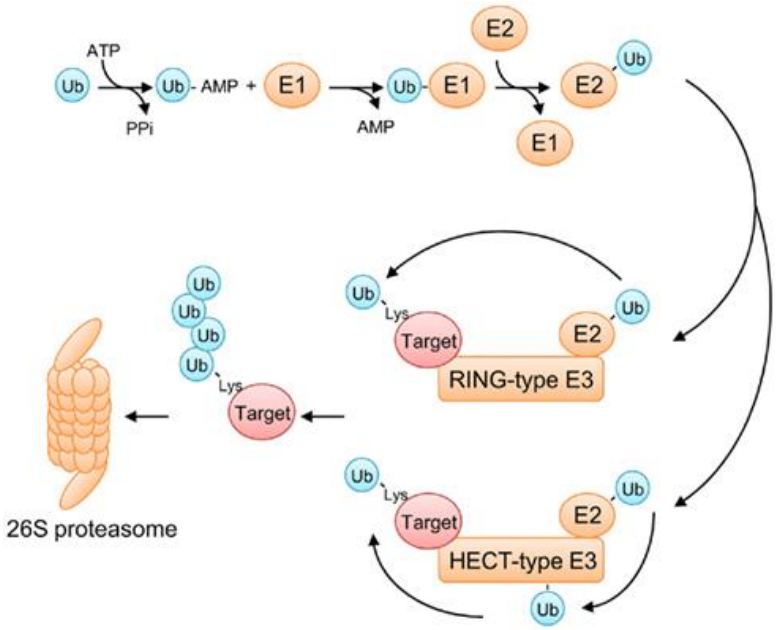

Figure 1.1 The ubiquitination cascade
The ubiquitination requires the consecutive action of the ubiquitin-activating enzyme E2, the ubiquitin-conjugation enzyme E2, and the ubiquitin-ligating enzyme E3. The free ubiquitin (Ub) is activated under ATP hydrolysis and linked via a thioester bond to the E1. Subsequently, it is transferred to the E3. Depending on the type of the E3 ligase, ubiquitin is directly transferred onto the lysine residue of the substrate (HECT and RBR type) or intermediately bound to the E3 ligase (RING type). The further processing of the substrate depends on the linkage type and can result in proteasomal degradation (adopted from Magori, Citovsky 2011).

The biggest fraction of ubiquitin is conjugated as monoubiquitin (Clague et al. 2015). In the endolysosomal system, monoubiquitin can target proteins for sorting in MVBs (multivesicular bodies), similar to K63 chains. In other cases, monoubiquitination provides additional interaction sites and recruits binding partners. For example, the heterologous transcription activator LexA-VP16 fused to monoubiquitin is extracted from chromatin by p97 (Ndoja et al. 2014). This case is also an example for a non-proteolytic function in ubiquitin signaling.

The formation of short chains can directly happen by the initial complex of E2, E3 and substrate. On the other hand, some E2-E3 complexes only recognize ubiquitin itself as a substrate. They can build chains on monoubiquitinated substrates or elongate the short “initiator” chains (Ye, Rape 2009). The linkage specificity can depend on the E2 or the E3: In the case of the RING E3 ligases, the corresponding E2 controls the linkage type. On the other hand, HECT and RBR E3 ligases control

linkage specificity independently of the E2. The topology of the chain depends on the modified lysine or methionine. For example, the distinct distance and flexibility of the different chain types is utilized by different binders to discriminate between the chains and enables differential signaling (Komander, Rape 2012). The K48 and K63 chains are the best studied types. K63 linkage is a signal typically found in protein trafficking, signal transduction and DNA repair pathways. K48 linkages are usually a signal for proteasomal degradation. However, inhibition of the proteasome results in an increase of all lysine linkages except K63, indicating that also all other chain types, not only K48 chains, can target proteins for degradation (Xu et al. 2009). Additional layers of complexity are added by mixed linkage types, branched chains, and posttranslational modifications on ubiquitin itself (Swatek, Komander 2016).

Ubiquitination is a reversible modification and the removal is an important part of regulatory mechanisms. Around 100 deubiquitinating enzymes (deubiquitinases, DUBs) can cleave the chains either en bloc or more commonly, one by one. So far, five families of DUBs are known. USP (ubiquitin-specific protease), UCH (ubiquitin C-terminal hydrolases), OTU (ovarian tumor proteases) and josephins are cysteine proteases that can be inhibited by chemicals like NEM (N-Ethylmaleimide). Members of the fifth family are Zn^{2+} metalloproteases called JAMM (JAB1/MPN/MOV34, or MPN^{+}). In both cases, the GG sequence at the C-terminus of ubiquitin is needed for the removal of ubiquitin. Similar to E2s and E3s, DUBs can exhibit linkage specificity towards the different ubiquitin chain types. The DUB activity is important for a variety of cellular functions: The maintenance of the level of free ubiquitin, cleavage of the linear ubiquitin chains originating from biosynthesis, regulation of the signaling by ubiquitin in the diverse pathways or the rescue of ubiquitin from degradation in proteasomal or lysosomal pathways (Komander et al. 2009). For example, the DUB AMSH can counteract E3 ligases in the ESCRT pathway and therefore act as a negative regulator of degradation (Clague et al. 2012).

1.1.2 The proteasome

The proteasome is a huge, ubiquitously expressed protein complex present in the cytosol and nucleus (Figure 1.2 A). It consists of 33 different subunits and can be divided into a core that associates with different caps. The 20S core particle contains the proteolytic sites in a barrel-like structure. The barrel is built of four stacked, heteroheptameric rings. The middle rings consist of β-subunits and contain in total six active sites. The two outer rings consist of α-subunits and form a pore that prevents

folded proteins from entry into the proteolytic chamber. The core can bind to caps or regulatory particles. The 20S core together with the 19S cap makes up the 26S proteasome (Inobe, Matouschek 2014). The 19S cap is the best studied regulatory particle and can be divided into two parts. One part is the base with a heterohexameric AAA+ ATPase (Rpt1-6) together with Rpn1, Rpn2, and Rpn13. The ATPase binds to the α-subunits of the 20S core with the C-terminal HbYX motif and induces the pore opening. The second part, the lid, consists of Rpn3, Rpn5, Rpn6, Rpn7, Rpn8, Rpn9, Rpn12, and Rpn15/Sem1 (Figure 1.2 B). The 19S cap can recruit ubiquitin binders (UbL-UBA proteins) or deubiquitinases. Some subunits of the cap like Rpn13 and Rpn11 can also bind or cleave ubiquitin, respectively. Binding of substrate and ATP induce conformational changes that align the cap and the core on a common axis, accelerating the substrate degradation (Förster et al. 2013).

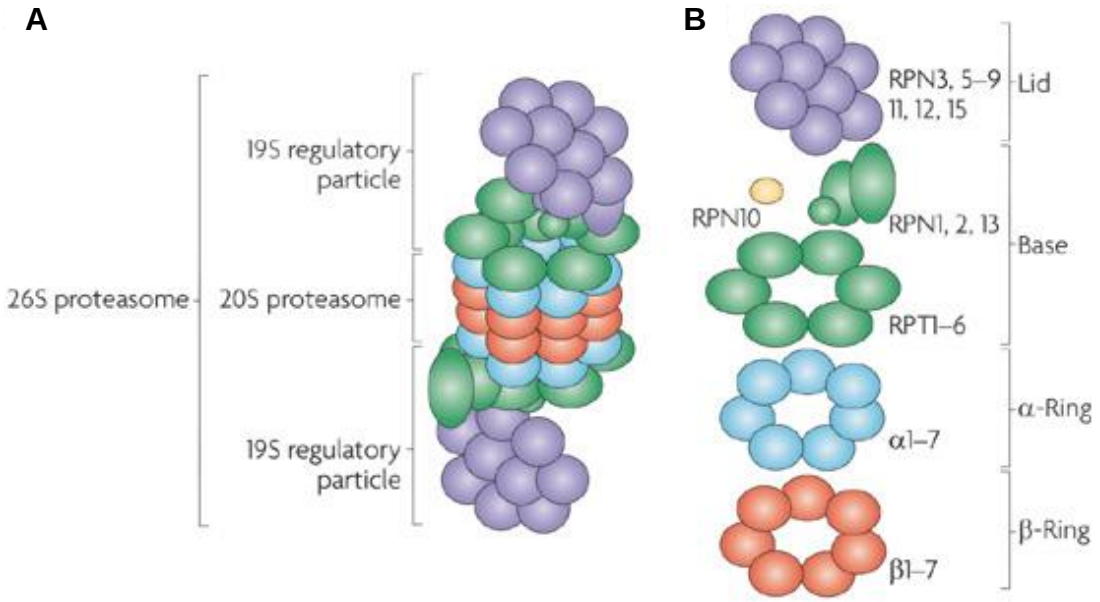

Figure 1.2 Structure and components of the 26S proteasome
A) Overview of the assembled 26S proteasome. It consists of the catalytic core of the 20S proteasome and the 19S regulatory particle. B) Single components of the 26S proteasome. The 20S core consists of two stacked heptameric β-rings and two outer heptameric α-rings. The base of the regulatory particle is divided into the base and the lid. They consist of a hexameric ATPase (regulatory particle triple-A 1-6) and regulatory particle non-ATPase (RPN) subunits (adopted from Murata et al. 2009).

Unmodified proteins can be degraded directly if they can associate to the proteasome and contain an unstructured tail long enough to reach into the 19S base (Erales, Coffino 2014). However, usually ubiquitinated proteins are recruited and degraded. Here, too, an unstructured region is important for initiation of proteolysis. As the degradation signal or degron consists of two parts, ubiquitination and the unstructured region can be distributed onto different proteins. This way, a quaternary

structure can be segregated and only one partner degraded (Inobe et al. 2011). Ubiquitin can bind directly or indirectly to the 19S cap and a chain length of at least four ubiquitins is needed for efficient degradation (Thrower et al. 2000). Due to the associated E3 ligases and DUBs, the chain length can be modified while the substrate is bound to the proteasome. The deubiquitination can serve as a recycling mechanism of ubiquitin but also as a regulatory step of degradation: The DUBs remove the distal ubiquitin moieties first. Together with the chain length, this creates a time limit for degradation. If the initial unfolding process of the substrate is slower than the deubiquitination, the substrate may escape degradation (Lee et al. 2011).

Besides the 19S regulatory particles, three other caps for the core are described. Two of them, 11S and Blm10/PA200, are ATP independent and only little is known about their function. 11S is a toroidal heptamer that induces the gate opening in the subunits of the 20S proteasome similar to the 19S particle. It is implicated to be involved in the immune response. Blm10/AP200 forms a long, single chain that wraps at the top of the 20S proteasome and does not seem to trigger the opening of the subunits (Kish-Trier, Hill 2013). The third type of cap, the p97 homolog Cdc48/VAT, was so far only found in archaea. VAT was shown to functionally interact with the 20S proteasome via the HbYX motif in the C-terminus (see 1.2.1) (Barthelme, Sauer 2012).

1.2 The AAA+ ATPase p97

The hexameric ATPase p97 (also called VCP for valosin containing protein or Cdc48 in yeast) is an essential and ubiquitously expressed protein, found in high abundance in the cytoplasm and nucleus of the cell (Peters et al. 1990). It is highly conserved in eukaryotes. As a member of the AAA+ family (ATPases associated with diverse cellular activities), it uses the energy provided by ATP hydrolysis to induce conformational changes in substrate molecules.

p97 was found to be involved in many diverse pathways (Wolf, Stolz 2012; Dargemont, Ossareh-Nazari 2012; Bug, Meyer 2012, Figure 1.3). For example, it extracts Aurora B and Ku80 from chromatin (Ramadan et al. 2007; van den Boom et al. 2016) and mediates the degradation of CDC25A and IκBα depending on signaling events (Riemer et al. 2014; Li et al. 2014). Furthermore, p97 is an important component of the regulation of protein quality control and homeostasis throughout the cell. It associates with various organelles where it promotes the degradation of misfolded proteins, for example in endoplasmic reticulum-associated degradation

(Wolf, Stolz 2012, see below) or mitochondria-associated degradation (Taylor, Rutter 2011; Wu et al. 2016). Moreover, it promotes degradation of nascent polypeptides at stalled ribosomes (Verma et al. 2013).

A unifying theme in these pathways is the association of p97 with ubiquitin or ubiquitinated substrates. The binding to ubiquitin itself is weak and mainly mediated by over 30 ubiquitin adapters and additional cofactors. These interactions regulate p97 and recruit the enzyme to the distinct pathways.

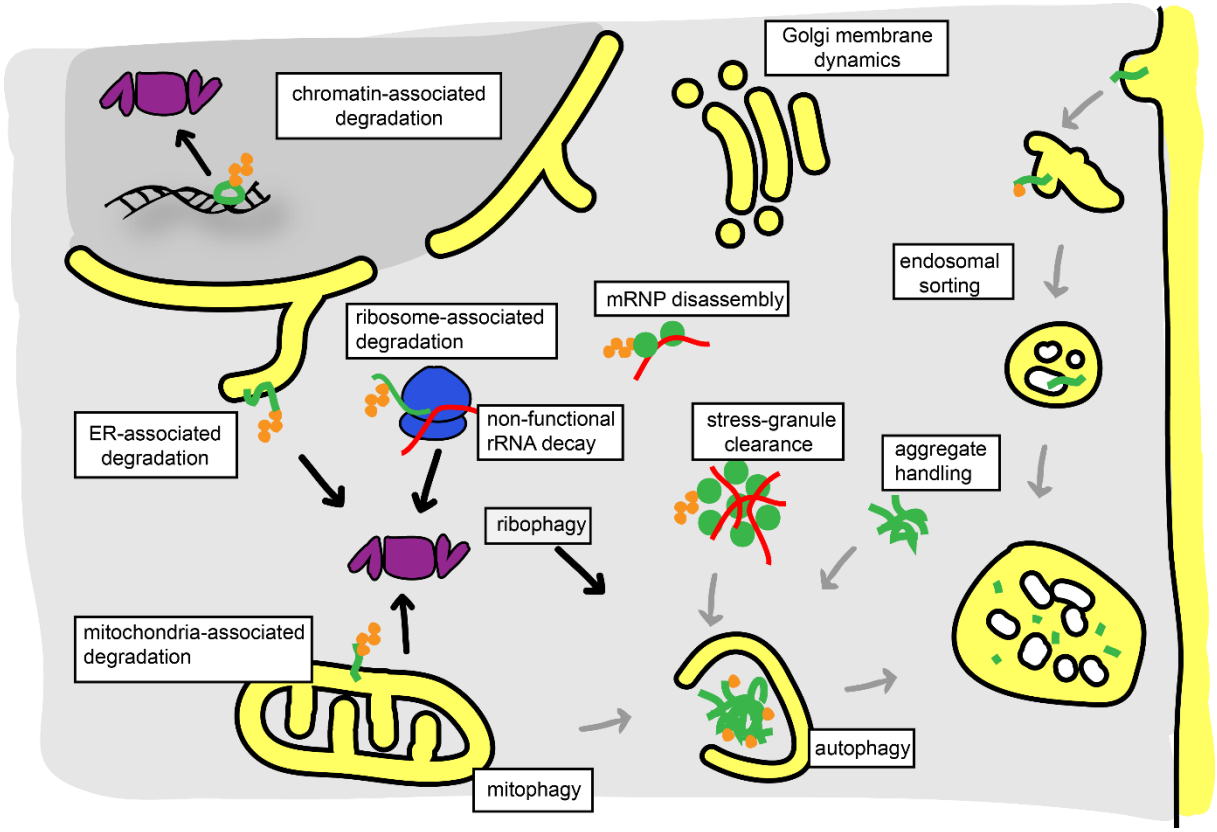

Figure 1.3 Cellular functions of p97
p97 extracts substrate destined for proteasomal degredation like in ER-associated degradation. In other cases, it promotes degradation by autophagy, for example stalled ribosomes, but also catalyzes the dissociation of proteins from chromatin. For effects of disease-associated mutant of p97, see also section 1.2.3. Green: substrates; orange: ubiquitin; purple: proteasome; red: RNA; blue: ribosome.

The cofactors bind with different domains or motifs to the p97 N domain or in some cases to the C-terminus. The largest group of N domain-binding cofactors contains a UBX (ubiquitin regulatory X) or the structurally similar UBX-L (ubiquitin regulatory X-like) domain (Buchberger et al. 2015). UBX and UBX-L are structurally similar to ubiquitin but have additional, distinct features in their S3/S4 loops that are important for p97 binding (Hanzelmann et al. 2011; Kang, Yang 2011). The function of p97 is closely linked to ubiquitinated substrates but p97 itself shows only low affinity to

ubiquitin (Ye et al. 2003). The interaction with the ubiquitinated substrates is mediated by cofactors. A subset of the UBX proteins can bind to ubiquitin with a UBA (ubiquitin-associated) domain (Buchberger et al. 2015). The UBX-UBA containing cofactors are therefore also described as substrate recruiting cofactors. Of note, other cofactors can bind p97 and ubiquitin with different domains, too. For example, AIRAPL (arsenite-inducible RNA-associated protein-like protein) contains a VIM (VCP-interacting motif) for p97 binding and a UIM (ubiquitin-interacting motif) for ubiquitin binding (Glinka et al. 2014). Besides acting as scaffolds, some cofactors show enzymatic activity, for example E3 ligases like gp78 or dequbiquitinases like YOD1 (Fang et al. 2001; Messick et al. 2008). The two related proteins p37 and p47 modulate the ATPase activity of p97 (Zhang et al. 2015). However, the organization of the cofactor system and the roles of many of the known cofactors are under investigation (Meyer, Weihl 2014).

According to the currently prevailing model, p97 forms “core complexes” with major cofactors (Meyer, Weihl 2014; Hänzelmann, Schindelin 2017). These major cofactors bind mutually exclusive. The binding of “accessory” cofactors localize the core complex to a defined pathway (Meyer et al. 2012). The UFD1–NPL4 (ubiquitin fusion degradation protein 1, nuclear protein localization protein 4) heterodimer, p47 and UBXD1 (ubiquitin regulatory X domain 1) are described as such major cofactors (Meyer et al. 2012; Buchberger et al. 2015). All three can occupy two binding sites in the hexamer. p47 uses a SHP box and a UBX domain (Bruderer et al. 2004). UFD1 binds p97 with a SHP box and NPL4 uses a UBX-L domain to bind to one or two neighboring N domains (Hanzelmann, Schindelin 2016). UBXD1 binds to the N domain via a VIM motif and to the C-terminus with its PUB (PNGase/UBA or UBX containing proteins) domain (Kern et al. 2009).

The mutual exclusive binding of major cofactors can be partially explained by overlapping binding sites. For example, p47 and UFD1-NPL4 bind to the same groove in the N domain with a UBX or UBX-L domain, respectively (Dreveny et al. 2004; Isaacson et al. 2007) and compete for this binding site (Bruderer et al. 2004). However, access to the binding sites in p97 is not generally blocked. For example, accessory cofactors can bind to the N domain simultaneously with the major cofactors UFD1-NPL4 and UBXD1 (Glinka et al. 2014; Papadopoulos et al. 2017). How these restrains in the stoichiometry are achieved is not fully understood.

The most-studied function of 97 involves the core complex with UFD1-NPL4 in ERAD (endoplasmic reticulum associated degradation), an important part of protein quality control during protein biosynthesis. Nascent proteins are bound to chaperones in the ER lumen (Nakatsukasa, Brodsky 2008). If the proteins cannot fold properly, they become primed for degradation (Nishikawa et al. 2001). In a next step, the protein needs to be transported out of the ER lumen or membrane. A channel is assumed to be necessary, similar to the Sec61 channel for translocation (Hampton, Sommer 2012). After parts of the protein are exposed to the cytosol, it can be ubiquitinated and subsequently completely transported into the cytosol (Wang et al. 2007). ER-associated E3 ligases are for example Hrd1 (HMG-coA Reductase Degradation 1) and gp78 (Glycoprotein 78) (Bordallo et al. 1998; Zhong et al. 2004), both cofactors of p97. The complex of p97 and UFD1-NPL4 binds to the ubiquitinated substrates and ATP hydrolysis by p97 is needed for the substrate translocation (Ye et al. 2001). Furthermore, p97 acts as an interaction hub for other ERAD-associated proteins such as UBXD8 or the DUB Ataxin-3 (Suzuki et al. 2012; Zhong, Pittman 2006). Finally, the substrates are handed over to the 26S proteasome for degradation (Zhang, Ye 2014).

Another role of p97 is found in the endolysosomal system. There, p97 forms a complex with UBXD1 (Kirchner et al. 2013). Recently it was shown that p97 and UBXD1, together with YOD1 (Ubiquitin thioesterase OTU1) and PLAA (phospholipase A_2 activating protein), are also involved in the clearance of damaged lysosome by autophagy or in short, lysophagy. During this process, the complex targets and processes K48 linked ubiquitin chains on the damaged lysosome. This step in the endo-lysosomal damage response (ELDR) is essential for the formation of the autophagosome (Papadopoulos et al. 2017).

UBXD1 belongs to the class of UBX containing cofactors of p97. A physiological role of UBXD1 was found in endolysosomal transport of caveolin (Figure 1.4). Together with p97, it was implicated in targeting of monoubiqitinated caveolin. Mutations in p97 can cause degenerative diseases (see 1.2.3). One of these p97 mutants was found to impair the transport of caveolin, potentially by lower binding between UBXD1 and the p97 mutant (Ritz et al. 2011; Schuetz, Kay 2016). UBXD1 is special in that it does not use the UBX domain to bind to p97 (Madsen et al. 2008). Instead, UBXD1 has a PUB domain for C-terminal binding and a VIM motif for N-terminal binding. Moreover, the N-terminus harbors an additional binding element for the N-D1 interface of p97.

Interestingly, also the disease-associated mutations in p97 are found at this interface, offering a possible explanation for the decreased interaction between UBXD1 and the p97 mutants. Furthermore, UBXD1 inhibits the p97 ATPase activity. As a mechanism, it was suggested that it locks the N domains in the down conformation with the help of its N-terminal binding region (Trusch et al. 2015; Schuetz, Kay 2016).

YOD1 binds the p97 N domain with a C-terminal UBX-L domain. It is a deubiquitinase of the OTU (ovarian tumor) family (Figure 1.4). Especially longer, K11-linked ubiquitin chains are cleaved, but its specificity is broadened by the N-terminal Zinc finger domain towards K27, K29, K33 and also K48 chains (Mevissen et al. 2013). The zinc finger domain, like the UBX-L domain, was shown to be necessary for *in vivo* retrotranslocation of ERAD substrates. There, it is also associated with p97 (Ernst et al. 2009). YOD1 activity impaired the retrotranslocation of a nonubiquitinated substrate, implicating a negative regulation of ERAD components by the DUB (Bernardi et al. 2013).

PLAA consists of a WD40 domain followed by a PFU domain for ubiquitin binding and the C-terminal PUL domain that interacts with the p97 C-terminus (Figure 1.4). The PUL domain forms a helical structure with a long, positively charged groove to which the p97 C-terminus binds (Qiu et al. 2010). The yeast homolog of PLAA, Doa1/Ufd3 was shown to be associated with ESCRT-0 and the efficient sorting of ubiquitinated substrates into multivesicular bodies (Ren et al. 2008). Doa1 also regulates ubiquitin levels by an unknown mechanism (Qiu et al. 2010).

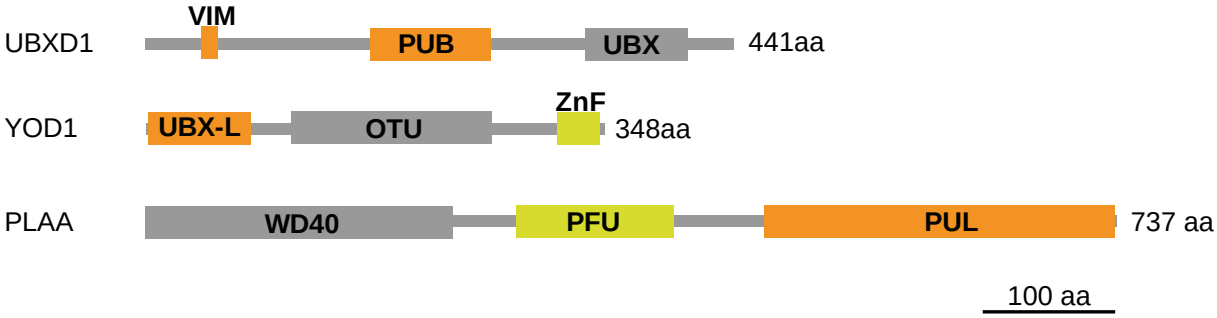

Figure 1.4 Domain structure of UBXD1, YOD1, and PLAA
The size and domains of the three ELDR cofactors UBXD1, YOD1, and PLAA are shown. Orange: domains or motifs binding to p97; yellow: domains binding to ubiquitin.

1.2.1 Structure and domains

p97 belongs to the family of AAA+ proteins and harbors two consecutive ATPase domains (D1 and D2 domains). The active unit is a hexamer where the ATPase

domains form two stacked rings with a diameter of around 12 nm and a height of around 7 nm. The N domains form a second ring around D1 with a diameter of around 15 nm (Figure 1.5 A+B).

The N domain is separated into two lobes, the N-terminal Nn part and C-terminal Nc part. Nn consists of a double ψ-barrel, Nc consists of a four-stranded β-barrel (Yeung et al. 2008) (Figure 1.5 C). The cleft between the two subdomains is an important adaptor interaction site, which binds UBX, UBX-L, VIM and VBM motifs of cofactor proteins. The SHP box binding site is in the vicinity of the cleft on the Nc subdomain and simultaneous binding of UBX/UBX-L and SHP box is sterically possible (Hanzelmann, Schindelin 2016).

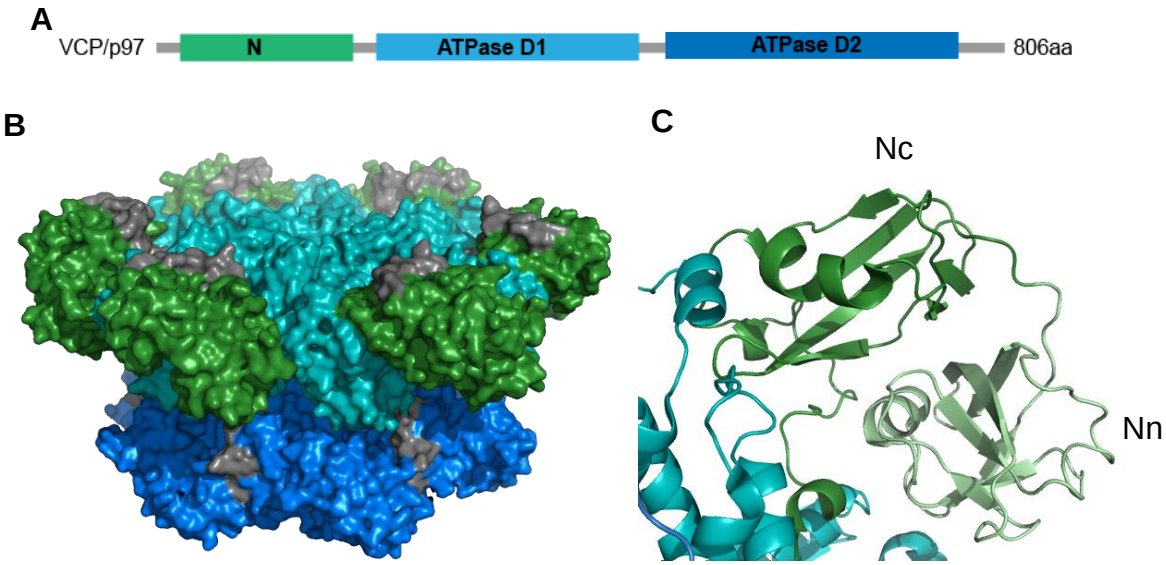

Figure 1.5 Structure of the p97 hexamer
A) Domain structure of p97. Green: N domain; light blue: D1; dark blue: D2; Grey: linker. B) Hexameric structure of p97 with ADP in D1 and no nucleotide in D2 (pdb 5ftk). Colored as in A). C) Detailed view of the N domain of p97 (pdb 3cf3): view from the D1 towards the N domain. Colored as in A), but with additional coloring for the N subdomains. Light green: Nn double ψ-barrel; green: Nc four-stranded β-barrel

The two ATPase domains are very similar in sequence. Regarding their structure, the D2 domain adopts a more “open” state (Davies et al. 2008; Magnaghi et al. 2013). The D1 domain is important for hexamerization as truncations without N or D2 domain still form hexamers. It was shown that the full length protomers can assemble even in absence of nucleotides, though presence of nucleotides accelerates the process (Wang et al. 2003). The two ATPase domains also differ in activity, with D2 being the main contributor to hydrolysis (see 1.2.2.2). The C-terminus is a flexible tail and rarely visible in structural datasets. Its interactions with the PUB (PNGase/UBA

or UBX containing proteins, also called PUG) and PUL (PLAP, Ufd3p, and Lub1p) domains of cofactors are correspondingly elusive. At the very end of the C-terminus, p97 harbors the HbYX motif (hydrophobic, tyrosine, any amino acid) that is part of the longer PIM (PUB interacting motif). In other AAA+ ATPases, the HbYX motif is part of the interface with the 20S proteasome (see 1.1.2). The tyrosine at position 805 is reported as a phosphorylation site that if phosphorylated blocks interaction with the PUB domain of cofactors. The PUL domain found in cofactors binds also to the PIM but with weaker affinities (Zhao et al. 2007).

1.2.2 Molecular mechanisms in p97

p97 converts chemical energy from ATP hydrolysis into mechanical work. It extracts or segregates substrates from membranes or protein complexes, or it unfolds the client proteins (Stolz et al. 2011). However, the molecular mechanism of this process is currently intensively debated. A typical feature of AAA+ ATPases is their central pore that that is used by some enzymes for substrate translocation, causing global unfolding. An example for an AAA+ ATPase with this mechanism is VPS4 (Yang et al. 2015). Another AAA+ ATPase on the other hand, NSF, uses the movement of the N domains to segregate proteins in a single burst (Ryu et al. 2015). Very recent studies could reconstitute the unfoldase activity of wild type p97 *in vitro* (Blythe et al. 2017; Bodnar, Rapoport 2017).

1.2.2.1 Models for substrate processing

Three models for the role of the central channel were suggested: First, the substrate is only looped into the D2 pore. The D2 pore is lined with the denaturing “arginine collar” (R586, R599) and aromatic amino acids (551WF552), possibly helping in an unfolding process (DeLaBarre et al. 2006). This mechanism was considered because ubiquitinated proteins, the typical substrates of p97, were thought to be too unwieldy to be threaded through the pore (Stolz et al. 2011). On the other hand, the DUBs and ubiquitin ligases among the p97 adaptors render a sequential de- and re-ubiquitination possible.

In a second model, the substrate may enter “sideways” from the D1-D2 interface and leave through the D2 pore. Axial openings in the D1-D2 interface were observed in different structures that could serve as entry points. A normal mode analysis claimed that the D1 pore is rigid, especially due to residue H317. Rotational and elongating movements of the D2 domain would pull a substrate through the D2 pore (Na, Song 2016).

In a third model, the substrate is threaded completely through the D1 and D2 pores. However, some structural data implicated narrow pores, particularly the D1 site seemed to be blocked by amino acids 313-323 (DeLaBarre et al. 2006). In other structures, especially those derived from cryo-EM, this constraint seems to be lifted (Yeung et al. 2014; Banerjee et al. 2016). In the archaeal p97 homolog VAT, important pore lining sequences include aromatic or hydrophobic residues (KYYG in D1 and KMVG in D2). However, a corresponding sequence in mammalian p97 is only found in D2 (550MWFG553). By mutation of the D1 pore loop 277KLAG280 to 277KYYG280 and additional deletion of the N domain, unfoldase activity of this mutant p97 could be shown *in vitro*. As the mutations in D1 were needed, it implicates a complete threading of substrates through the pore (Rothballer et al. 2007). A very recent study established an *in vitro* unfolding assay. A fluorescent model substrate was ubiquitinated and the fluorescence is reduced by Cdc48-UFD1-NPL4 in a time dependent manner. The efficiency of unfolding increased with the ubiquitin chain length and reached a maximum at four to five ubiquitin moieties. Interestingly, K48-linked chains, but not K63-linked chains were processed. Furthermore, a polyubiquitinated substrate could be crosslinked either to D1, the intra-luminal site of the pore, or D2 in yeast Cdc48. The authors concluded that the substrate is translocated through the entire pore from D1 to D2 driven by ATP hydrolysis in D2, which causes global unfolding. For the release of the unfolded substrate, the DUB activity of YOD1 was needed (Bodnar, Rapoport 2017). Simultaneously, another group showed in a similar assay with human p97 that the unfolding did not occur with the cofactors p47 or UBXD7. Here, too, longer chains were processed more efficiently and also branched chains improved the unfolding (Blythe et al. 2017).

In all three models, ATP hydrolysis is mandatory for the function of p97. This prerequisite was demonstrated in different *in vitro* unfolding experiments (Rothballer et al. 2007; Blythe et al. 2017; Bodnar, Rapoport 2017) and also in numerous cell based studies (Esaki, Ogura 2010; Meerang et al. 2011; Riemer et al. 2014). Furthermore, the different nucleotide states correlate with different conformations of p97 (Banerjee et al. 2016). Therefore, understanding the nucleotide binding and the ATPase activity is important to establish a comprehensive model of the p97 function.

1.2.2.2 ATPase activity

In total, p97 has twelve ATPase domains distributed on six protomers with two different binding sites each. Each ATP binding site is influenced by the other in the same protomer and by neighboring protomers, spanning an intricate network that is not understood so far. An additional layer of complexity is added by the N domains and adaptors that influence the activity (Niwa et al. 2012; Zhang et al. 2015). These connections are for example addressed by investigating the activities and nucleotide affinities in different mutants of p97. One important set of mutants harbors single point mutations of residues in the Walker A (K251 and K524) or Walker B (E305 and E578) motifs. Walker A mutants are deficient in nucleotide binding, Walker B mutants deficient in ATP hydrolysis. Among the four possible Walker mutants, only Walker B in D1 (or B1 in short) shows activity at wild type level (Chou et al. 2014). Furthermore, experiments in yeast implicated that the hydrolysis in D1 is not essential (Ye et al. 2003; Esaki, Ogura 2010). Along with these observations, the main ATPase activity of p97 was attributed to the D2 domain. However, the attribution of D1 as inactive was challenged when an ND1 fragment (1-480, ND1L) was found to be active. The relevance of this activity in the full length protein is unclear. At least in *in vitro* experiments, the D2 domain seems to be a negative regulator of the D1 domain (Tang, Di Xia 2013; Chou et al. 2014). The B1 mutant, but not the Walker B in D2 (B2) mutant showed unfolding activity *in vitro*, mirroring the ATPase activity of the mutants (Blythe et al. 2017; Bodnar, Rapoport 2017).

An interesting property of the D1 domain is its very stable binding to ADP. Even under nucleotide-free purification conditions, ADP is bound in D1. The reported amounts prebound ADP ranges from 0.5 to 1 per p97 monomer (DeLaBarre, Brunger 2003; Davies et al. 2008; Briggs et al. 2008; Tang, Di Xia 2013). The amount of prebound nucleotides is also reflected by the affinities of the different domains to the different nucleotides. The Walker A mutants or the ND1L truncation are used to differentiate between binding to the two ATPase domains. The reported affinities vary with the methods used, but the ratios between binding to D1 and to D2 are consistent. The D1 domain has higher affinities for ATP and ADP than the D2 domain (Table 1.1 A, comparing K524A with K251A). Furthermore, ADP has a slightly higher affinity for the D1 domain than ATP (A, comparing ADP with ATP). However, this changed when the protein was depleted of prebound nucleotide with apyrase, resulting in an elevated affinity for ATPγS (B).

Table 1.1 Nucleotide affinities for different p97 mutants
The data was taken from the indicated publications. Two values in a box are the results from a two site binding model.

A

Binding in	Mutation	Nucleotide affinity [nM]		
		ADP	ATP	ATPγS
D1	K524A	142	264	9.5 / 417
D2	K251A	6400	8670	1870
D1+D2	Wild type	123 / 3100	140 / 4700	42 / 1200
none	K524A/K251A	22300	25500	11200

SPR data from Chou et al. 2014. The proteins were not depleted of prebound nucleotide.

B

Binding in	Mutation	Nucleotide affinity [nM]		
		ADP	ATPγS	ATPγS (apyrase)
D1	ND1L	880	890	110

ITC data from Tang, Di Xia 2013. Comparison of ATPγS affinities between apyrase treated and non-treated protein. Apyrase hydrolyzes ATP and ADP to AMP.

Activity and affinity measurements showed the mutual influence of the ATPase domains, but also the N domain became apparent as an important regulator. A hint at the mechanism was found in mutations of p97 associated to the disease MSP1 (Multisystem Proteinopathy 1). The influence of MSP1 mutations on the functions of p97 is still under investigation. Interestingly, the mutations are only found in the N-D1 interface or in the N-D1 linker, while the ATP binding sites themselves are not changed (see 1.2.3). Nevertheless, some disease-associated mutations cause a higher ATPase activity (Tang, Di Xia 2013). By restraining the flexibility of the N domain, either by mutations in the N-D1 linker or crosslinking N to D1, ATPase activities of an MSP1 mutant or the wild type were reduced (Niwa et al. 2012). The first crystal structure of the N domains in the so called up-conformation was achieved with an MSP1 mutant in the ND1L fragment. This correlated with the binding of ATPγS to D1 (Tang et al. 2010). In earlier studies with wild type p97, only ADP was found in D1. Another observation was the lower occupancy of nucleotides in D1 in different disease associated mutants, leading to the suggestion that the exchange from ADP to ATP is accelerated in the mutants (Tang, Di Xia 2013). Later, cryo-EM data of full length wild type p97 confirmed the connection between ATPγS in D1 and the N domain in up-conformation (Banerjee et al. 2016). There, the N domains in up-conformation showed lower electron densities, hinting at a possible asymmetry that

may be obscured by symmetry operations during structure determination (Tang, Di Xia 2013; Schuller et al. 2016; Banerjee et al. 2016). Also NMR data showed a higher flexibility of the N domain in presence of ATPγS or in different MSP1 mutants. In this study, different pathways for allosteric interactions were proposed that influence the interaction with other protomers, the nucleotide binding site, or the N-D1 interaction (Schuetz, Kay 2016). However, if the conformation of the N domain is a result of ATP binding in D1 or vice versa is unclear. Some adaptors are associated with an N domain conformation, too, as was shown for p47, FAF1 and UFD1-NPL4 (Ewens et al. 2014). All four bring the N domains in an up-conformation, while UBXD1 is proposed to favor the down-conformation (Trusch et al. 2015; Schuetz, Kay 2016). *In vitro,* both p47 and UBXD1 have an inhibitory effect on the p97 ATPase activity, but seem to favor different N domain positions. It is unknown if the displacement of the N domains, in concert with bound cofactors, transfers force on a substrate or if it is a regulatory mechanism. Besides the change in N domain conformation, there are two other prominent interdependent movements in the hexamer during the hydrolysis cycle. First, a twist of D1 and D2 against each other around the central axis occurs. The rotation is dependent on ATP binding to D2, but not hydrolysis (Noi et al. 2013). The second movement is a narrowing of the D2 pore upon binding of ATP (Banerjee et al. 2016). Of note, the pores appear wider in solution-based structures like cryo-EM than in crystal structures (Beuron et al. 2006). These two structural changes are attributed to exert mechanical force onto the substrate.

A proposed model for the ATPase cycle assigns a regulatory role to D1 (Figure 1.6 A). It differentiates between the ADP open and locked state, additionally to an empty and ATP bound state. In the empty state with unknown conformation of the N domain, ATP can bind and the N domain is found in the up conformation. This state allows ATP hydrolysis in D2. However, it is not clear if hydrolysis in D1 and D2 happens sequentially or if the two ATPase cycles occur in a connected, but independently proceeding manner as this model assumes. Upon hydrolysis of ATP, the N domain flips down and the corresponding D2 is inactive. Importantly, the D1 domain is at first in a locked state, meaning that ADP cannot be readily exchanged against ATP (Tang, Di Xia 2016). The model can be expanded with the new data from unfolding assays (Figure 1.6 B). The binding of ATP to D1 strengthens the binding of UFD1-NPL4 (Chia et al. 2012) and reduces or elevates the global ATPase activity with or without substrate, respectively. If the whole complex is assembled,

hydrolysis in D1 is reduced to maintain the active conformation. In the meantime, the D2 domain can progressively unfold the substrate until ATP in D1 is hydrolyzed. Then, the N domains adopt the down conformation. For substrate release, the remaining folded ubiquitin moieties are cleaved off by a DUB and the substrate, including a short ubiquitin chain, is pulled completely through the pore before finally dissociating from p97. The dissociation is supported by the DUB Otu1 (the YOD1 homolog in yeast) (Bodnar, Rapoport 2017).

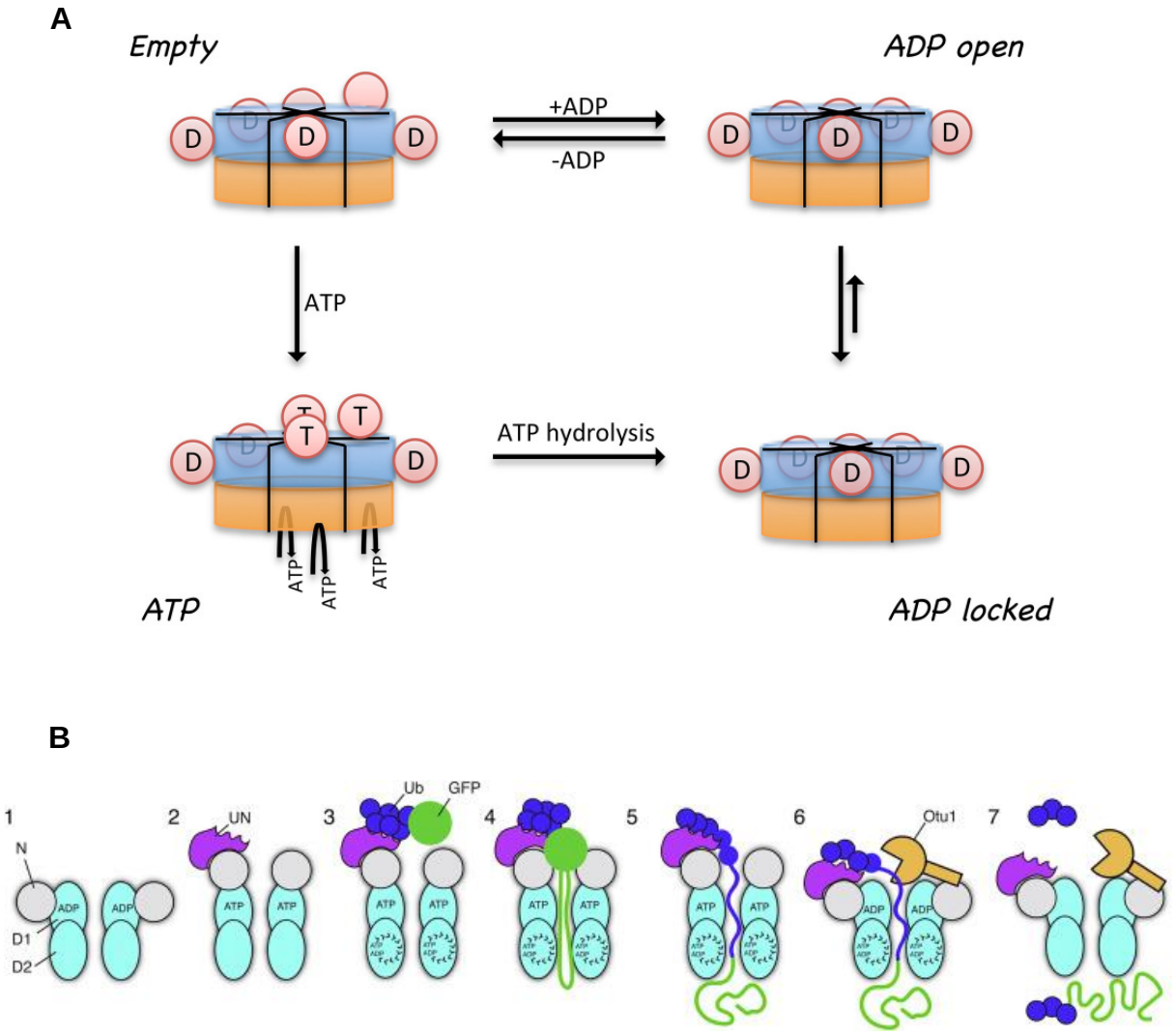

Figure 1.6 Model for the regulation of the ATPase cycle in p97
A) Model with a focus on the hydrolysis in D1. N domains are shown in red, D1 in blue and D2 in orange. D denotes ADP in D1 and a corresponding down conformation, T denotes ATP in D1 with an up conformation. An empty D1 is unlabeled. A D2 domain can hydrolyze ATP only in case D1 is occupied by ATP (adopted from Tang, Di Xia 2016). B) Model for the translocation of a ubiquitinated substrate (ubiquitin in blue, GFP in green). UN: UFD1-NPL4; Ub: ubiquitin (adopted from Bodnar, Rapoport 2017)

1.2.3 Degenerative diseases caused by mutations in p97

Over 30 point mutations in p97 are known that cause autosomal dominant degenerative diseases. They are subsumed under the term multisystem proteinopathy 1 (MSP1) and include IBM (inclusion body myopathy), FD (frontotemporal dementia), Paget's disease of bone, FALS (familial amyotrophic lateral sclerosis) and CMT (Charcot-Marie-Tooth disease) (Tang, Di Xia 2016). They are late-onset diseases and the first indicators often occur in muscle tissue, but also bone and brain can be affected. The same mutation can differ in phenotype and severity depending on the patient. In patient tissue, hallmarks of the diseases are aggregates or inclusions, often positive for TDP-43 or ubiquitin. Structurally, the mutations are located at the interface between N and D1 domain with no obvious connection to binding sites of ATP or cofactors (Meyer, Weihl 2014). How the mutations cause the different phenotypes is not clear. An important question is if the mutations confer a loss-of-function or a gain-of-function. At least some of them result in an elevated ATPase activity (Niwa et al. 2012; Tang, Di Xia 2013), but it is not clear if this always translates to higher activity in the cellular functions or represents and idle running, decoupled ATPase activity. Several recent findings support the gain-of-function hypothesis: First, less pre-bound ADP is found in D1, resulting in a faster, deregulated nucleotide exchange in D1 that may result in hyperactivity (Tang, Di Xia 2016). Second, experiments in *Drosophila melanogaster* showed that a p97 mutant could rescue a mitochondrial defect, arguing against a loss-of-function (Zhang et al. 2017). Third and most recently, in an *in vitro* unfolding assay a mutant showed higher unfolding activity compared to the wild type (Blythe et al. 2017). However, the studies were not carried out comprehensively including all disease mutants, but focused predominantly on R155H and A232E. Besides an influence on p97 activity itself, another possibility how the mutations affect different pathways is the deregulation of p97-cofactor interactions (Fernández-Sáiz, Buchberger 2010). This was shown for UBXD1 that binds less to the R155H mutant (Ritz et al. 2011). Furthermore, the two cofactors p47 and p37 regulate the ATPase activity of p97 and this regulation is impaired in different MSP1 p97 mutants (Zhang et al. 2015).

1.2.4 Inhibitors of p97

With p97 emerging as a key player in protein homeostasis, the development of inhibitors of p97 moved into focus. Cancer cells are "addicted" to certain traits that enable them to grow in spite of their abnormalities. One of these abnormalities is

proteotoxic stress and therefore, they need a highly efficient UPS (ubiquitin-proteasome system). As p97 is an important part of this system, it emerged as a target for cancer therapy (Vekaria et al. 2016). Another similar strategy to target cancer cells via the protein quality control axis is already in clinical practice with proteasome inhibitors like bortezomib. Accordingly, there is ongoing research in developing p97 inhibitors (Chapman et al. 2015).

Eeyarestatin I (EerI) was found in a library screen for ERAD inhibitors (Figure 1.7 A). It inhibits the degradation of class I major histocompatibility complex or T-cell receptor α without inhibition of the proteasome (Fiebiger et al. 2004). Subsequent studies showed that EerI inhibits ERAD by association with the p97-UFD1-NPL4 complex. There, it negatively regulates a deubiquitinating process. However, EerI does not affect the ATPase activity of p97 (Wang et al. 2008). Combined with bortezomib, EerI induced apoptosis even in bortezomib resistant cells, demonstrating the promising concept of targeting different components of the protein quality control simultaneously (Auner et al. 2013).

The competitive inhibitor DBeQ (Figure 1.7 B) was found in another screen. It was selective, reversible, ATP competitive, and inhibited the ATPase activity of p97 with an IC_{50} of 1 µM. Treated cells responded for example with upregulation of the UPR (unfolded protein response) marker CHOP (CCAAT/enhancer-binding protein homologous protein) and caspase activation (Chou et al. 2011). In later studies, DBeQ was found to act on both the D1 and D2 domain of p97 but two derivatives (ML240 and ML241) were selective for D2 (Chou et al. 2014). While both derivatives inhibited p97 potently, only ML 240 impaired autophagy and induced apoptosis, indicating the possibility to develop pathway-specific inhibitors of p97 (Chou et al. 2013). The ATP-competitive inhibitors also lost potency against p97 if it was bound to p47, further supporting the possibility to target specific p97 functions (Fang et al. 2015a). The structure of ML240 was refined to the compound CB-5083 (Figure 1.7 C) with an IC_{50} in the low nanomolar range and entered clinical trials (Anderson et al. 2015).

Two inhibitors were found in another screening, one allosteric and one covalently binding. The covalent inhibitor NMS-859 (Figure 1.7 E) targets C522. This residue is known to be regulated by an oxidative modification that results in ATPase inhibition (Noguchi et al. 2005). Since C522 is near to the critical Walker A residue K524, ATP binding is blocked by NMS-859, similar to the widely used K524A mutant (Magnaghi

et al. 2013). Other compounds like Withaferin A analogs also target C522 (Tao et al. 2015). The allosteric inhibitor was further improved, yielding NMS-873 (Figure 1.7 D) with an IC_{50} of 30 nM. It induced established biomarkers of p97 inhibition such as CHOP, polyubiquitinated proteins and caspase-3. Its binding site was found with a derivative that carried an azido moiety. This moiety could be crosslinked to p97. After digestion and MS analysis, a modified peptide was found in the region of the D1-D2 interface at positions 615KN616. A docking simulation supported this site as a possible binding pocket. Mutations in this area lead to a loss of binding and loss of inhibition by NMS-873, confirming the binding site. As a possible mechanism of inhibition, NMS-873 could disrupt the communication between intersubunit signaling motif (ISS) and the Sensor I region and subsequently between the protomers. This area is important for interprotomer communication and nucleotide sensing. Accordingly, nucleotide binding was affected by NMS-873 in that the compound increased p97's affinity towards ADP. Furthermore, ATP binding was necessary for binding of NMS-873, as NMS-873 did not bind to the K524A mutant that cannot bind ATP in D2. In the context of the ATPase cycle in the hexamer, NMS-873 probably interferes with the hydrolysis by prohibiting the interaction of the D2 arginine finger with ATP in the following D2 domain. Another effect is the inhibition of ADP release from the D2 domain in which NMS-873 itself is bound (Magnaghi et al. 2013).

UPCDC30245 is another allosteric inhibitor of p97. Its binding site could be determined with cryo-EM to be located at the D1-D2 interface in the same area as NMS-873. Based on the structural data, it was suggested that UPCDC30245 inhibits the conformational change that occurs between the ADP and ATP bound form of the D2 domain. Accordingly, the bound inhibitor was found in data sets of the ADP conformation whereas binding to the ATP form would produce steric clashes (Alverez et al. 2015; Banerjee et al. 2016). This is in line with the elevated affinity of p97 towards ADP upon NMS-873 binding.

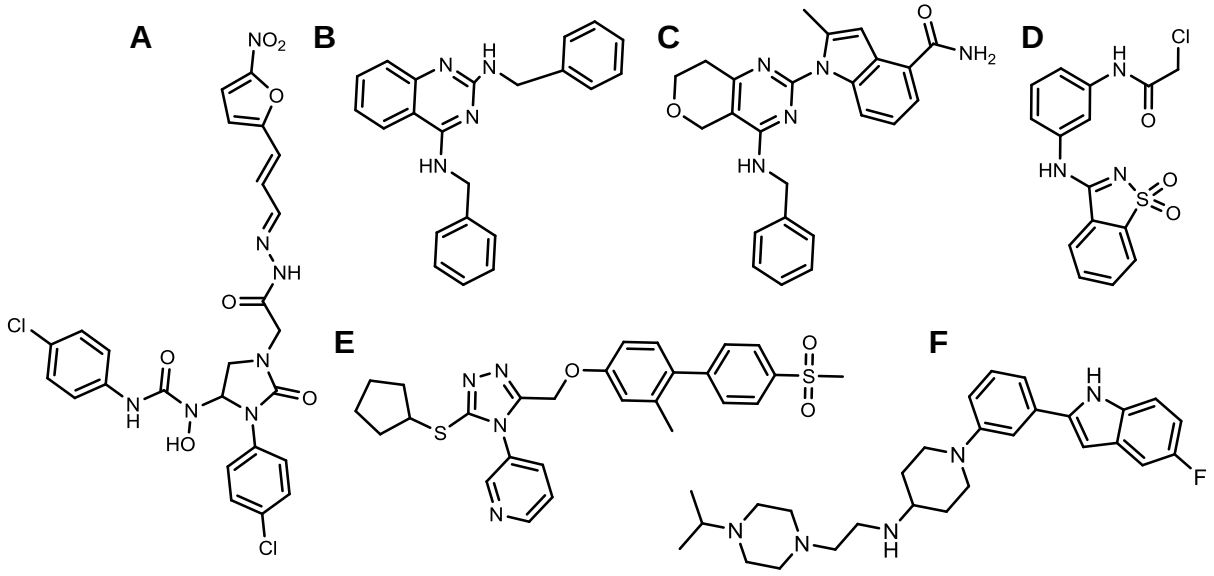

Figure 1.7 Structures of described inhibitors of p97
A) Eeyerstatin I B: DBeQ (competitive) C) CB-5083 (competitive, D2 specific) D) NMS-859 (covalent attachment to C522) E) NMS-873 (allosteric, D2 specific) F) UPCDC30245 (allosteric)

1.3 The ESCRT pathway and the AAA+ ATPase Vps4

During this study, the AAA+ ATPase VPS4 that is related to p97 became relevant for our investigations. For that reason, its cellular function is introduced.

Endocytosis describes the process of the invagination of the plasma membrane and the formation of vesicles through the abscission of the membrane. Endocytic vesicles bud from the plasma membrane to transport cell surface factors and extracellular material to the endosome. As an example, this mechanism regulates the cell surface expression of the receptor tyrosine kinase EGFR (epidermal growth factor receptor) (Goh, Sorkin 2013), but also viruses uses this machinery to infect cells (Shtanko et al. 2014). Moreover, the release of enveloped viruses (for example HIV) requires the ESCRT (endosomal sorting complex required for transport) machinery, including VPS4 activity (Votteler, Sundquist 2013).

The ESCRT pathway is an important part of the processing of ubiquitinated cargo in the endosomal/lysosomal system. During the maturation of an endosome, the cargo can be sorted with the help of the ESCRT pathway into intraluminal vesicles (ILV) so that an MVB (multivesicular body, also called MVE for multivesicular endosome) develops (Huotari, Helenius 2011). The ESCRT pathway is controlled by a sequential assembly of different protein complexes (Figure 1.8). ESCRT-0 is a heterodimer with the subunits HRS (hepatocyte growth factor (HGF)-regulated Tyr-kinase substrate)

and STAM (signal transducing adaptor molecule) (Asao et al. 1997). HRS recognizes endosomes decorated with phosphatidylinositol 3-phosphate (PI3P) (Raiborg et al. 2001). Furthermore, HRS and STAM can bind to ubiquitinated proteins at the endosomal membrane (Bache et al. 2003). The ESCRT-I subunit TSG101 (Tumor Susceptibility Gene 101) is recruited by the amino acid motif PSAP in HRS. TSG101 is part of a heterotetramer with VPS28 (vacuolar protein sorting-associated protein 28), VPS37 and hMVB12. Ubiquitinated substrates are recognized by TSG101 and hMVB12 (Christ et al. 2017). However, the interaction of ESCRT-I to membranes is only weak and its recruitment depends on ESCRT-0 (Kostelansky et al. 2007). The interaction between ESCRT-I and ESCRT-II in mammals is probably mediated between VPS28 and EAP45 (Christ et al. 2017). EAP45 also provides the interaction with the membrane via PI3P and with ubiquitin (Slagsvold et al. 2005). Additionally to EAP45, the ESCRT-II complex consists of EAP30 and two subunits of EAP20. The EAP20 subunits mediate the interaction with the ESCRT-III protein CHMP6 (charged multivesicular body protein 6) (Yorikawa et al. 2005). CHMP6 can also bind directly to the ESCRT-I subunit hVPS28 (Pineda-Molina et al. 2006). The ESCRT-III complex differs from the other complexes in that its subunits do not form defined complexes already in the cytosol but polymerize on the membrane. Binding between EAP20 and CHMP6 forms a nucleation complex and the other ESCRT-III proteins, CHMP7, CHMP5, CHMP4 (isoforms A, B, C), CHMP3, CHMP2 (isoforms A, B), CHMP1 (isoforms A, B), and IST1 (increased salt tolerance 1) are recruited. The proteins do not assemble in the cytosol because the negatively charged C-terminus folds back to the N-terminus, causing auto-inhibition (Williams, Urbe 2007). Upon displacement of the C-terminus, the proteins can polymerize (Alonso Y Adell et al. 2016). The membrane interaction of the subunits is mediated by the positive charges in the N-terminus, myristoylation of CHMP6, and a membrane inserting domain in CHMP4 (Yorikawa et al. 2005; Buchkovich et al. 2013). CHMP4 is also suggested to provide the biggest fraction of the ESCRT-III polymer (Alonso Y Adell et al. 2016).

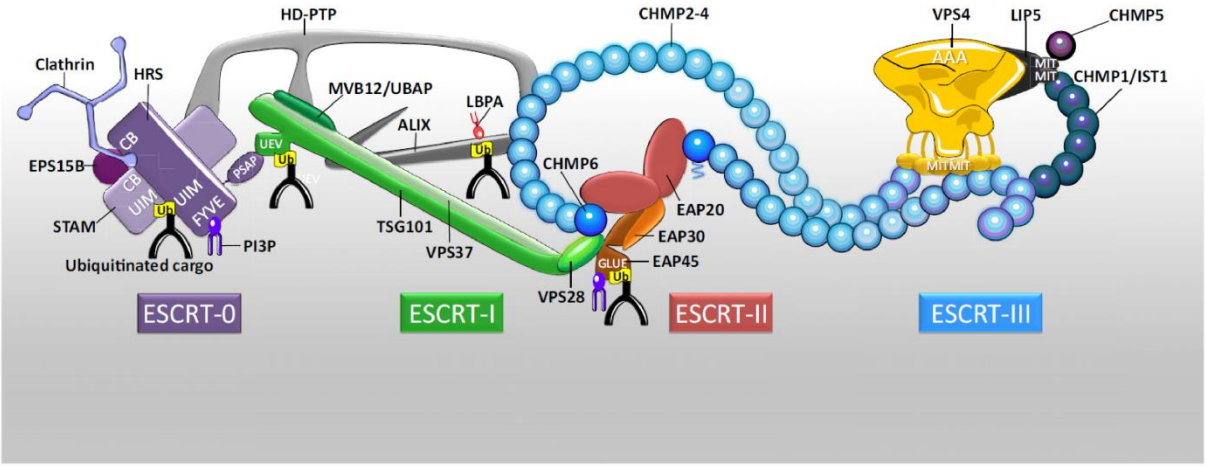

Figure 1.8 Overview of the ESCRT complexes in endolysosomal sorting
The sorting of cargo after endocytosis requires the coordination of four protein complexes. ESCRT-0 interacts with ubiquitinated cargo, the clathrin coat, and lipids (PI3P). Typically, ESCRT-I and ESCRT-II are recruited to ESCRT-0 and the cargo, though also alternative pathways exist (in grey). The ESCRT-III polymer drives vesicle formation and abscission of the vesicles, together with the ATPase VPS4. VPS4 also recycles the ESCRT-III subunits (Christ et al. 2017).

In the biogenesis of MVBs, ESCRT proteins and VPS4 are needed for budding and scission of ILVs (Adell et al. 2014). However, the mechanism of membrane remodeling and scission is so far unknown. The ESCRT-III polymer is thought to be the main driver of the process. It can form spirals, tubes, and cones, though the functional relevance of the different forms is unclear (Schöneberg et al. 2017). VPS4 is recruited by the exposed MIMs (MIT interaction motif) in the C-termini of ESCRT-III proteins at the membrane. The ESCRT-III related protein LIP5 binds with its VSL (Vta1/SBP-1/Lip5) domain to the β-domain of VPS4. LIP5 contains two further MIT (microtubule interacting and trafficking) domains to interact with other ESCRT-III proteins. Furthermore, the VSL domain of LIP5 causes dimerization. Therefore a model was proposed where multiple VPS4-LIP5 complexes form a lattice on ESCRT-III (Yang, Hurley 2010). The mechanic force provided by the ATPase activity of VPS4 is needed for disassembly of ESCRT-III. Already the partial disassembly of the ESCRT-III polymer destabilizes it and causes depolymerization (Yang et al. 2015).

1.3.1 Structure and activity of VPS4

VPS4 is a type I AAA+ ATPase and cooperates with the ESCRT machinery in membrane deformation and fission events. As part of this evolutionary conserved system, VPS4 is found in all eukaryotes and archae. In higher eukaryotes, two isoforms, VPS4A and VPS4B, exist. They display a high degree of sequence similarity of 80 % to each other and 60 % to yeast VPS4. The isoforms can assemble in heteromeric complexes. VPS4B can functionally replace VPS4 in yeast and VPS4B alone is sufficient for viral release (Scheuring et al. 2001; Kieffer et al. 2008). The functional difference between the isoforms is not clear yet but they may be involved in different branches of the ESCRT pathway (Monroe, Hill 2016). VPS4 is the only direct consumer of energy during endocytosis, making it a prominent target for inhibition. A potent, specific inhibitor would be a valuable research tool. So far, no specific inhibitors of VPS4 are known. However, DBeQ, developed as a p97 inhibitor, was shown to be active against VPS4B, too (Magnaghi et al. 2013).

A protomer of VPS4 consists of an N-terminal MIT domain, a flexible linker, and a single ATPase domain followed by a short C-terminus. The ATPase domain is further subdivided in the large and small ATPase domain (Figure 1.9). The small ATPase domain contains the β-domain insertion found in higher eukaryotes but not in yeast or related ATPases like spastin (Scott et al. 2005b).

Figure 1.9 Domain structure of human VPS4
VPS4A is slightly shorter than VPS4B due to deletions in the N-terminal part (based on Scott et al. 2005a; Scott et al. 2005b).

Similar to other AAA+ ATPases, VPS4 oligomerizes to fulfill its function but the stoichiometry of active VPS4 is under debate. In the inactive state, it forms probably dimers in the cytoplasm (Babst et al. 1998; Scott et al. 2005b), In some cases, also monomeric states were reported (Inoue et al. 2008). In the active oligomer, different stochiometries ranging between 6-14mers were proposed, though data hinting at hexamers or dodecamers of two stacked hexamers was reported most often (Landsberg et al. 2009; Monroe et al. 2014; Caillat et al. 2015). The p97 D1 domain was chosen as a structural model for the hexameric ring due to the high sequence

similarity and because p97 D1 forms a hexamer, too (Scott et al. 2005a). *In vivo*, the oligomerization of VPS4 could be induced by its high local concentration at the ESCRT-III complex together with nucleotide binding. Recent studies favor a simple hexamer of VPS4 as its active conformation (Monroe et al. 2014; Caillat et al. 2015). The crystal structure of msVPS4ΔMIT from *Metallosphera sedula* from the phylum *Crenarcheota* revealed an asymmetric pseudohexamer, showing for the first time an active conformation in a structural data set. The data implicated a model where VPS4 oligomerizes upon ATP binding and structural changes in two opposing protomers lead to the mechanical work. Furthermore, five low affinity sites and one high affinity site for ADP were found in ITC experiments, explaining the asymmetry in the ring structure that results in a pseudohexamer (Caillat et al. 2015). The central pore of VPS4 shows typical features found in other AAA+ ATPases, for example hydrophobic pore residues and an arginine collar (Gonciarz et al. 2008). Indeed, VPS4 uses the energy from ATP hydrolysis to disassemble the ESCRT-III complex by translocating the ESCRT-III substrates trough the pore, causing global unfolding (Yang et al. 2015).

1.4 Aims of the thesis

The molecular mechanism of p97 as well as the interactions with cofactors are still of major interest to understand its role in the cell. Inhibitors are valuable tools to investigate the function of a protein in the cellular context and to understand the activity of an enzyme on the molecular level. Furthermore, p97 evolved as an interesting drug target, both for cancer therapy by targeting cells that depend on highly efficient protein homeostasis and for treatment of degenerative diseases caused by gain-of-function mutations.

At the start of this thesis, only few inhibitors of p97 were described. We wanted to characterize a novel small organic molecule that was found in a high throughput screen against p97 activity. Furthermore, we aimed to improve the inhibition or specificity by investigating the important structural features of the inhibitor. Moreover, we set out to reveal the mechanism of inhibition, especially by identifying the binding site of the inhibitor. Finally, we wanted to investigate the inhibitory effect of I8 on the related AAA+ ATPase VPS4B and compare it to p97.

2 Results

The work in our laboratory focuses on the AAA+ ATPase p97. This chaperone is a complex machine involved in many different cellular pathways. We are interested in elucidating its cellular function as well as its molecular mechanism. Small molecule inhibitors are important tools for the research of a protein's functions as a fast and easy alternative to genetic techniques like RNAi. They provide a way to understand the function and mechanism of a protein in the cellular context and on a molecular level. Every newly identified inhibitor needs to be characterized in order to understand its mechanism of action. Therefore, the first goal of this study of a novel small molecule was the initial characterization that included the activity to p97 and possible off-target effects, its reversibility, and kinetic measurements. Subsequently, we focused on elucidating the inhibitory mechanism of the molecule.

2.1 Initial characterization of a HTS hit

A high throughput screening was conducted in a private company. A library of small molecules was tested for the inhibition against purified p97 in an NADH coupled ATPase assay. We chose one hit from the screen for further characterization (Figure 2.1). We called this molecule I8 (inhibitor 8).

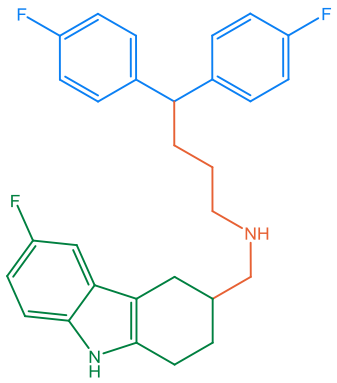

Figure 2.1 Chemical structure of the HTS hit I8
The molecule can be divided into three different parts: the bisphenyl group (blue), the alkyl linker with an amine (orange) and a tetrahydrocarbazole ring system (green).

The small molecule I8 (462.56 g/mol) harbors two moieties: a fluorinated bisphenyl group (Figure 2.1 blue) and a tetrahydrocarbazole (Figure 2.1 green) ring system connected by an alkyl chain containing a secondary amine (Figure 2.1 orange).

In a first step, we wanted to validate the HTS result. We tested the inhibitory effect of I8 against p97 and, in addition, against two other AAA+ ATPases. NSF is a type II AAA+ ATPase closely related to p97 and already in use in our laboratory. It

segregates SNARE complexes that form during the fusion of membranes (Ryu et al. 2016). VPS4B, a type I AAA+ ATPase, has been shown to be inhibited by DBeQ, a known competitive inhibitor of p97 (Magnaghi et al. 2013). Therefore we were interested if our compound I8 would show activity against VPS4B as well. We used the malachite green assay to measure the ATPase activity of the three enzymes. The malachite green assay is a colorimetric endpoint assay to detect inorganic phosphate in which the enzyme of interest hydrolyses ATP for the desired incubation time. Afterwards, an acidic molybdate containing reagent stops the reaction. The inorganic phosphate that is released by ATP hydrolysis forms a complex with molybdate and the complex is detected by measuring the absorption at 630 nm. P97 and NSF have been shown to have good basal activity, while VPS4B needs a substrate to be active (Merrill, Hanson 2010). We used the C-terminal fragment of the ESCRT-III protein CHMP1B (amino acids 106-199) to activate VPS4B. 0.2 µM of ATPase were incubated for 30 min (p97 and NSF) or 10 min (VPS4B) at 25 °C with 2 mM ATP. For VPS4B, 5 µM of CHMP1B 106-199 was added as activator (Figure 2.2).

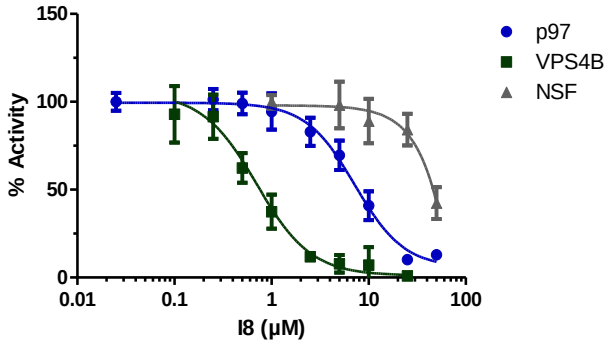

	IC_{50} (µM)	95% CI	Remaining act. at 50 µM (s.d.)
p97	7.22	6.10 to 8.55	
NSF	-	-	42.4 (9.1)
VPS4B	0.71	0.61 to 0.81	

Figure 2.2 Effect of I8 on three AAA+ ATPases
The activity against p97 was validated and the effect against two other AAA ATPases tested. The activity was measured with the endpoint malachite green assay. Shown are mean and error (s.d.) of three replicates. NSF was inhibited to a lesser extent then p97 while VPS4B was more sensitive towards I8.

The inhibitor I8 was indeed active against p97 and less so against NSF. VPS4B activity on the other hand was already inhibited by a ten times lower concentration than p97.

Since the chemical structure of I8 does not contain a reactive group, we expected a reversible inhibition of p97 by I8. To investigate this, we incubated p97 with I8, diluted the sample stepwise in reaction buffer and measured the activity with the standard malachite green assay. Indeed, dilution released the inhibition (Figure 2.3), showing that I8 inhibits p97 reversibly.

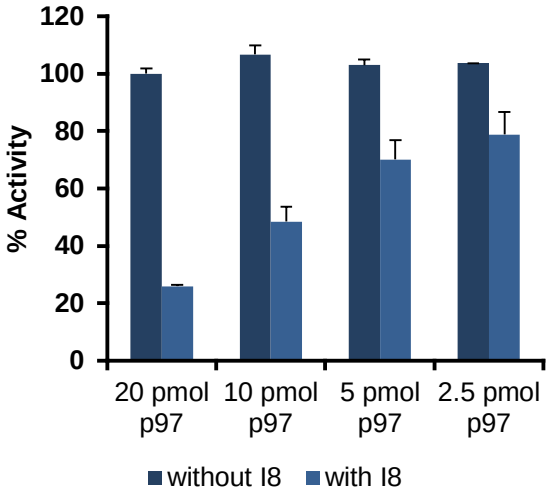

Figure 2.3 Dilution shows reversibility of I8
20 pmol p97 were incubated with 20 µM I8 and a twofold dilution series was made. ATPase activity was measured with the standard endpoint malachite green assay. Mean of three experiments. Errors are s.d. Note that dilution restored the relative activity of p97, showing reversible inhibition.

In a next step we wanted to investigate the effect of I8 on the enzyme kinetics of p97 and VPS4B. The kinetic measurements require low ATP concentrations. Under these conditions, product inhibition by ADP can become a secondary effect that interferes with the measurements. We used the continuous NADH coupled ATPase Assay to circumvent this problem. In this assay the initial ATP concentration is kept constant by a coupled reaction with pyruvate kinase and lactate dehydrogenase and their substrates phosphoenolpyruvate (PEP) and reduced nicotinamide adenine dinucleotide (NADH), respectively. Phosphoenolpyruvate and pyruvate kinase replenish ATP from ADP produced by the ATPase. The formed pyruvate is metabolized by lactate dehydrogenase to lactate. During this step, NADH is oxidized to NAD^+ and loses an absorption peak at 340 nm. The decline of absorption at 340 nm over time is detected in a spectrophotometer. If the ATP hydrolysis is the rate limiting step, the rate of NADH consumption equals the reaction rate of the ATPase. VPS4B showed strong inhibition by I8 (Figure 2.2). We therefore wondered whether inhibition by I8 would show the same kinetic mechanism for p97 and VPS4B and therefore included VPS4B in the measurements (Figure 2.4).

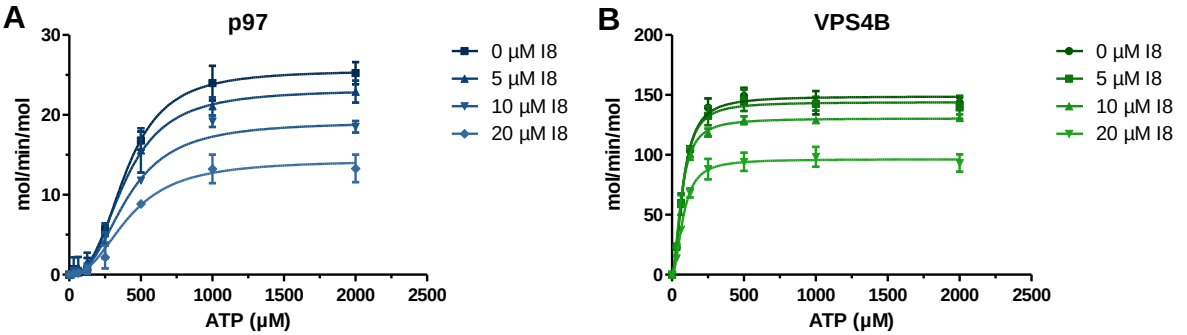

C

I8 (µM)	p97			VPS4B		
	v_{max}	h	K_M	v_{max}	h	K_M
0	25.6±0.5	2.8±0.2	396±13	149±2	1.9±0.1	78.2±2.3
5	23.1±0.8	2.6±0.3	387±23	144±2	2.0±0.2	74.6±3.3
10	19.1±0.3	2.5±0.1	405±11	130±1	1.9±0.1	66.1±1.6
20	14.3±0.3	2.3±0.2	416±15	96±2	2.0±0.2	78.6±4.3

Figure 2.4 Inhibitory effect of I8 on the kinetics of p97 and VPS4B
For kinetic measurements at 37 °C, a continuous NADH coupled assay was used to prevent product inhibition at low ATP concentrations that can interfere with measurements if the endpoint malachite green assay is used. The activity was derived from the decline of NADH absorption at 340 nm.
A: ATP titration to 0.25 µM p97 at indicated concentrations of I8. Means of three independent experiments are shown. Error bars indicate s.d.
B: ATP titration to 0.1 µM VPS4B and 10 µM CHMP1B 106-199 at indicated concentrations of I8. Means of three independent experiments are shown. Error bars indicate s.d.
C: Fitted parameters of the Hill-equation for measurements of the inhibition of p97 and VPS4B by I8. Parameters: v_{max}: maximal enzyme velocity; h: Hill-coefficient, an indicator of cooperativity; K_M: Michaelis-Menten constant. Errors indicate s.d. of the fit.

Incubation of p97 with rising concentrations of I8 resulted ina drop in v_{max}, showing that the inhibition by I8 is not competitive. The Hill-coefficient showed a positive cooperativity of the hexamer, that is an increased affinity of an unoccupied binding site in p97 for ATP upon binding of ATP to another binding site. Together with the relatively high K_M, this resulted in a sigmoidal shape of the fitted curve. In contrast to the decreasing v_{max}, the K_M stayed constant, indicating a non-competitive inhibitory mechanism in which the complex of enzyme and inhibitor forms independently of the substrate (Figure 2.4 A+C).

The v_{max} of uninhibited VPS4B ATPase activity was higher by a factor of seven and the K_M lower by a factor of five compared to p97. The Hill-coefficient showed a positive cooperativity as it was the case for p97. As a consequence of the high v_{max} and low K_M of VPS4B, the fitted curve showed no sigmoidal shape. Like I8 mediated

inhibition of p97, inhibition of VPS4B by I8 caused a drop in v_{max} while the K_M stays constant (Figure 2.4 B+C), indicating that I8 inhibits both ATPases with the same mechanism.

The K_M describes the affinity between enzyme and substrate (in this case ATP). We wanted to further investigate the influence of I8 on nucleotide binding. To this end, we measured the anisotropy of the fluorescent nucleotide analog ATP-BODIPY (Figure 2.5). Binding of this probe results in an increase in anisotropy. In the case of tight binding or low K_d, less protein is needed to achieve saturation. p97 was titrated in a twofold serial dilution to 20 nM of ATP-BODIPY in the presence of DMSO or 20 µM I8. In a next step, the experiment was modified to address a possible influence on ADP binding. Therefore, ADP was added at a constant concentration of 1 µM, causing competition with ATP-BODIPY.

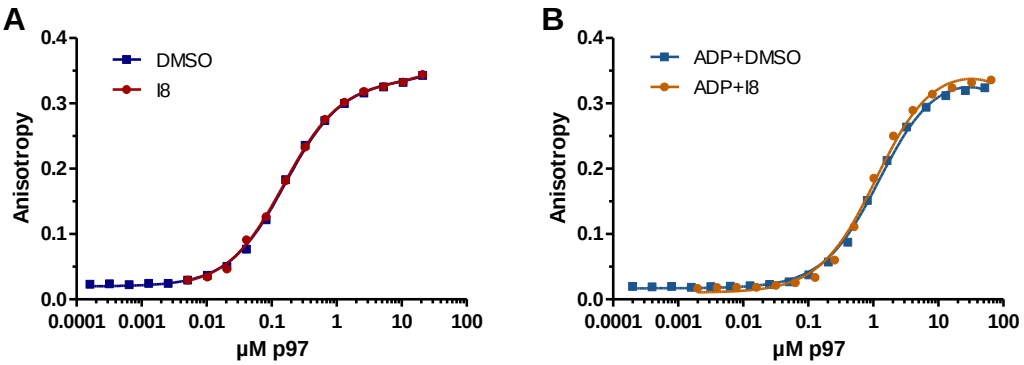

C

ATP-B + compound	K_d of ATP-B (nM)	K_d of ADP (nM)
-	162±6.0	-
I8	153±7.8	-
ADP	1247±74.4	149
ADP+I8	1108±114.9	171

Figure 2.5 I8 does not affect nucleotide binding affinity to p97 wt
p97 wt was titrated to 20 nM ATP-BODIPY. In a second set of experiments, 20 µM I8 and/or 1 µM ADP were added. In the presence of ADP, the measured K_d of ATP-BODIPY was used to calculate the K_d of ADP. ATP-B: ATP-BODIPY. Errors are s.d. of the fit of one experiment. Neither the K_d of ATP-Bodipy nor the derived K_d of ADP was altered by adding I8.

ATP-BODPIY bound to p97 with a K_d of 162 nM, which is in line with previously published values (Chou et al. 2014). The addition of I8 did not result in a shift of the curve to higher concentrations of p97, resulting in a constant affinity between p97 and ATP-Bodipy (162 nM vs. 153 nM, Figure 2.5 A+C). Next, we tested the affinity of ADP. Compared to the measurements without ADP (Figure 2.5 A), a shift of the

curve towards higher concentrations became visible, showing the competition between ATP-Bodipy and ADP (Figure 2.5 B). The addition of I8 did not result in a further shift. Thus, the affinitie of ADP stayed constant (149 nM vs. 171 nM, Figure 2.5 C). The data from these anisotropy experiments are consistent with the kinetic results and supports a non-competitive mechanism.

2.2 Structure activity relationship SAR

The IC_{50} value of I8 is in a range comparable to other first hits from high throughput screens for p97 inhibitors like DBeQ (precursor of CB-5083) or NMS-862 (precursor of NMS-873), with values of 9.1 µM and 2.8 µM, respectively (Magnaghi et al. 2013). We subsequently aimed to improve the inhibition of p97 by I8 by generating I8 derivatives to facilitate further experiments.

2.2.1 SAR with p97

The structure activity relationship (SAR) studies were done in cooperation with AG Kaiser at the ZMB at the University Duisburg-Essen, where all syntheses were done by Jan Krahn. For these structure activity relationship studies, the standard malachite green assay was used. p97 (0.2 µM) was incubated for 30 min at room temperature with 1 mM ATP. An overview of the remaining p97 activities for the tested derivatives of I8 is given in Figure 2.6.

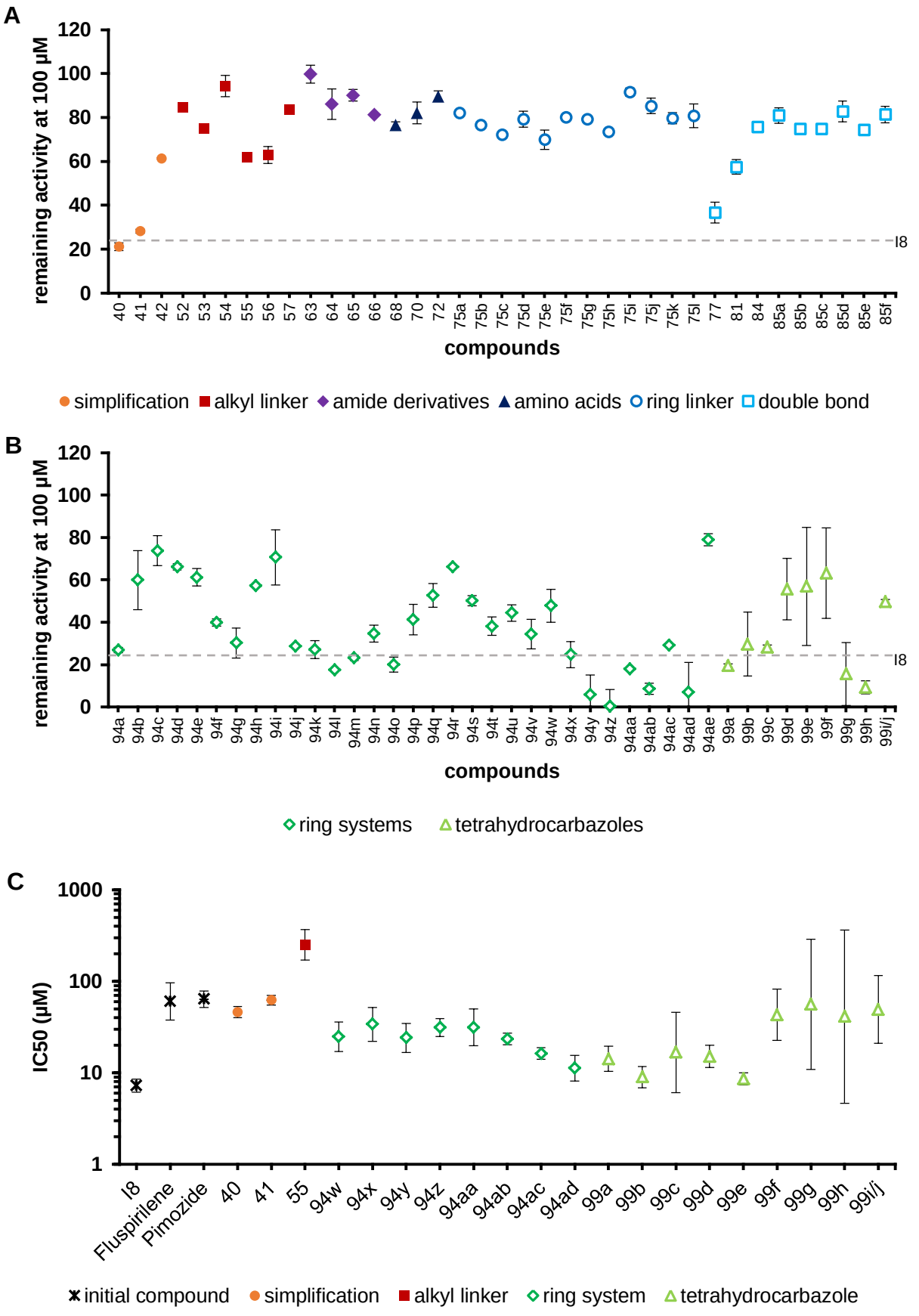

Figure 2.6 Overview of the derivatives of I8 tested against p97
All measurements were done with the endpoint malachite green assay.

A: Single point measurements of different classes of derivatives of I8. The grey line marks the remaining activity of p97 in the presence of 100 µM I8. Means of two experiments shown. Errors bars represent s.d.
B: Continuation of A. The grey line marks the remaining activity of p97 in the presence of 100 µM I8. Means of two experiments shown. Errors bars represent s.d.
C: IC_{50} values were determined for selected compounds that showed good inhibition. Means of two experiments shown. Errors bars represent 95% CI.

As examples, the structures of some derivatives from Figure 2.6 are given in Figure 2.7.

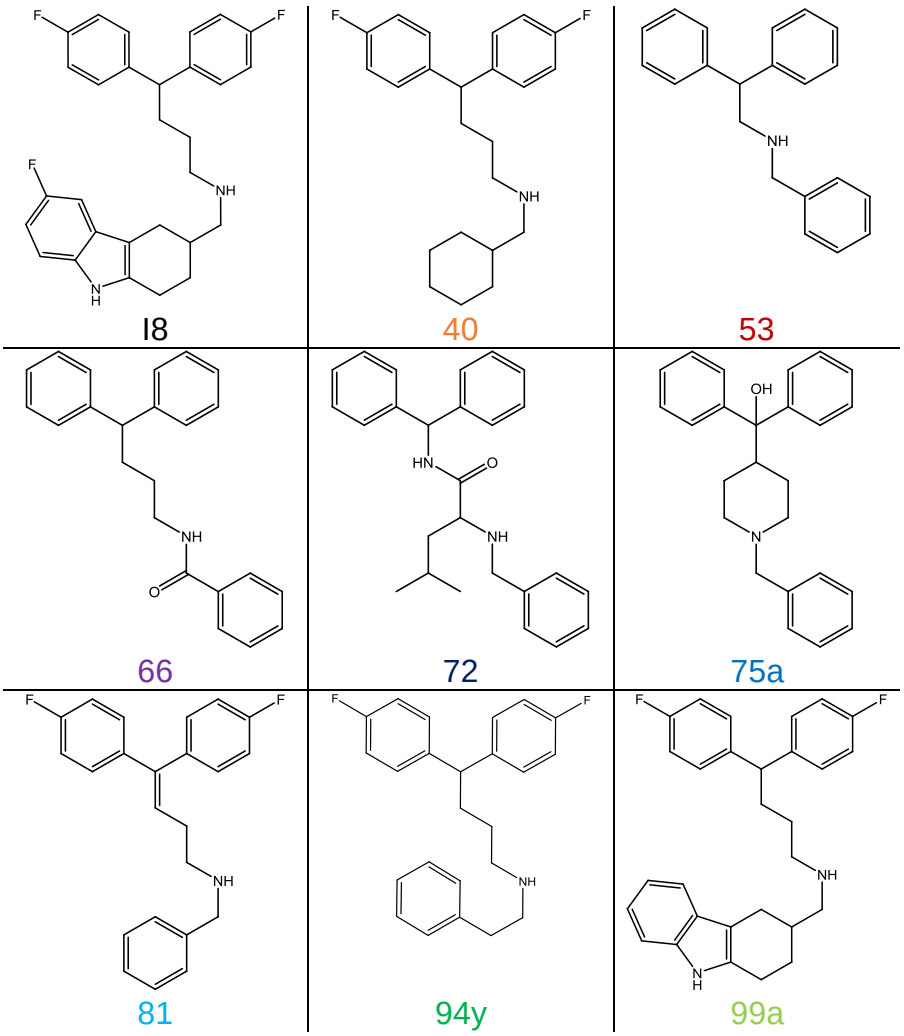

Figure 2.7 exemplary structures from the SAR studies in Figure 2.6
I8: lead structure; 40: simplification of I8 used for synthesis; 55: variant with changed alkyl linker; 66: amide derivative instead of alkyl linker; 72: amino acid instead of alkyl linker; 75a: ring system instead of alkyl linker: 81: double bond in alkyl linker; 94a: simple ring system instead of tetrahydrocarbazole; 99a: tetrahydrocarbazole, here without a substituent

Most compounds were based on simpler, less potent derivatives (e.g. compound 40, Figure 2.7), but were sufficient to evaluate parts of the I8 structure (Figure 2.6 A+C). The alkyl chain derivatives showed that a shorter chain or a different position of the

secondary amine lead to a lower inhibition (Figure 2.6, alkyl linker). In general, changes in the alkyl chain led to a loss of inhibition, as shown for derivatives with changes in the length of the linker or the position of the amine (e.g. compound 55, Figure 2.7), introducing an amide bond (e.g. compound 66, Figure 2.7) or amino acids (e.g. compound 72, Figure 2.7). Using a ring system as a linker (e.g. compound 75a, Figure 2.7) or constraining the orientation of the bisphenyl group by adding a double bond (e.g. compound 81, Figure 2.7) also resulted in a loss of inhibition. Two antipsychotic drugs from the diphenylbutylpiperidine class, Fluspirilene and Pimozide also contain a fluorinated bisphenyl group. Both showed a similar inhibition compared with each other towards p97, highlighting the importance of this group (Figure 2.6 C).

We next focused on alternatives to the tetrahydrcarbazole ring system (Figure 2.6 B). Substitution with a simple benzyl group (e.g. compound 94y, Figure 2.7) showed minor improvements compared to the cyclohexyl group (compound 40, Figure 2.7). The best results were achieved by working with the original tetrahydrocarbazole and changing the substituents (Figure 2.6 B+C). Exchange of the fluoride in I8 to a chloride in 99b or the absence of a substituent (e.g. compound 99a, Figure 2.7) resulted in good inhibition but still in the range of I8.

We synthesized and tested many different compounds and gained an understanding of the relevance of different structural parts of I8. However, we could not improve our lead structure.

2.2.2 SAR with VPS4B

We wanted to know if there were some differential effects of the derivatives between p97 and VPS4B. Selected compounds that showed good inhibition towards p97 were tested against VPS4B (Figure 2.8). VPS4B (0.2 µM) was incubated for 10 min at 25 °C with 1 mM ATP. 2 µM of CHMP1B 106-199 was added as activator.

None of the compounds showed a loss or gain of function. On the contrary, the relation between IC_{50} values for p97 or VPS4B was rather constant with ten times lower values for VPS4B. Thus, we did not find a way to change the specificity of I8. This may underline the high similarity of VPS4B and p97 not only in structure but also in mechanism.

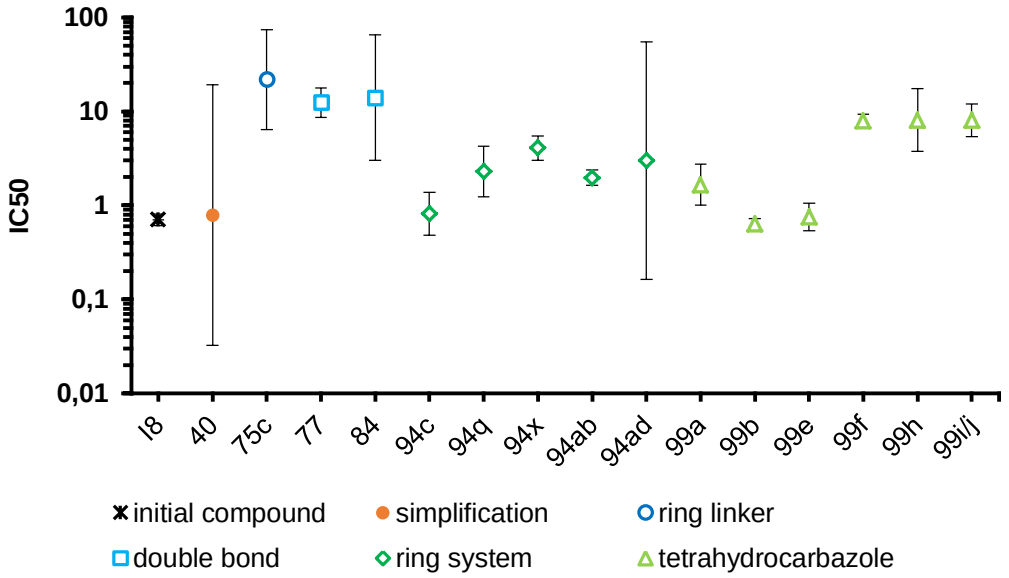

Figure 2.8 Overview of the derivatives of I8 tested against VPS4B
The IC_{50} values for selected compounds were determined with the endpoint malachite green assay. Mean of two experiments. Errors are 95% CI.

2.3 Mechanistic investigations

A new inhibitor bears the possibility to investigate the mechanism of an enzyme. This is especially true for an allosteric inhibitor that does not directly compete with nucleotide binding.

2.3.1 Comparison to known inhibitors

NMS-873 is a known allosteric inhibitor of p97. An azido derivative of NMS-873 was found to cross link to N616 of p97 and the p97 N616F mutant is insensitive towards NMS-873 (Magnaghi et al. 2013).

CB-5083 is a competitive inhibitor of p97. Its binding site is not known, but cells challenged with CB-5083 developed different mutations to become resistant. The most effective was T688A (Anderson et al. 2015). However, the sites of resistance mutations do not necessarily reflect the binding sites as NMS-873 resistant cells showed a A530T mutation, more than 17 Å apart from N616 (Her et al. 2016).

We wanted to know if I8 and NMS-873 act by the same mechanism and tested I8 together with NMS-873 and CB-5083 against the N616F mutant (Figure 2.9). The malachite green assay was used to measure the activity of 0.2 µM p97 after incubation with 2 mM ATP for 30 min at 25 °C and various concentrations of inhibitor.

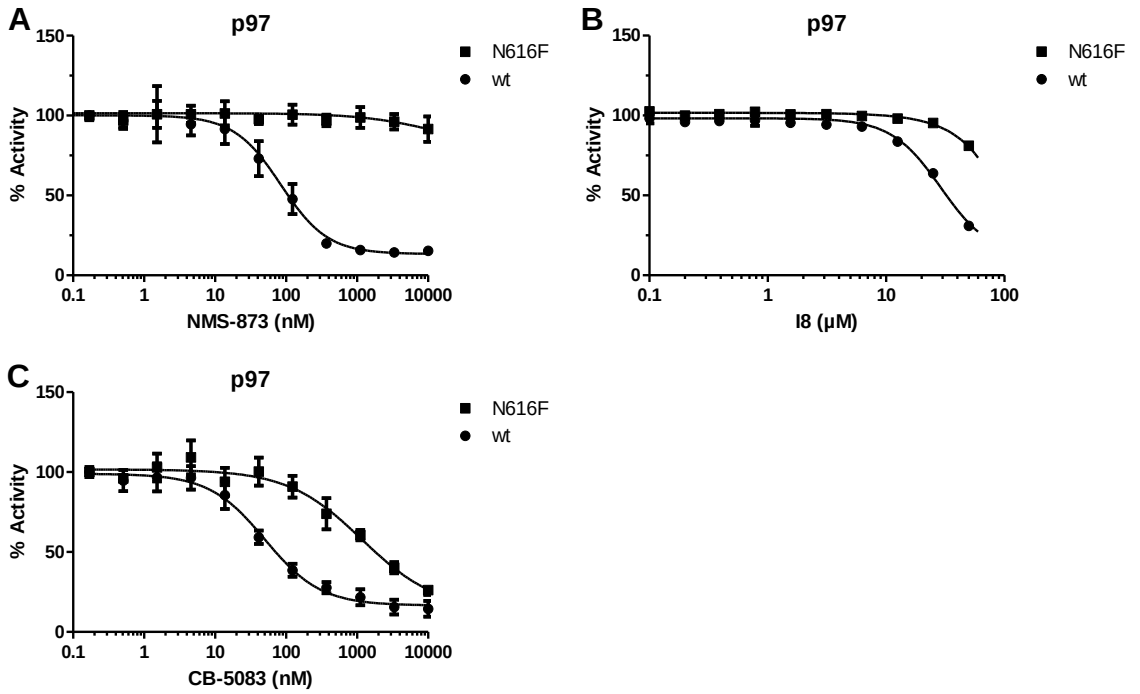

IC_{50}	NMS-873 (nM)	95% CI	CB-5083 (nM)	95% CI	I8 (µM)	95% CI
wt	84.14	72.19 to 98.08	50.45	41.50 to 61.35	29.05	20.93 to 40.33
N616F	-	-	1170	589.3 to 2323	-	-

Figure 2.9 Effect of different inhibitors on p97 wt or p97 N616F
Activity measurements of p97 wild type (wt) and p97 N616F were done with the endpoint malachite green assay.
A: The p97 N616F mutant has wild type level ATPase activity and is not inhibited by NMS-873. Mean of three experiments. Errors are s.d.
B: I8 shows reduced efficacy towards the N616F mutant, similar to CB-5083 (C). Mean of three experiments. Errors are s.d.
C: As a negative control, the unrelated, competitive inhibitor CB-5083 is used. The N616F mutant is less sensitive towards CB-5083. Mean of three experiments. Errors are s.d.
D: IC_{50} values of the fits of the graphs A, B and C. Mean of three experiments. Errors are 95 % CI.

In line with the literature (Magnaghi et al. 2013), the p97 N616F mutant showed activity at wild type level and was not inhibited by NMS-873 (Figure 2.9 A). The inhibition of p97 N616F by I8 was weakened compared to p97 wild type, though due to the limited solubility of I8 at higher concentrations, the curves were incomplete (Figure 2.9 B). Interestingly, the p97 N616F mutant also showed resistance against CB-5083 (Figure 2.9 C). Since the N616F mutation affected also CB-5083, it is uncertain if the reduced efficacy of I8 was a result of reduced binding of I8 or if the mutation introduced subtle changes to p97 who affected regulatory interactions in the hexamer.

2.3.2 Binding studies of I8

2.3.2.1 A rhodamine probe binds to p97

The kinetic data showed that I8 inhibits p97 and VPS4B with an allosteric mechanism (Figure 2.4). Its binding site is therefore important for the mechanism of ATP hydrolysis or indirectly by disrupting a path of allosteric communication in the hexamer. Knowing the binding site can therefore give important information on p97 function.

First, we used ITC measurements of I8 and p97. However, due to low affinity and low solubility of I8, we could not obtain K_d values or information about the stoichiometry of I8 binding. We then used anisotropy measurements as these worked good for the nucleotide binding studies. Jan Krahn from AG Kaiser synthesized a fluorescent probe of I8. A fluorescent TAMRA moiety was linked with a short alkyl chain to the carboxy derivative 99g of I8. 0.1 µM of the probe was used in the anisotropy binding assay with twofold serial dilutions of p97 (Figure 2.10).

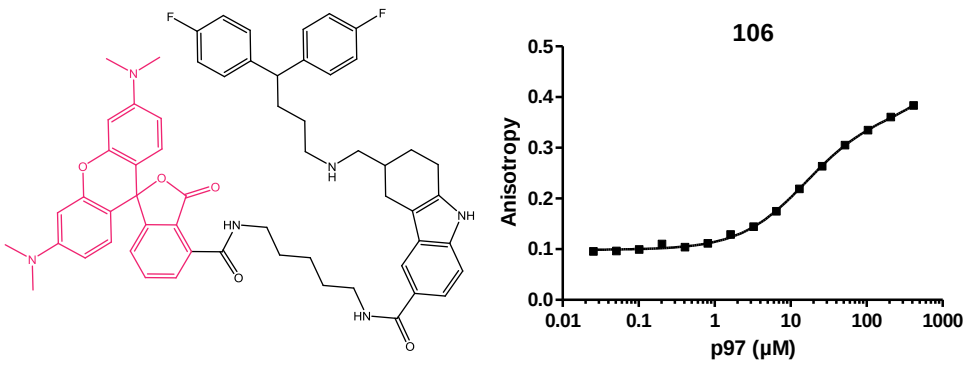

Figure 2.10 A fluorescent derivative of I8
A derivative (106) of I8 binds to p97 (K_d = 15.64 ± 0.96 µM). A Carboxytetramethylrhodamine (TAMRA, colored in red) was coupled to the carboxy group of the derivative 99g with a short alkyl chain, substituting the flour at the tetrahydrcarbazole of I8.

Due to the rhodamine moiety interfering with the malachite green based activity assay, we could not determine the probe's IC_{50}, but it showed inhibition towards p97. To be sure that the probe and I8 bind to the same site, an anisotropy competition assay was conducted (Figure 2.11).

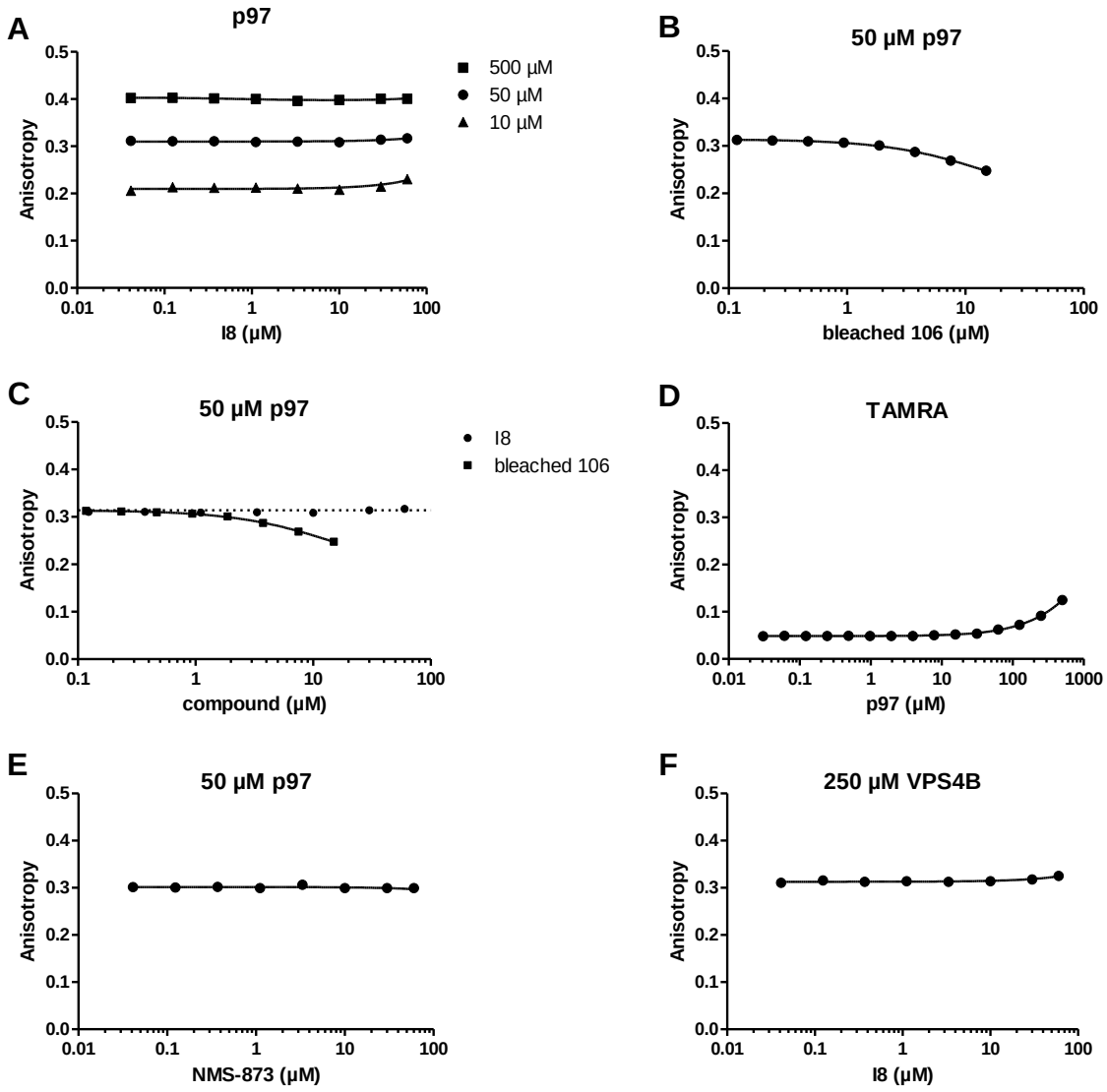

Figure 2.11 Anisotropy competition experiments to find the K_i of I8
The probe was used at a concentration of 0.1 µM.
A: Titration of threefold serial dilution of I8 to different concentrations of p97. No change in anisotropy visible.
B: Titration of twofold serial dilution of the bleached probe to 50 µM p97. Competition occurs. The fitted K_i (~22 µM) of the bleached probe is similar to the measured K_d (15 µM) of the fluorescent probe. Because of the missing lower plateau of the curve, the fit depends slightly on the constraints of parameters.
C: Direct comparison of A and B. Under the same experimental set up the bleached probe but not I8 shows competition. An explanation is a different binding site for I8 and compound 106.
D: Titration of a twofold serial dilution of p97 to TAMRA, the rhodamine moiety of compound 106. The signal rises only at high concentrations above 100 µM. That means at the p97 concentrations used, unspecific binding of TAMRA is not the reason for lacking competition.
E: Titration of threefold serial dilution of NMS-873 to 97. No change in anisotropy visible.
F: Titration of threefold serial dilution of I8 to VPS4B. No change in anisotropy visible.

We could not observe competition of I8 or NMS-873 with the probe towards p97 (Figure 2.11 A and E). No change in anisotropy was detected for the titration of I8 to VPS4B as well, indicating that there was no competition between the probe and I8 (Figure 2.11 F). As a positive control, 500 µM of the probe was bleached with an HXP short arc lamp over 48 hours. This bleached probe worked in this experimental set up and lowered the signal of the fluorescent probe (Figure 2.11 B). The highest possible concentration from the bleached 500 µM stock was 15 µM so that the competition was low, but clearly distinguishable from the trend of the I8 curve (Figure 2.11 C) showing that the probe and I8 have different binding sites. Since the rhodamine moiety was the most obvious difference between the probe and I8, we wondered if this might be the reason for an unspecific binding event. A titration of TAMRA to p97 showed no binding at 50 µM p97, ruling out this possibility (Figure 2.11 D).

2.3.2.2 Alanine screen of VPS4B mutants to validate a binding site

Various approaches were undertaken to find the binding site of I8 with the help of mass spectrometric analyses. Jan Krahn from AG Kaiser synthesized different probes bearing azido moieties that were covalently linked to p97 or VPS4B. The crosslink changes the m/z ratio of the tryptic peptide so that its peak disappears (or more precisely shifts) in comparison to the untreated protein sample. The advantage of this approach is that the modified peptide does not need to be detected. The detection can be challenging since the exact kind of modification and therefore the mass shift is not known. The cross linking and mass spectrometry was done by Farnusch Kaschani from AG Kaiser.

After crosslinking and analysis, two modified peptides could be identified only in VPS4B. The peptides were located in N-terminal MIT domain (amino acids 24-46) and in the ATPase domain (amino acids 256-289):

```
24- AGNYEEALQLYQHAVQYFLHVVK-46
256- TEFLVQMQGVGVDNDGILVLGATNIPWVLDSAIR-289
```

In a next step, we focused on the peptide in the ATPase domain since this is the region homologous between VPS4B and p97. We wanted to validate the hit by an alanine screen (Figure 2.12).

A

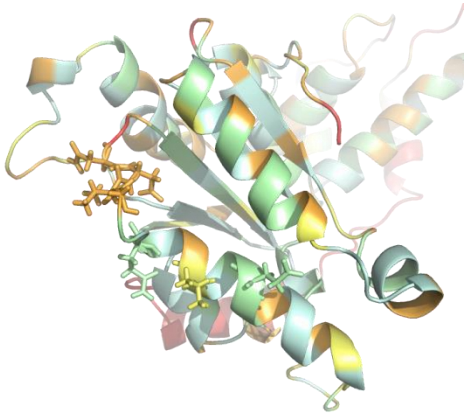

Helix3A	E257A V260A Q263A
Loop4A	GVDN266AAAA

B

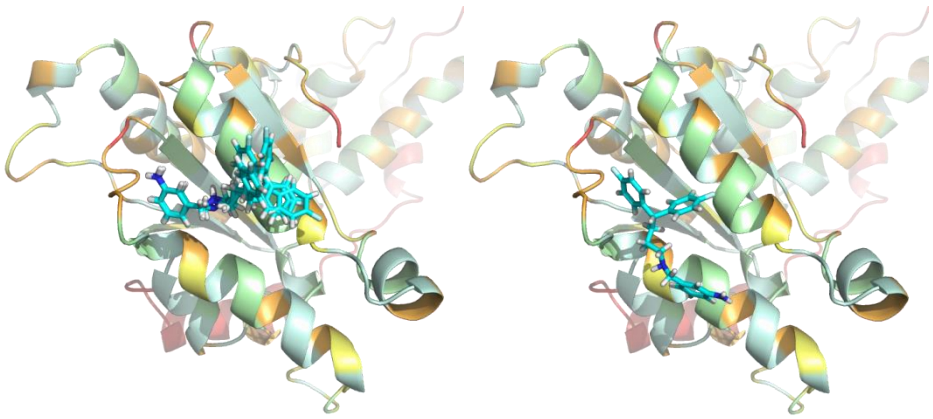

C

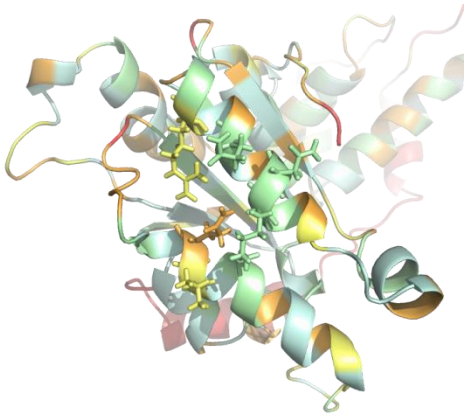

Upper helix	K218A	N218A	Q221A	R224A
Lower helix	V260A	Q261A		

Figure 2.12 Evaluation of an MS hit

The structure of VPS4B (pdb 2zao) is shown. The amino acids are colored according to the conservation between VPS4B and p97. Light blue: identical; light green: high similarity; yellow: low similarity; orange: no similarity, red: missing in p97

A: The two multi alanine mutation sites, located in the identified peptide.

B: Results from a docking simulation of the probe to VPS4B. Two different orientations of the probe are shown. On the left picture, the probe is spanning from the lower to the upper helix. Shown is an overlay of three docking results that differ only in the orientation of the bisphenyl part. On the right picture, the probe is aligned along the identified peptide.

C: The single alanine mutations chosen based on the docking simulation, with a focus on the upper helix.

The peptide in the ATPase domain is rather long and can be divided in an N-terminal helical part and a C-terminal loop part. At these sites, we introduced two multi alanine mutations Helix3A and Loop4A (Figure 2.12 A).

Johannes van den Boom from our lab conducted a docking simulation of the probe to VPS4B. A VPS4B trimer was modeled to a p97 trimer (pdb code 3CF1) and the azido probe was subsequently docked to the protomer in the middle (Figure 2.12 B, only middle protomer shown). Six further mutations were chosen based on the docking simulation that are not only located in the identified peptide but also in the upper helix (Figure 2.12 C).

We did not have the means for a direct binding assay, therefore we tested the purified VPS4B mutants for resistance against I8 (Figure 2.13). For activity measurements, we used the malachite green assay with 0.2 µM ATPase, 1 mM ATP and 4 µM CHMP1B 106-199 as activator. Reaction time was 10 min at 25 °C.

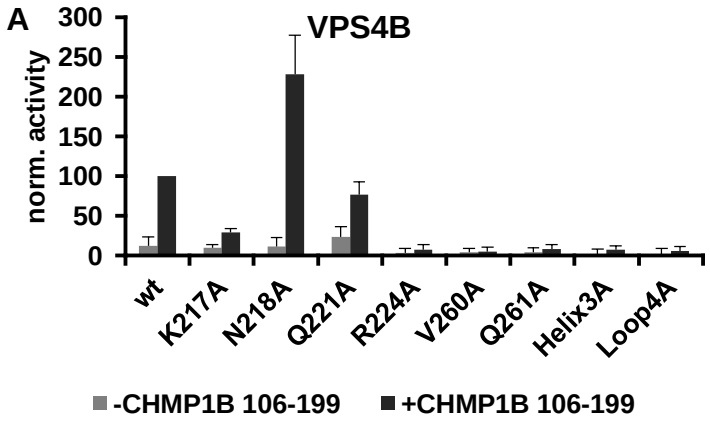

B

VPS4B	IC_{50} (µM)	95% CI
wt	0.71	0.61 to 0.81
N218A	1.5	1.4 to 1.7
Q221A	0.72	0.54 to 0.96

Figure 2.13 Activity of the VPS4B mutants
A) Activities were measured with the endpoint malachite green assay with or without the activating CHMP1B fragment. Means of three experiments shown. Errors bars represent s.d. B) IC_{50} values of I8 against VPS4B wild type and the two active mutants from the screen in A).

Most mutations are inactive and could therefore not be used to test the activity of I8 (Figure 2.13 A). The N218A exchange is a gain of function mutation, however it was still inhibited by I8. Q221A showed an activity comparable to the wild type, but was also sensitive to I8 (Figure 2.13 B). We could therefore not confirm the peptide as the binding site of I8. However, we can exclude the part in the upper helix (figure, amino acids) as important contributors for the binding of I8.

The inactivity of the multi alanine mutants could be a consequence of improper folding. To further investigate this possibility, we recorded CD (circular dichroism)

spectra of the two mutants and the wild type (Figure 2.14). Circular polarized light interacts with the chiral proteins and the ratios of the different secondary structures (helices, sheets and loops) generate characteristic spectra. 0.2 g/l of the proteins were measured in chloride free potassium phosphate buffer and the curves of the mutants normalized to the wild type.

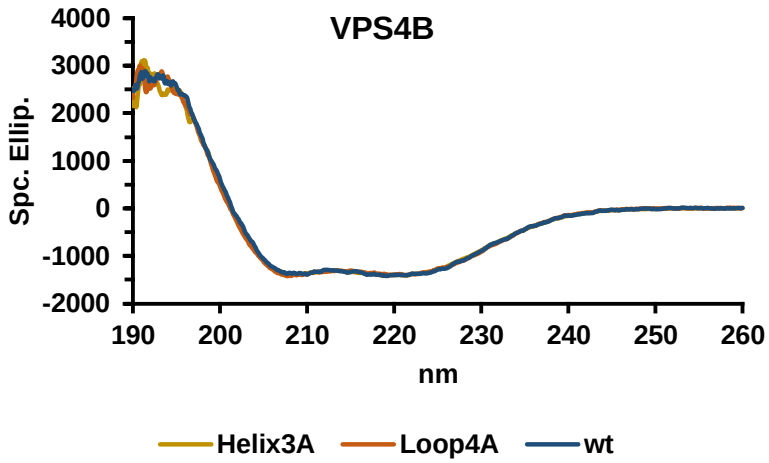

Figure 2.14 CD spectra of VPS4B wt and the mutants Helix3A and Loop4A
The proteins were measured in 50 mM chloride free potassium phosphate buffer at pH 7.4. The mutations do not introduce discernable changes in the secondary structure that could explain a loss of activity.

The spectra of the mutants showed no deviation from the wild type, meaning the mutations cause no gross misarrangement in the secondary structure. Moreover, a single, conservative mutation like V260A abolished the activity completely, showing the sensitivity of this area to disturbances.

2.3.3 Effect of I8 on p97 mutants

Since we had no probe to test the binding between I8 and p97, we tried to investigate the inhibitory mechanism of I8 by using different mutants of p97. This established approach uses the different Walker mutations that either cannot bind (Walker A) or cannot hydrolyze (Walker B) ATP to distinguish between the activity of the D1 or D2 domain. Therefore, this approach can be used to determine the specificity of an inhibitor for an ATPase domain. We used the malachite green assay with 0.2 µM ATPase, 2 mM ATP and 35 min incubation at 25 °C.

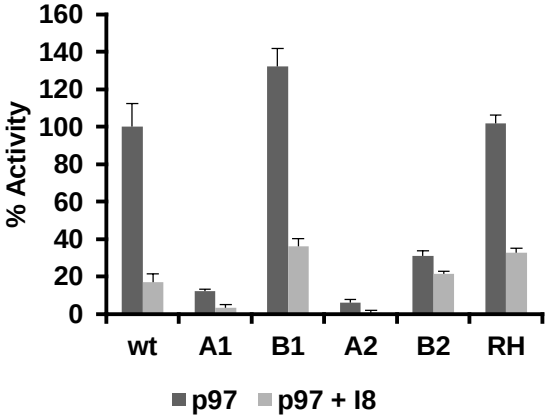

Figure 2.15 Influence of 20 µM I8 on p97 mutants
Activity measurements with the endpoint malachite green assay. Wt: p97 wild type; A1: Walker A in D1, K251A; B1: Walker B in D1, E305Q; A2: Walker A in D2, K524A; B2: Walker B in D2, E578Q; RH: MSP1 associated mutation R155H.

The mutants B1 and RH showed robust activity at wild type level. The two Walker A mutants were inactive. The mutant B2 showed intermediate activity. Only for B2, a loss of inhibition by I8 is visible. Since the activity in the B2 mutant stems from the D1 domain, this finding suggests that I8 may reduce mainly the activity of the D2 domain. Of note, the B2 mutant had a low activity that was less robust than the activity of the wildtype or B1 mutant.

The ND1L mutant (1-480) was described as an active truncation compared to a shorter fragment (1-458). It can therefore be used as an alternative to the B2 mutant. In my hands, the activity was not as high as reported (30% vs. 80% of wild type (Zhang et al. 2015)) but at similar levels as B2, hampering the activity measurements (Figure 2.16).

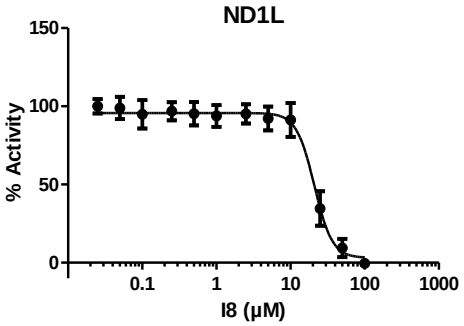

	IC_{50}	95% CI
ND1L	20.93	18.92 to 23.15

Figure 2.16 Activity of I8 against the p97 ND1L fragment
The p97 ND1L fragment (1-480) was incubated with various concentrations of I8 and its activity measured with the endpoint malachite green assay.

The ND1L fragment was inhibited by I8 to a similar extent as the wild type, suggesting that I8 bound ND1L and influenced the D1 activity. However, the Hill slope of -4 was unusually steep, indicating possible secondary effects like aggregation.

2.3.4 Conformational changes in p97 or VPS4B upon I8 treatment

The ATPase activity of p97 is coupled to different structural changes. One prominent feature is the up and down movement of the N-domains that correlates with ATP binding in D1 (Banerjee et al. 2016). While it is clear that movement and activity are linked, it is not known if the conformational state is a result of the activity or if it controls the activity. Either way, this implies that inhibiting p97 with I8 or with other inhibitors may cause changes in the structure. We used limited proteolysis of p97 and VPS4B to test this hypothesis (Figure 2.17). The ATPase was incubated with trypsin and aliquots were taken at different time points. For analysis of the digested fragments, these aliquots were separated with SDS-PAGE and stained with colloidal Coomassie.

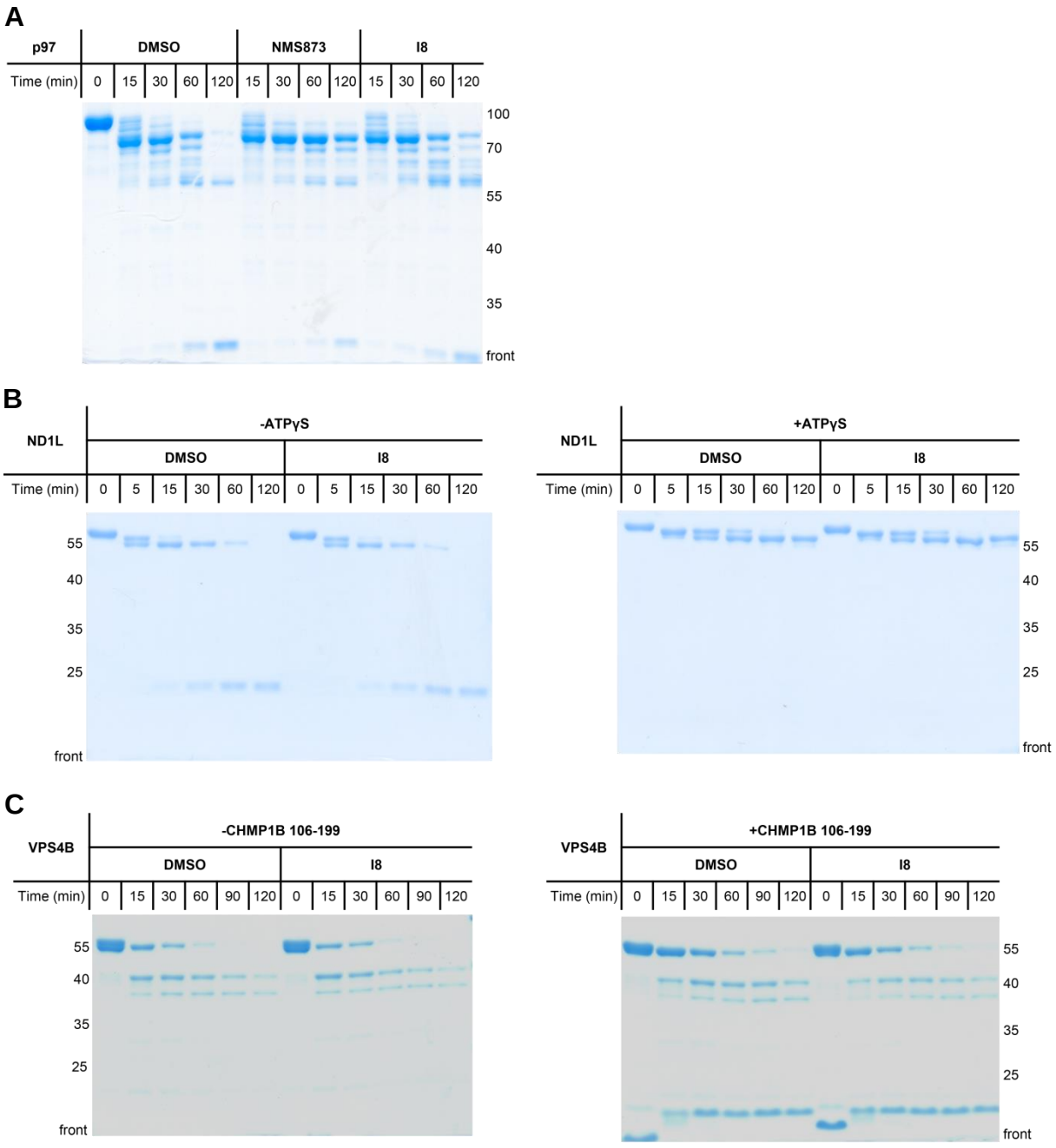

Figure 2.17 Limited proteolysis of p97, ND1L or VPS4B with Trypsin
10 µM of the indicated protein (A: p97; B: ND1L; C: VPS4B) was incubated with 70 µM inhibitor and 7.5 ng/µl trypsin. Incubation temperature for p97 and VPS4B was 30 °C, for ND1L 37 °C. After the indicated time, aliquots were taken, separated with SDS-PAGE and stained with colloidal Coomassie.

Full length p97 (Figure 2.17 A) is readily degraded at 30 °C. An intermediate fragment at ~75 kDa build up during the first 15 minutes and was subsequently degraded to a ~55 kDa fragment. According to Magnaghi et al., this was an N-D1 fragment. The addition of NMS-873 or I8 to p97 caused a stabilization of the high molecular weight fragment at ~75 kDa. Therefore, I8 and NMS-873 probably had a stabilizing effect on the D2 structure. Consistent with the stabilization, small

fragments in the running front were depleted. The stabilizations by the inhibitors could be a direct effect by masking cleavage sites or an indirect effect. In the latter case, a structural rearrangement might make the D2 domain more compact and less susceptible for trypsin digestion.

In the case of the tryptic digestion of ND1L, a higher temperature (37°C) was needed to observe degradation (Figure 2.17 B). A relative stable fragment at ~24 kDa accumulated in the course of two hours. Addition of I8 had no effect on the degradation of ND1L. This can serve as a control that I8 does not inhibit trypsin activity. On the other hand, ATPγS stabilized ND1L efficiently, only a fragment of ~5 kDa is lost after two hours.. It is known that ATPγS binding to D1 correlates to the up conformation of the N domains (Banerjee et al. 2016). Apparently, this also had protective effects against trypsin.

VPS4B was very susceptible to the digestion at 30 °C (Figure 2.17 C). A big fraction of the protein is digested after 15 minutes. Two of the resulting smaller fragments (~40 kDa and ~38 kDa) were more stable. Addition of CHMP1B 106-199 (~15 kDa) delayed degradation of the full length protein and a third fragment at ~17 kDa was stabilized during the first 30 minutes. This fragment did not appear without CHMP1B 106-199 and was stable during the remaining time course. The flexible linker between MIT and ATPase domain has a high content of lysines and therefore possible cleavage sites for trypsin. This offers an explanation for the fast digestion during the first 15 minutes. The activator CHMP1B 106-199 binds to the N-terminal MIT domain where it could shield otherwise accessible peptide bonds, explaining the new band at ~17 kDa. Another effect could be a stabilization of the linker region resulting in the delayed degradation of full length VPS4B. The addition of I8 had no visible effect on the stability of the proteins.

We searched further for a possible mechanism of I8. In contrast to other AAA ATPases, p97 is known to form remarkably stable hexamers that form even in the absence of nucleotide or substrates. *In vitro*, 6 M urea is needed to disassemble p97 (Wang et al. 2003). Because the monomers are inactive, disassembly by I8 may be a way of inhibition. To test the hypothesis, we conducted size exclusion chromatography with a 1:1 ration of p97:I8 (Figure 2.18).

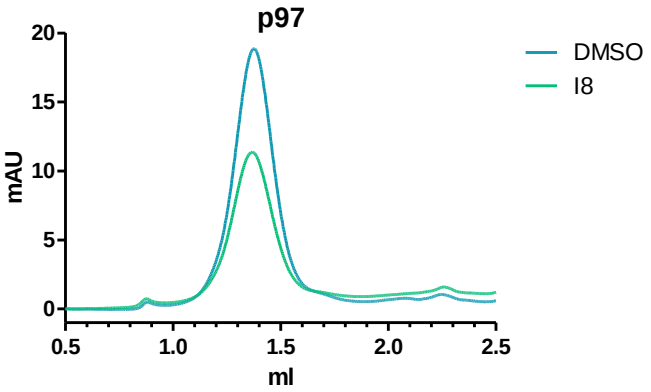

Figure 2.18 Size exclusion chromatography of p97 with or without I8
20 µM I8 or DMSO was added to 20 µM purified p97 and to the running buffer. The mixture was loaded onto a Superose 6 3.2/30 column. Protein was detected at 280 nm. The flow rate was set to 0.04 ml/min.

During a size exclusion chromatography, a change in size or even conformation should result in a peak shift. Besides a monomerization, also the formation of higher order assemblies could result in inactivity of the enzyme. No difference in elution volume was observed. The difference in peak height is due to loading of the column. In these experiments, I8 did not show an influence on the p97 hexamer.

2.4 The assembly of the ELDR components are not influenced by I8

The ATPase p97 is involved in many different pathways. Papadopoulos et al. investigated the case of the endolysosomal damage response (ELDR) where we found p97 acting in concert with a distinct set of adaptors: YOD1 (a DUB), UBXD1 and PLAA (Papadopoulos et al. 2017). The components act in an intermediate step of lysophagy: Before the damaged lysozyme can be degraded, the ELDR components turn over K48-linked ubiquitin chains. In immunofluorescence experiments, they were colocalizing on damaged lysosomes. In immunoprecipitation experiments from cell lysates, the components were also associated with each other. In the immunoprecipitation experiments however, PLAA was not found together with p97 wild type but with the dominant negative p97 B2 mutant that can bind ATP in D2 but cannot hydrolyze it. The B2 mutant is known for this “trapping” effect.

As a part of the study of the endolysosomal damage response, we wanted to reconstitute the complex *in vitro*. To this end, we expressed and purified the single components in bacteria or insect cells. We tested the binding of the ELDR components via a GST-pull down of recombinant ubiquitin. The protein was fused to a C-terminal GST tag that cannot be cleaved by deubiquitinases (Ub-GST). Two of

the ELDR components, YOD1 and PLAA, are already known to contain at least one ubiquitin binding site and could act as possible scaffolds (Mevissen et al. 2013; Fu et al. 2009). The proteins were incubated for 90 minutes at room temperature to avoid precipitation. After elution from beads with reduced glutathione, the proteins were analyzed with an SDS-PAGE and subsequent colloidal Coomassie staining (Figure 2.19).

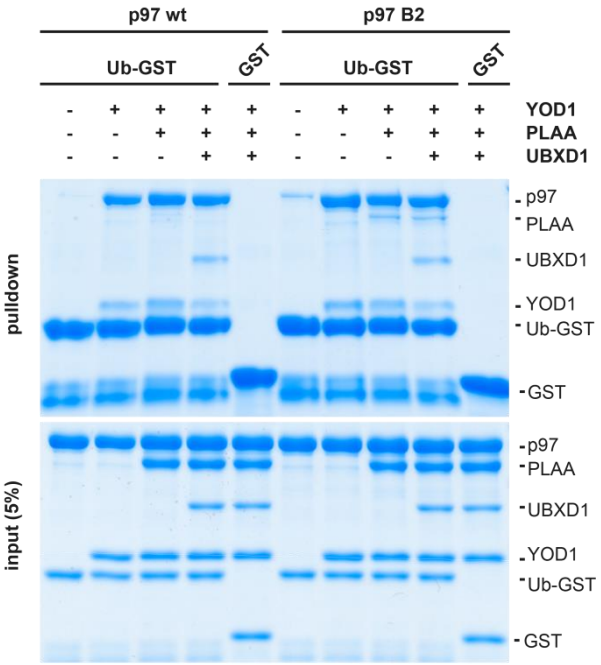

Figure 2.19 The ELDR components can be reconstituted *in vitro*
Pulldown of Ubiquitin-GST (Ub-GST) or GST with the different ELDR components (p97 12 µM; YOD1 8 µM; UBXD1 3 µM; PLAA 6 µM). The indicated proteins were incubated in buffer containing 2 mM ATP. Co-isolated proteins were detected with colloidal Coomassie staining after SDS-PAGE. GST served as a pulldown control. P97 did not bind alone but together with YOD1 to Ub-GST. UBXD1 could also integrate into the complex. Only in the p97 B2 background, PLAA is associated with Ub-GST.

p97 bound to Ub-GST together with YOD1, but not alone. UBXD1 was detected in the pulldown, too. In ITC experiments with the EDLR components performed in our lab, Daniel Grum found a change in stoichiometry if YOD1 and UBXD1 bind simultaneously to p97. The ratio p97:YOD1 was 6:6 and for p97:UBXD1 it was 6:3. But for the tertiary complex of p97:YOD1:UBXD1 it was found to be 6:3:3. Apparently, UBXD1 limits the YOD1 binding to p97. In this pulldown, this was reflected by the weaker band of YOD1 in the sample with UBXD1 compared to the one without UBXD1.

We could show that the ELDR components can bind together to Ub-GST *in vitro* (Papadopoulos et al. 2017). A special case is PLAA: It was only associated with the

other components if the dominant negative p97 B2 mutant was used. We next asked if I8 could mimic or abrogate this “trapping” phenotype. We used the Ub-GST pull down in the same set up to test the hypothesis (Figure 2.20).

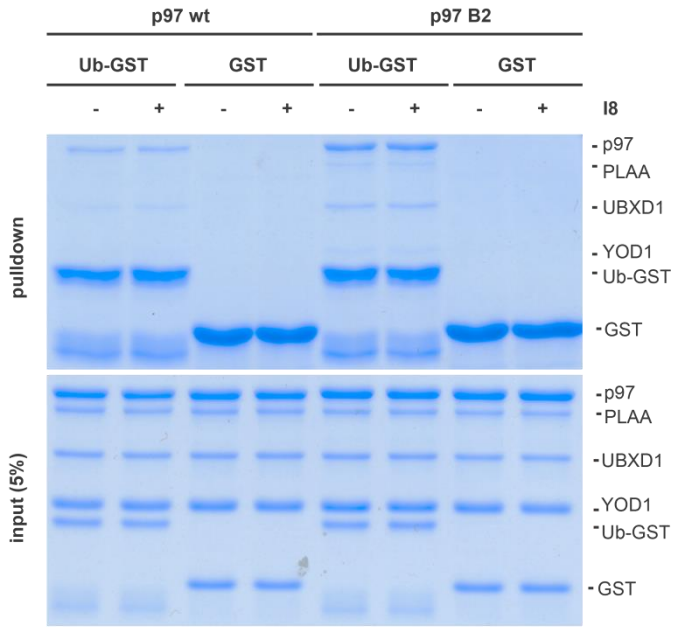

Figure 2.20 The ELDR components assemble in presence of I8
Pulldown of Ubiquitin-GST (Ub-GST) or GST with the different ELDR components (p97 8 µM; YOD1 8 µM; UBXD1 3 µM; PLAA 3 µM) with or without 10 µM I8. The indicated proteins were incubated in buffer containing 2 mM ATP. Co-isolated proteins were detected with colloidal Coomassie staining after SDS-PAGE. GST served as a pulldown control. The use of p97 B2 results in a stronger pulldown and association of PLAA. No difference between the samples with or without I8 was observed.

The pulldown showed again that the ELDR components were dependent on each other for binding to Ub-GST (compare Figure 2.20 and Figure 2.19). The weaker intensities in this experiment could result from the lower input levels of p97 (8 µM versus 12 µM), hinting at the hexamer as the central hub for the components. A higher efficiency of the pulldown with p97 B2 could be observed. I8 showed no influence on the complex of YOD1, UBXD1 and PLAA with either p97 wt or p97 B2. Therefore, I8 did not mimic the B2 “trapping” phenotype.

3 Discussion

A general strategy to study cellular functions is the impairment of single proteins. The impairment can be achieved by DNA based techniques (RNAi and CRISPR/Cas) or small molecules. The latter can be used in *in vitro* experiments, offer a high penetrance of the cell population, and are fast acting. Furthermore, the inhibited protein may still interact with its partners, in contrast to the genetic techniques. The option to use inhibitors in the controlled environment of cell free assays adds to their great versatility. With their help, significant progress regarding the molecular mechanism of a complex enzyme like p97 or its contribution in the different cellular pathways becomes possible (Chou et al. 2014; Papadopoulos et al. 2017; van den Boom et al. 2016). Small molecules are therefore important complementary research tools (Weiss et al. 2007). A second property of high interest is their potential to be developed into drugs as happened in the development of proteasome inhibitors (Kisselev, Goldberg 2001). In this regard, inhibition of p97 can be used to target cancer cells addicted to the ubiquitin proteasome system (Luo et al. 2009).

In this study, we describe the small molecule I8 as an inhibitor of p97. I will discuss potential binding sites and inhibitory mechanisms in p97 and also in the context of the related AAA+ ATPase VPS4B. Furthermore, the inhibition by I8 will be compared to the effects of other known inhibitors and possible effects on the inter- and intra-domain communication in p97 will be discussed.

3.1 I8 is a reversible, allosteric inhibitor of p97

In cooperation with a private company, we received the new chemical compound I8 that was found in a high throughput screening (HTS) against p97 ATPase activity. We set out to investigate its activity against p97 and confirmed an IC_{50} value in the low micromolar range (7 µM, Figure 2.2), in range of typical values of compounds found in HTS campaigns. Therefore, we wanted to study this compound in detail.

A fundamental difference between inhibitors is whether they bind reversibly or irreversibly. We tested I8 in this regard by a serial dilution experiment. I8 does not contain a reactive electrophile so that we expected a reversible inhibition. As experimental conformation, we used a serial dilution assay. A reversible inhibitor can be removed by dilution which results in a regained specific activity. In line with our expectation, we determined the binding of I8 to be reversible. Reversible inhibition is usually favored over irreversible inhibition in drug development for several reasons: Although irreversible inhibitors can have high potencies and prolonged effects, their

off-target effects are considered more harmful than reversible inhibitors (Bauer 2015). Additionally, irreversible inhibition can lead to immune-mediated toxicity (González-Bello 2016). Reversible inhibition on the other hand can be used in chase experiments, an important aspect of versatile research tools.

In our kinetics analysis, we determined a Hill-coefficient of h>2, showing cooperation in the p97 hexamer. Data from literature on this topic is ambiguous. Some studies support our observation (DeLaBarre et al. 2006; Magnaghi et al. 2013) and structural data show that arginine fingers interact with bound nucleotides in neighboring ATPase domains, giving a structural explanation for the cooperativity (DeLaBarre, Brunger 2003). In other studies however, no cooperativity was reported (Chou et al. 2014; Her et al. 2016). In the latter cases however, endpoint activity assays were used. Therefore, the absence of the observed cooperativity might be an artifact maybe caused by product inhibition at low ATP concentrations.

We carried out our initial characterization of I8 at high ATP concentrations and therefore under conditions of high competition. Still, the inhibitor showed good inhibitory effects, indicating a mechanism different from competitive inhibition. Our kinetics analysis of the inhibition of p97 by I8 shows that v_{max} is reduced and K_M stays constant, suggesting a non-competitive mechanism (Figure 2.4). However, a direct fit of the kinetic data to a non-competitive model is not possible as the model does not account for the observed cooperativity. A non-competitive inhibitor can bind to the free enzyme or the enzyme substrate complex and does not influence the affinity between enzyme and substrate (in this case p97 and ATP). To further investigate the mechanism, we used anisotropy measurements of ATP-BODIPY and p97 to measure the affinity between p97 and the different nucleotides. In this experiment, we detect no change in affinities between p97 and ATP or ADP (Figure 2.5). This observation differs from the effect that was observed for the p97 inhibitor NMS-873 (Magnaghi et al. 2013). In that case, the affinity between p97 and ADP was increased, indicating a different allosteric mechanism between I8 and NMS-873. Of note, our anisotropy measurements were conducted with full length p97 wild type. As the D1 domain shows dominant binding of nucleotides over the D2 domain, binding to D1 is predominantly assessed. To further investigate the hypothesis of non-competitive inhibition, the effect of I8 on the nucleotide affinities towards the Walker A mutants of p97 can be measured in future experiments.

3.2 Important structural features of I8

As an initial hit from an HTS campaign, I8 shows only moderate potency. Therefore, we wanted to improve the potency and selectivity of the molecule by probing the chemical space. In the scope of our structure-activity relationship (SAR) study of over 90 derivatives, we show that the bisphenyl group in I8 is an important structural feature (Figure 3.1). The phenyl rings may mediate the binding with the protein by π-interactions (Kozelka 2017). We show that the fluorination in the para-position elevates the potency of the inhibitor (comparing compound 41 and 42) but did not investigate the influence at the ortho- or meta-positions. Fluorine substituents are introduced for example to improve bioavailability and metabolic stability (Purser et al. 2008). For *in vitro* studies however, different effects are important to be considered. Due to the high electron negativity of the fluorine, the benzyl rings are relatively electron poor. Consequently, interactions with electron rich areas at the protein surface could be strengthened. However, the bisphenyl group is also part of the antipsychotic drugs pimozide and fluspirilene (Figure 3.1).

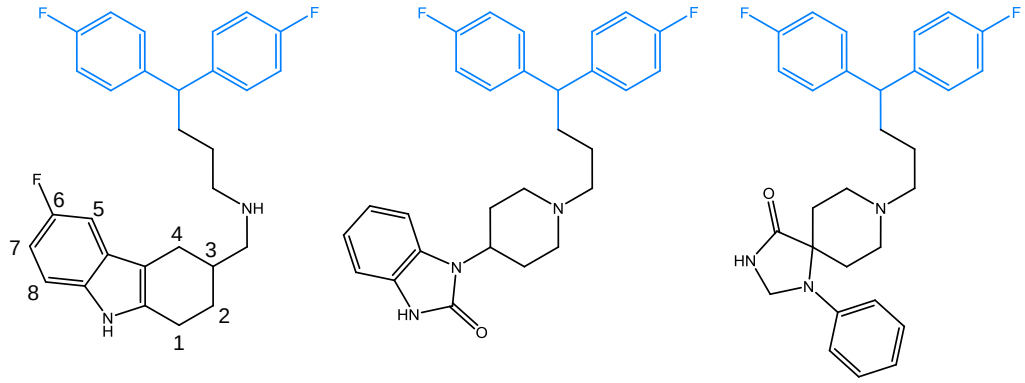

Figure 3.1 Structures of I8, pimozide and fluspirilene
From left to right: I8, pimozide and fluspirilene. All three compounds contain the fluorinated bisphenyl group highlighted in blue. In the structure of I8, the numbering for the aromatic part of the tetrahydrocarbazole is given.

Pimozide and fluspirilene were developed and used as dopamine receptor antagonist (Muscat et al. 1990; Wang 2002), but for both of them, a variety of targets are described, including the hERG K^+ channel and the USP1/UAF1 complex (Kang et al. 2000; Chen et al. 2011). The bisphenyl group itself may therefore provide limited selectivity. A secondary amine linker of defined length connects the bisphenyl group to the second prominent part of I8, a fluorinated tetrahydrocarbazole. Changes of the halite to positions 5 and 8 had only minor effects on the potency whereas a substituent at position 7 results in incomplete inhibition (Figure 2.6). Also the introduction of a second halite has only minor an effect on the potency. The fluorine

can be substituted with chlorine but the introduction of bigger groups like carbonyls is detrimental to the potency of I8. This could be a sign of steric limitations in a binding pocket. It may also provide an explanation why I8 does not compete with its rhodamine derivative (Figure 2.10): The rhodamine moiety is a substitute of the fluorine at the tetrahydrocarbazole and may prevent access to the binding pocket.

3.3 I8 inhibits VPS4B, but not NSF or proteasomal ATPases

Alina Dressler in our group observed a high toxicity of I8 compared with NMS-873 in MTS assays in HeLa cells. There, cell viability was markedly reduced by I8 already after 5 hours. We considered this fast toxicity as an indication that p97 is not the only target of inhibition, as the p97 inhibitor NMS-873 showed effects only after 24 hours. Grzegorz Dobrynin in our group conducted a selectivity test in a reporter cell line that helps differentiate between inhibition of p97 and inhibition of the proteasome. The cell line expresses two substrates, Ub-GFP and ODD-luciferase that are both degraded in the proteasome, but only Ub-GFP in a p97 dependent manner. Ub-GFP, but not ODD-luciferase was stabilized by I8. Thereby, Grzegorz Dobrynin showed that I8 does not inhibit the proteasome and we excluded that the observed toxicity arises from proteasome inhibition. Both assays by Alina Dressler and Grzegorz Dobrynin were conducted in a cell based system. They demonstrate the advantageous straightforwardness of assays based on the inhibition by small molecules compared with genetic techniques.

DBeQ was the first described compound that reversibly inhibited the ATPase activity of p97 by competition with ATP (Chou et al. 2011) and was used thereafter in different studies (for example Haines et al. 2012; Watkinson et al. 2013; Fang et al. 2015b). However, DBeQ was later found to also inhibit the p97-related AAA+ ATPase VPS4B (Magnaghi et al. 2013). Hence, we tested I8 against other AAA+ ATPases to further explore its specificity. I8 has negligible activity against the AAA+ ATPase NSF but shows high potency against VPS4B, whereas NMS-873 shows no activity towards both ATPases. Off-target effects of DBeQ and I8 could explain their high toxicity in the MTS assay. Importantly, I8 and DBeQ are structurally unrelated and have distinct mechanisms according to the kinetics analysis. Nevertheless, they are both ineffective against NSF and the proteasome and inhibit VPS4B and p97). The overlap of the activities of I8 and DBeQ might stem from the fact that both inhibitors are active against the D1 and D2 domain of p97 as D2 selective compounds do not inhibit VPS4B (Magnaghi et al. 2013; Chou et al. 2014).

VPS4 is an interesting target for small molecule inhibitors, since it is the only mechanoenzyme in the ESCRT pathway. Therefore, I8 could provide a viable way to inhibit the pathway or more specifically the formation of intraluminal vesicles. Inhibition of VPS4 has a potential for cancer treatment as the ESCRT pathway is associated with tumorigenesis (Mattissek, Teis 2014). However, the role of VPS4 in tumorigenesis is not clear: Low levels of VPS4B are connected to higher malignancy of breast cancer cells, possibly by elevated growth factor signaling (Lin et al. 2012). On the other hand, VPS4 is involved in the final steps of cytokinesis and VPS4 activity is connected to proliferation signaling (Davies et al. 2011). Therefore, VPS4 inhibition by a small molecule could have positive or negative effects on tumor growth and survival. Another pathologically relevant function of the ESCRT pathway is its association with viral infection. For example, some viruses require formation of MVBs for infection, and this formation requires VPS4B activity (Pasqual et al. 2011). Furthermore, the ESCRT machinery is used by enveloped viruses like Ebola for release of virions from the cell membrane (Li, Blissard 2012). Therefore, inhibition of VPS4 may prevent spreading of certain viral infections.

3.4 Where is the binding site of I8?

3.4.1 Coarse-grained views on effects of I8 binding

We demonstrate that inhibition by I8 and NMS-873 results in a similar protection of the D2 domain against trypsin digestion (Figure 2.17). In line with its higher potency, the effect is more pronounced for NMS-873. The experiment implicates a more compact D2 domain upon I8 binding, and this might influence cofactor binding. However, we detected no evidence for a change in the composition of the ELDR components UBXD1, YOD1 and PLAA in presence of the inhibitor (Figure 2.20). Of note, the protective effect of the inhibitors against tryptic digestion can be indirect, as inter- and intra-domain communications within the hexamer exist. Thus, inhibitor binding in D1 could result in protective changes in D2.

In further limited proteolysis experiments, we show that the digestion of the ND1L fragment is not influenced by I8 but depends on the nucleotide state (Figure 2.17). Even without nucleotide, ND1L is very stable against digestion. Addition of ATPγS forces the N domains into the up conformation (Banerjee et al. 2016) and concomitantly the resistance against trypsin is increased, possibly by masking otherwise accessible lysine or arginine residues. A protective effect of I8 on ND1L

against limited proteolysis could be obscured by different reasons. First, the ND1L fragment is already quite stable, even before addition of I8. It is possible that this stability cannot be further increased or the increase cannot be resolved in this assay. The second reason is that I8 may only bind to the D2 domain, which is absent in the ND1L fragment. This is implicated by the binding sites of the other known allosteric p97 inhibitors NMS-873 and UPCDC30245 in the D2 domain (see 3.4.2 and 3.5). However, a discrimination of I8 between the two ATPase domains of p97 seems unlikely because I8 also targets VPS4B, and the VPS4B ATPase domain is structurally homologous to both ATPase domains in p97. Moreover, I8 cannot stabilize VPS4B in our limited proteolysis experiments. Thus, in this experiment, VPS4B resembles ND1L. I8 might therefore not be a domain selective inhibitor in regard to p97, similar to DBeQ (see 3.3).

Interestingly, our data regarding inhibition of ND1L by I8 is ambiguous. The decline in activity happens over a very small inhibitor concentration range of only ~10 µM, hinting at some unusual kind of inhibition (Figure 2.16). Usually, this interval spans around two orders of magnitude (Auld et al. 2012). A possible explanation for the rapid decline could be an increased aggregation rate of ND1L in presence of I8 compared to full length p97. The higher susceptibility of aggregation of ND1L would then be caused by the truncation of the D2 domain since we detect no aggregation of full length p97 in size exclusion chromatography in presence of I8. Furthermore, the B2 mutant but not the B1 mutant of p97 shows a slight resistance against I8 inhibition. Taken together, these results indicate that I8 likely targets the activity in both ATPase domains, possibly with a preference for the D2 domain.

3.4.2 Narrowing down a possible binding site

The inhibition of p97 and VPS4B by I8 results in the same changes in the kinetics parameter (a reduced v_{max} and constant K_M, Figure 2.4). We therefore reason that a similar mechanism with homologous binding sites might exist in p97 and VPS4B. We have no compounds available to test a direct binding to p97, but an azido derivative of I8 was successfully crosslinked to VPS4B. Subsequently, we identified a modified peptide by mass spectrometry in collaboration with AG Kaiser. To confirm the binding site, we mutated residues in the peptide and in a neighboring helix based on docking simulations (Figure 2.12). In most cases the point mutations rendered the protein inactive. This prevented the assessment of a possible lower potency of I8 against these mutants that would indicate a loss of binding. However, two mutants with

mutations in the neighboring, upper helix were active and inhibited with the same potency as the wild type. We therefore excluded this helix as part of the binding site.

The modified VPS4B peptide we found in the MS analysis is located in the ATPase domain of VPS4B and comprises glycine 271. Glycine 271 is the structural homolog of histidine 340 in p97 D1 and asparagine 616 in p97 D2 (Figure 3.2 A+B). In the type II AAA+ ATPase NSF, the homolog amino acids to glycine 271 are asparagine 366 in D1 and lysine 639 in D2 (Figure 3.2 C+D). The alignments of the modified peptide with the ATPase domains of p97 and NSF show that it has higher homology with the p97 D2 and NSF D1. This correlates with the attribution that the NSF D1 and p97 D2 domains are the active ATPase domains of the respective enzyme. Therefore, I8 might preferentially bind in the active ATPase domain. Furthermore, the homologue residues of p97 and NSF are asparagines and spatially more extensive than the glycine in VPS4B and could introduce steric limitations that may explain the reduced potency of I8 towards NSF and p97 compared with VPS4B.

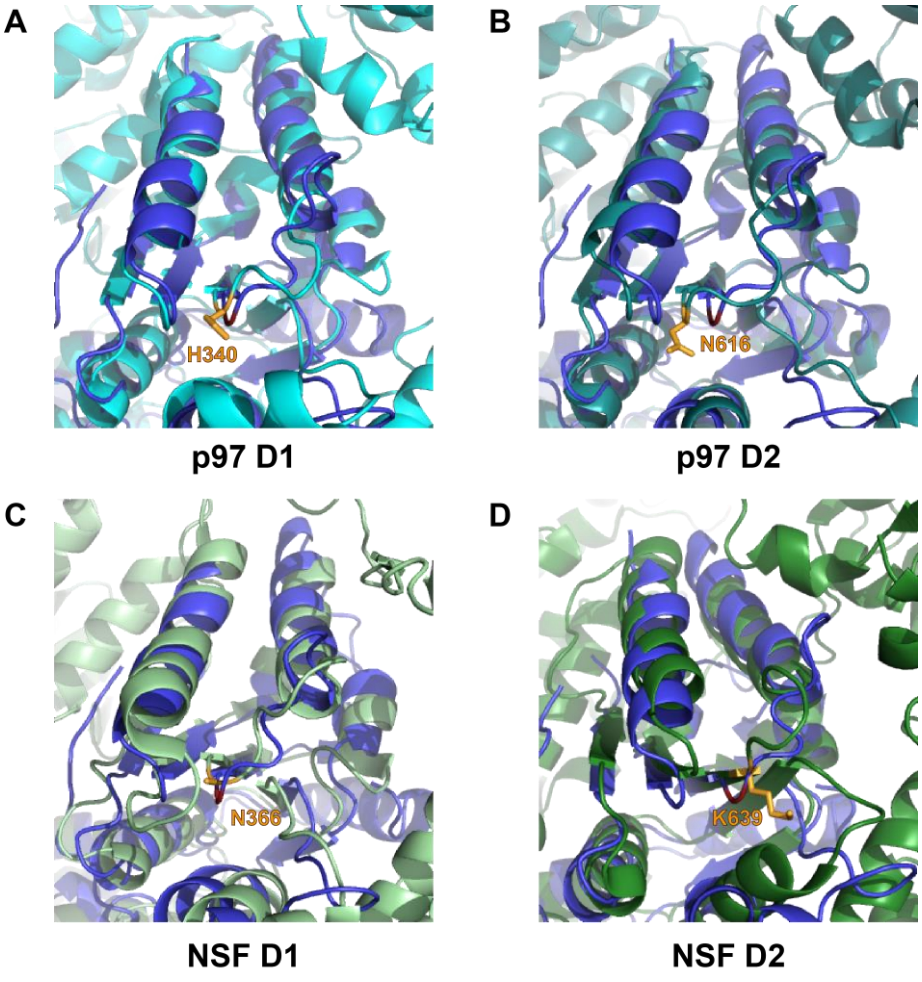

Figure 3.2 Structural alignment of the ATPase domain of VPS4B to the ATPase domains of p97 and NSF

The ATPase domain of VPS4B (blue, pdb 2zao) is aligned to A) p97 D1 (cyan, pdb 5ftk) B) p97 D2 (teal, pdb 5ftk) C) NSF D1 (light green, pdb 3j95) D) NSF D2 (dark green, pdb 3j95). The homologue amino acids to VPS4B glycine 271 (red) are shown in orange in stick representation. The pore is located at the top in all pictures.

The homology between glycine 271 in VPS4B and asparagine 616 in p97 provides a connection to the inhibitor NMS-873. Asparagine 616 was found crosslinked to an azido derivative of NMS-873. Subsequently, the azido derivative was modeled into the D1-D2 interface of two neighboring p97 subunits (Magnaghi et al. 2013). Mapping the modified peptide we found to p97 D2 reveals an overlap with the binding site of NMS-873 (Figure 3.3 B). Therefore, the binding sites of the two inhibitors may be in the same area. However, NMS-873 does not inhibit VPS4B (Magnaghi et al. 2013). This implicates that although I8 and NMS-873 may share partially their binding sites, they are different enough so that I8 can additionally bind and inhibit VPS4B.

Intriguingly, the structure of the inhibitor UPCDC30245 bound to the p97 D2 domain showed that asparagine 616 is also involved in the binding of UPCDC30245, providing hydrophobic interactions for the inhibitor (Figure 3.3 B).

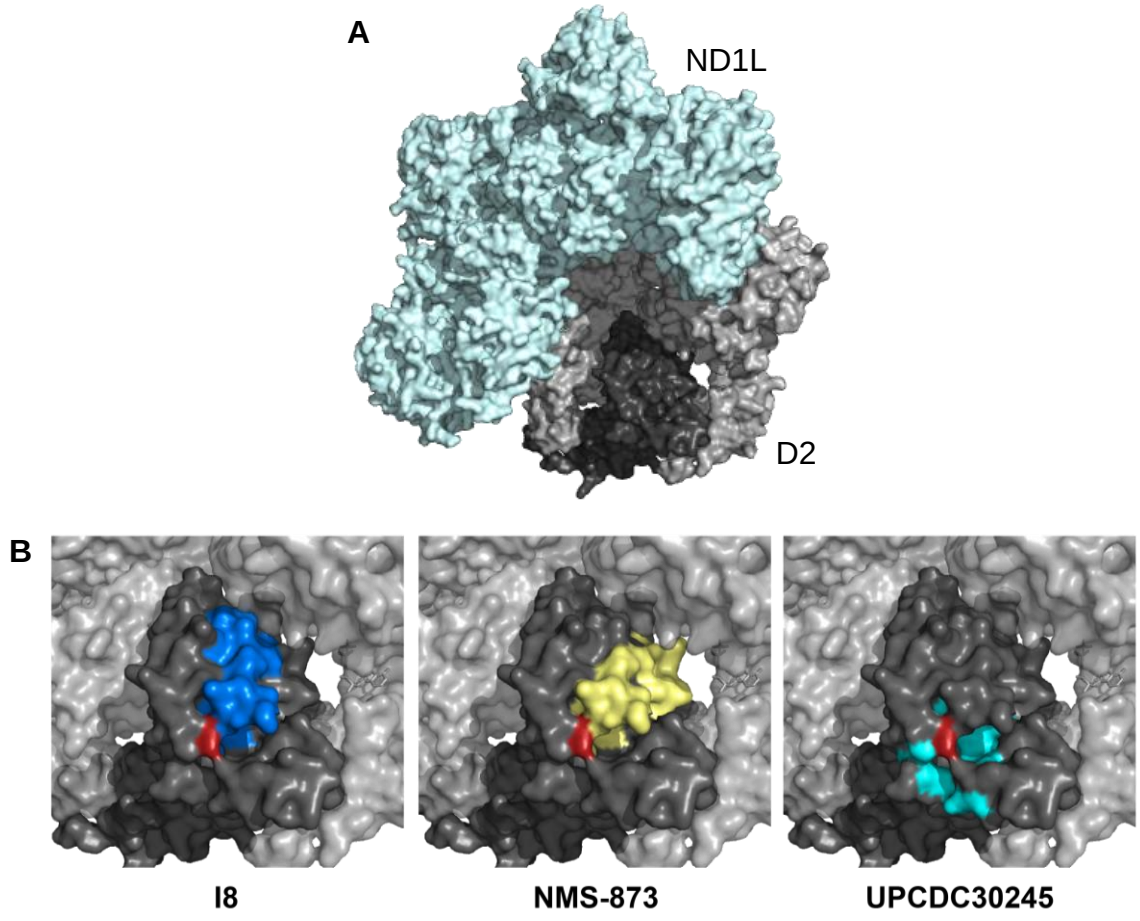

Figure 3.3 Binding sites of three different inhibitors

A) Overview of the whole p97 hexamer in the same orientation as in B). Two ND1L fragments are removed to show the D2 ring. ND1L in cyan, D2 in gray. A single D2 protomer is highlighted in dark grey (pdb 3cf3). B) Zoom in on the highlighted D2 domain from A). Peptides found in the MS analysis are shown in blue for I8 (peptide 602-634) and in yellow for NMS-873 (peptide 609-638, Magnaghi et al. 2013). According to a docking simulation, additional interactors are found in the D1 domain (N460 and L463, not shown). The interaction sites of UPCDC30245 are shown in cyan according to Banerjee et al. 2016. Asparagine 616 (red) is part of all three patches.

UPCDC30245 binds via a fluorinated indole group. Superposition of the inhibitor bound state with the ATPγS bound state (without inhibitor) showed steric clashes in the inhibitor binding pocket. The authors concluded that thereby UPCDC30245 prevents the exchange of nucleotides during the ATPase cycle (Banerjee et al. 2016). Of note, the indole structure of UPCDC30245 is also part of the tetrahydrocarbazole of I8 (Figure 3.4) and we show that the tetrahydrocarbazole is an important moiety of I8 (see 3.2).

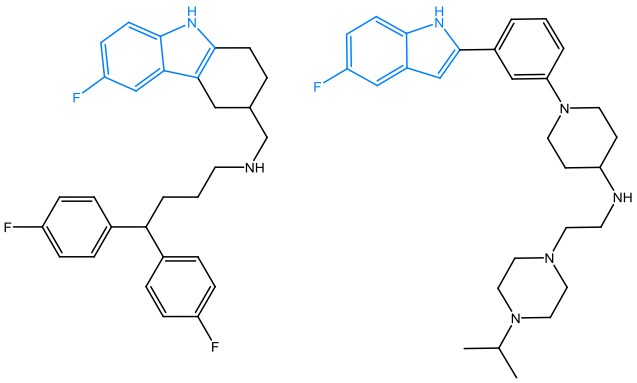

Figure 3.4 Structures of I8 and UPCDC30245
Structure of I8 (left) and UPCDC30245 (right). The common structural feature is highlighted in blue.

Considering the similarities in the structures of UPCDC30245 and I8 and the homology between glycine 271 and asparagine 616, their binding sites may be also similar. The electronegativity of the fluorine or other substituents was shown to be important contributors for the binding of UPCDC30245. For example, also bigger substituents like a nitro-derivative showed high potency (Alverez et al. 2015). Thus, steric limitations seem to be only a minor concern, contrary to our observations for I8. To further clarify the extent of the similarity between I8 and UPCDC30245, the inhibitory effect of the latter towards VPS4B could be tested. A high potency towards VPS4B may further hint at a similar binding site.

3.5 A common inhibitory mechanism of different inhibitors?

We compared the inhibition by I8 with inhibition by the commercially available inhibitors NMS-873 and CB-5083. For NMS-873, the binding site and a resistant p97 mutant are known. However, this NMS-873 insensitive N616F mutant was only tested *in vitro*. There, the enzymatic activity was slightly elevated but not as strong as in other mutations that result in a 2-3 fold increase in activity (Magnaghi et al. 2013; Tang, Di Xia 2013). These mutations cause a gain-of-function of p97 activity that leads to the late-onset disease MSP1. Therefore it could be reasoned that also the N616F mutation may not result in an immediate defect of cellular p97 function.

Interestingly, we show that not only I8 is less effective against p97 N616F but also the inhibitor CB-5083 is 20 times less potent against the mutant (Figure 2.9). Like NMS-873, CB-5083 is D2 specific. However, CB-5083 shows competitive behavior with ATP at the D2 domain whereas NMS-873 acts allosterically and prevents the release of ADP from D2 (Magnaghi et al. 2013; Anderson et al. 2015; Zhou et al. 2015). Considering these data, a common binding site appears unlikely. One explanation why the p97 N616F mutant shows resistance against CB-5083 is that the p97 N616F mutant may have an altered intra- or inter-subunit communication that leads to a loss of efficacy of CB-5083. Magnaghi et al. suggested that NMS-873 disrupts the inter-protomer motion transmission, resulting in impaired hydrolysis. Besides preventing the binding of NMS-873, the N616F mutation may have a strengthening effect on the connection between the subunits. Thereby, the N616F mutation could elevate the catalytic efficiency. In this case, CB-5083 and I8 can still bind and compete with the nucleotide, but the stronger connection between the protomers could diminish the inhibitory potency of the inhibitors.

A similar idea was suggested for the A530T mutation in p97. This particular mutation was found in cells resistant to NMS-873. Subsequently, it was found that NMS-873 still binds to purified p97 A530T. Consistently, the mutant is still inhibited by NMS-873 although less potently by a factor of four. Additionally, p97 A530T has a higher catalytic efficiency compared to wild type p97 and associates stronger with certain cofactors like UFD1-NPL4. It was suggested that the mutant circumvents the inhibitory effect of NMS-873 due to its more “robust” activity (Her et al. 2016).

How could the connection or communication between subunits be strengthened in the p97 N616F mutant? Asparagine 616 is located in a turn within a stretch of amino

acids that connect the sensor I region and the ISS (inter-subunit signaling) motif (Figure 3.5).

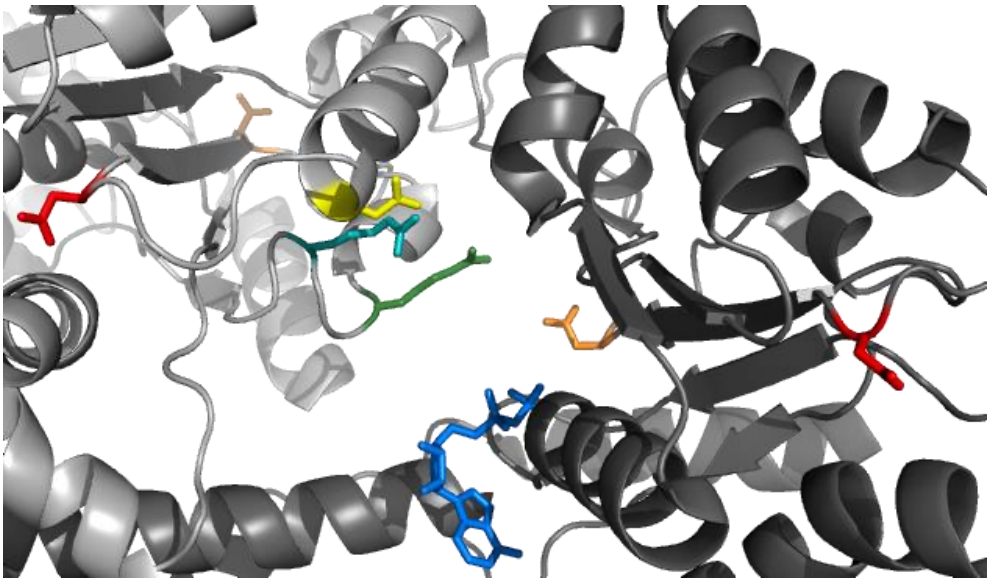

Figure 3.5 Communication network between two neighboring D2 domains
View on two neighboring D2 domains in light and dark shades of grey (left and right, respectively) from the outside of the hexamer (pdb 5ftk). Marked amino acids are part of the ISS motif (aspartate 609, yellow), the sensor I region (asparagine 624, orange), or the arginine finger (arginine 635, cyan and arginine 638, green). Asparagine 616 is marked in red. ADP is shown in blue.

The ISS motif coordinates the arginine finger that reaches into the nucleotide binding pocket of the neighboring protomer while the sensor I interacts with the ATP γ-phosphate of its own protomer (Davies et al. 2008; Huang et al. 2012). Mutation to phenylalanine might cause a repositioning of the two elements, resulting in a changed inter-protomer communication and possibly in the reduced susceptibility to the inhibitors, as described above. However, structural data would be needed to confirm this hypothesis.

3.6 Future development of inhibitors

Our study revealed interesting new insights into the regulatory mechanisms in the p97 hexamer, for example regarding the communication between D2 domains. However, the comparison of the compound I8 with the optimized inhibitors CB-5083, NMS-873, and UPCDC30245 shows that it is less potent. So far, only the DBeQ derivative CB-5083 showed drug-like pharmacokinetics and -dynamics and is tested in clinical trials (Anderson et al. 2015). Additionally, recent studies support the notion that MSP1 mutations result in a gain of function of p97 (Zhang et al. 2017; Blythe et

al. 2017). Therefore, p97 inhibitors could also be used as treatments against this degenerative disease.

Importantly, I8 is the first described allosteric inhibitor of VPS4B and already more potent towards VPS4B than towards p97. By further iterations of the inhibitor, the selectivity could maybe be improved. Similar to the p97 inhibitors, such a potent VPS4B inhibitor can be used as a lead structure for drug development (see 3.3), but also as a research tool. For example, unresolved questions that could be addressed involve how the VPS4 activity of coordinated with the membrane remodeling by ESCRT-III proteins and what the role of VPS4 is in the final scission steps of vesicle formation besides recycling of ESCRT-III proteins. Furthermore, cell based studies would not have to rely on overexpression of dominant negative mutants or downregulation of endogenous VPS4 if an inhibitor is available.

Another point that can be addressed in the future development of new p97 inhibitors is their domain specificity. The potent inhibitors NMS-873, CB-5083, and UPCDC30245 all target the D2 domain (Magnaghi et al. 2013; Anderson et al. 2015; Banerjee et al. 2016). Activity and unfolding measurements showed that ATP hydrolysis in D2 is higher compared to D1. Furthermore, hydrolysis in D2 but not D1 is needed for unfolding activity (Chou et al. 2014; Blythe et al. 2017; Bodnar, Rapoport 2017). By using full length p97 during the search for and development of inhibitors, a bias towards the D2 domain may be introduced. Therefore, in the development of new molecules, the focus could lie on the ND1L fragment of p97. In this approach to p97 inhibition, the modulation of the p97 regulation instead of simple ATPase inhibition could be preferentially targeted.

The important regulatory function of the ND1L part of p97 is demonstrated by its role as the main interaction site with the cofactors. The cofactor binding can influence the conformational status of the hexamer and directly or indirectly influence the activity of the hexamer (Niwa et al. 2012; Banerjee et al. 2016; Trusch et al. 2015). Conversely, nucleotide binding is connected to the differential association of cofactors (Chia et al. 2012; Bulfer et al. 2016). Interestingly, the MSP1 mutants cluster in the ND1L fragment and some show deviations in the cofactor association (Ritz et al. 2011; Chou et al. 2014). An inhibitor targeting either D1 activity or cofactor binding might therefore provide interesting new insights into the regulatory communication in the hexamer and also in the interaction with cofactors. The interaction with cofactors could also be targeted as a way to develop pathway-specific inhibitors. For example,

the disease associated functions of p97 in cancer or in MSP1 are usually affecting the degradation pathways but not the membrane dynamics (Meyer, Weihl 2014). Thus, the tolerance for a possible treatment may increase with a more precise approach of inhibition.

4 Material and methods

4.1 Cloning

The PCR reactions for generating different mutants were done using *PfuUltra* II Fusion HS DNA Polymerase (Agilent Technologies). The composition of the general reaction mixture is given in Table 4.1.

Table 4.1 Reaction mixture for site directed mutagenesis

H_2O	37.5 µl
10x *PfuUltra* II reaction buffer	5 µl
dNTP mix (10 mM each dNTP)	3 µl
forward primer (10 µM)	1 µl
reverse primer (10 µM)	1 µl
template (10 ng/µl)	2.5 µl
PfuUltra II Fusion HS DNA Polymerase	0.5 µl
Total reaction volume	50 µl

The general PCR program for the amplification is given in Table 4.2.

Table 4.2 General PCR program for site directed mutagenesis.
T_{M1} denotes the melting temperature of one half of the primer, T_{M2} the melting temperature of the whole primer.

	Temperature	Time	
Initial Denaturation	95 °C	3 min	
Denaturation	95 °C	30 s	
Annealing	T_{M1}-5 °C	1 min	10 cycles
Elongation	72 °C	8 min	
Denaturation	95 °C	30 s	
Annealing	T_{M2} -5°C	1 min	20 cycles
Elongation	72 °C	8 min	
Final elongation	72 °C	7 min	
Storage	15 °C	paused	

For purification of PCR products, the NucleoSpin® Gel and PCR Clean-up kit (Macherey-Nagel) was used according to the manufactures instructions. The plasmids were amplified by transformation of chemically competent *E. coli* strains DH5α or XL1-blue. Transformation was done by heat shock. 50 µl of bacterial suspension was mixed with 1 µl plasmid DNA. After 10 min incubation on ice, the bacteria were incubated for 45 s in a water bath at 42 °C. Afterwards, the bacteria

were incubated again for 10 min on ice. 800 µl TB media was added before 1 h incubation at 37 °C at 300 rpm. Purification of plasmid DNA from E.coli was done with the NucleoSpin® Plasmid kit (Macherey-Nagel) according to the manufactures instructions. The purified DNA was verified by sequencing (Microsynth or GATC Biotech). Used plasmids are given in Table 4.3.

Table 4.3 DNA constructs used in this study

name	insert	source	species	tag	vector	Code
YOD1-His	YOD1	D. Grum, Essen	human	His	pET41b+	698
His-PLAA	PLAA	D. Grum, Essen	human	His	pFL	707
His-p97	p97	D. Grum, Essen	human	His	pET15b	708
UBXD1-His	UBXD1	D. Grum, Essen	human	His	pET41b+	715
pETUbV-GST	Ubiquitin	H.Meyer, New Haven	mouse	GST	pET23a+	928
pQE9.NSF	NSF	Alan Morgan, Liverpool	hamster	His	pQE9	54
VPS4A	VPS4A	Phyllis I. Hanson, St. Louis	mouse	His	pEt28a	716
VPS4B	VPS4B	Phyllis I. Hanson, St. Louis	mouse	His	pEt28a	717
CHMP1B106-199	CHMP1B	Phyllis I. Hanson, St. Louis	mouse	His	pEt28a	718
His-VPS4B H3A	VPS4B	this study	mouse	His	pET28a	1009
His-VPS4B L4A	VPS4B	this study	mouse	His	pET28a	1010
His-VPS4B K217A	VPS4B	this study	mouse	His	pET28a	1040
His-VPS4B N218A	VPS4B	this study	mouse	His	pET28a	1041
His-VPS4B Q221A	VPS4B	this study	mouse	His	pET28a	1042
His-VPS4B R224A	VPS4B	this study	mouse	His	pET28a	1043
His-VPS4B V260A	VPS4B	this study	mouse	His	pET28a	1044
His-VPS4B Q261A	VPS4B	this study	mouse	His	pET28a	1045
p97 RH	p97	this study	human	His	pET15b	780
p97 A1	p97	this study	human	His	pET15b	781
p97 B1	p97	this study	human	His	pET15b	782
p97 A2	p97	this study	human	His	pET15b	783
p97 B2	p97	D. Grum, Essen	human	His	pET15b	784
p97 His-ND1L	p97	this study	human	His	pET15b	938

4.2 Expression and purification of recombinant proteins

All proteins were snap frozen and stored at -80°C after purification. YOD1-His was expressed and purified by Daniel Grum.

4.2.1 Protein expression and purification from *E. coli*

For bacterial expression of recombinant proteins, either *E. coli* strains Rosetta2 (DE3) or SoluBL21 (DE3) were transformed and grown in TB media. The chemically competent bacteria were transformed with the appropriate plasmid (Table 4.3) via heat shock and grown to an OD_{600} of ~0.8 at 37 °C. Expression was induced with 0.4 mM IPTG and the bacteria were grown over night at 18 °C. The bacteria were centrifuged for 15 min at 4 °C and 3900 x g. The pellet was resuspended to a final volume of ~70 ml lysis buffer (50 mM HEPES pH 7.4, 150 mM KCl, 5 mM $MgCl_2$, 5 % Glycerol, 20 mM imidazole for His-tagged proteins) per pellet from 1 l medium. The pellet was stored at -80 °C or directly used to purify the protein.

4.2.1.1 His-p97 (wild type and mutants)

The pellet was resuspended in lysis buffer or thawed. After addition of DTT (0.5 mM), PMSF (0.1 mM), ATP (2mM) and Lysozyme, the mixture was stirred for 20 min at 4°C. Cells were lysed on ice via sonication with 5x30 s pulses with 30 s breaks (Bandelin Sonoplus, TT13). After three pulses, Triton X-100 was added to 0.1 %. Lysed cells were centrifuged for 45 min at 35,000 x g. The supernatant was filtered through a 0.8 µm filter and loaded onto a 5 ml HisTrap FF crude column (GE Healthcare) at ~2 ml/min. Next, the column was washed with 300 ml lysis buffer and eluted directly on a HiTrap Q HP 5 ml column (GE Healthcare) with 25 ml lysis buffer containing 300 mM imidazole. The anion exchange column was washed with 25 ml IEX buffer A (20 mM HEPES pH 7.2, 25 mM KCl, 5 mM $MgCl_2$, 5 % Glycerol). Ion exchange chromatography was performed using elution with a gradient from 30 % to 70 % IEX B (as IEX A, but 1 M KCl) over 5 column volumes and 1 ml/min on an ÄKTApurifier UPC10 (GE Healthcare). The elution of protein was monitored with UV absorption at 280 nm. The peak fractions were pooled and concentrated with a 100 kDa cut-off centrifugal concentrator (Sartorius).

4.2.1.2 His-VPS4B (wild type and mutants)

The pellet was resuspended or thawed and DTT (0.5 mM), PMSF (0.1 mM), ATP (2 mM) and Lysozyme added. The mixture was stirred for 20 min at 4°C. Cells were lysed on ice via sonication with 5x30 s pulses with 30 s breaks (Bandelin Sonoplus,

TT13). After three pulses, Triton X-100 was added to 0.1 %. Lysed cells were centrifuged for 45 min at 35,000 x g. The supernatant was filtered through a 0.8 µm filter and loaded onto a 5 ml HisTrap FF crude column (GE Healthcare) at ~2 ml/min. Next, the column was washed with 300 ml lysis buffer, 50 ml lysis buffer containing 2 mM ATP and finally equilibrated with 50 ml IEX A (20 mM HEPES pH 7.2, 25 mM KCl, 5 mM $MgCl_2$, 5 % Glycerol). The proteins were eluted directly on a HiTrap SP HP 5 ml column (GE Healthcare) with 25 ml IEX A containing 300 mM imidazole. The cation exchange column was washed with 25 ml IEX buffer A. Ion exchange chromatography was performed using elution with a step from 0 % to 40 % IEX B (as IEX A, but 1 M KCl) with 4 column volumes at 40 %. Flow rate was 1 ml/min on an ÄKTApurifier UPC10 (GE Healthcare). The elution of protein was monitored with UV absorption at 280 nm. The peak fractions were pooled and concentrated with a 10 kDa cut-off centrifugal concentrator (Sartorius).

4.2.1.3 His-CHMP1B 106-199

The pellet was resuspended or thawed and PMSF (0.1 mM) and Lysozyme added. The mixture was stirred for 20 min at 4°C. Cells were lysed on ice via sonication with 5x30 s pulses with 30 s breaks (Bandelin Sonoplus, TT13). Lysed cells were centrifuged for 45 min at 35,000 x g. The supernatant was filtered through a 0.8 µm filter and loaded onto a 5 ml HisTrap FF crude column (GE Healthcare) at ~2 ml/min. Next, the column was washed with 300 ml lysis buffer and equilibrated with 50 ml IEX A (20 mM HEPES pH 7.2, 25 mM KCl, 5 mM $MgCl_2$, 5 % Glycerol). The protein was eluted directly on a HiTrap Q HP 5 ml column (GE Healthcare) with 25 ml lysis buffer containing 300 mM imidazole. The anion exchange column was washed with 25 ml IEX buffer A (20 mM HEPES pH 7.2, 25 mM KCl, 5 mM $MgCl_2$, 5 % Glycerol). Ion exchange chromatography was performed using gradient elution at 1 ml/min on an ÄKTApurifier UPC10 (GE Healthcare). However, the protein eluted late at 100 % IEX B. The elution of protein was monitored with UV absorption at 280 nm. The peak fractions were pooled and concentrated with a 100 kDa cut-off centrifugal concentrator (Sartorius).

4.2.1.4 UBXD1-His

The chemically competent bacteria were transformed with construct 715 via heat shock and grown to an OD_{600} of ~2 at 37 °C. Expression was induced with 0.4 mM IPTG and the bacteria were grown over night at 18 °C. The bacteria were centrifuged for 15 min at 4 °C and 3900 x g. The pellet was resuspended to a volume of ~70 ml

lysis buffer (50 mM HEPES pH 7.4, 150 mM KCl, 5 mM $MgCl_2$, 5 % Glycerol, 20 mM imidazole) per pellet from 1 l medium. After addition of DTT (0.5 mM), PMSF (0.1 mM) and Lysozyme, the mixture was stirred for 20 min at 4°C. Cells were lysed on ice via sonication with 5x30 s pulses with 30 s breaks (Bandelin Sonoplus, TT13). The lysed cells were centrifuged for 45 min at 35,000 x g. The supernatant was filtered through a 0.8 µm filter and loaded onto a 5 ml HisTrap FF crude column (GE Healthcare) at ~2 ml/min. Next, the column was washed with 300 ml lysis buffer and equilibrated with 50 ml IEX A (20 mM HEPES pH 7.2, 25 mM KCl, 5 mM $MgCl_2$, 5 % Glycerol). The protein was eluted with 25 ml lysis buffer containing 300 mM imidazole. After 1:1 dilution with IEX A, the solution was loaded on a 5 ml HiTrap Q HP column (GE Healthcare). The anion exchange column was washed with 25 ml IEX A. Ion exchange chromatography was performed using elution with a gradient from 45 % to 100 % IEX B (as IEX A, but 200 mM KCl) over 100 ml and 1.5 ml/min on an ÄKTApurifier UPC10 (GE Healthcare). The elution of protein was monitored with UV absorption at 280 nm. The peak fractions were pooled and concentrated with a 10 kDa cut-off centrifugal concentrator (Sartorius).

4.2.1.5 His-NSF

The pellet was re-suspended in lysis buffer (100 mM HEPES pH 7.0, 500 mM KCl, 5 mM $MgCl_2$, 5 mM ATP, 2 mM DTT, 0.1 % Triton X-100). After addition of Roche complete EDTA-free protease inhibitor and Lysozyme, the mixture was stirred for 30 min at 4°C. Cells were lysed on ice via sonication with 4x30 s pulses with 30 s breaks (Bandelin Sonoplus). The lysed cells were centrifuged for 30 min at 35,000 x g. The supernatant was loaded onto a Ni-TED (Machery-Nagel) column via gravity flow. After washing (20 mM HEPES pH 7.0, 500 mM KCl, 1 mM $MgCl_2$, 0.5 mM ATP, 2 mM DTT, 10 % glycerol, 0.1 % Triton X-100, Roche complete EDTA-free protease inhibitor), the protein was eluted with washing buffer containing 250 mM imidazole. The eluted protein was concentrated and further purified via size exclusion chromatography. The concentrate was loaded onto a Superose 6 10/300 GL column that was equilibrated with running buffer (20 mM Hepes 7.4, 150 mM KCl, 1mM MgCl2, 5% Glycerin, 1 mM DTT). The pooled fractions were concentrated with a 10 kDa cut-off centrifugal concentrator (Sartorius).

4.2.1.6 Ub-GST

The chemically competent bacteria were transformed with construct 928 via heat shock and grown to an OD_{600} of ~0.7 at 37 °C. Expression was induced with 0.4 mM

IPTG and the bacteria were grown for 4h at 30 °C. The bacteria were centrifuged for 15 min at 4 °C and 3900 x g. The pellet was resuspended in ~70 ml lysis buffer (50 mM HEPES pH 8.0, 150 mM KCl, 5 mM $MgCl_2$, 5 % Glycerol, 20 mM imidazole) per pellet from 1 l medium. After addition of Lysozyme, the mixture was stirred for 30 min at 4°C. Cells were lysed on ice via sonication with 5x30 s pulses with 30 s breaks (Bandelin Sonoplus, TT13). The lysed cells were centrifuged for 30 min at 35,000 x g. The supernatant was filtered through a 0.8 µm filter and loaded onto a 5 ml HisTrap FF crude column (GE Healthcare) at ~1.5 ml/min. Next, the column was washed with 100 ml lysis buffer and elutes with 20 ml containing 300 mM imidazole and 1 mM DTT. The elution was loaded on a 5 ml GSTrap FF (GE Healthcare) with a flow rate of 0.5 ml/min and washed with 150 ml buffer. The protein as eluted with 40 ml buffer containing 20 mM GSH and 2 mM DTT. Finally, the eluate was loaded onto a HiTrap Q HP 5 ml column (GE Healthcare) and the flow through collected. The flow through was concentrated with a 10 kDa cut-off centrifugal concentrator (Sartorius).

4.2.2 Protein expression and purification from insect cells with the baculovirus system

4.2.2.1 His-PLAA

The full length PLAA protein could not be expressed solubly in E. coli. Therefore, we used a baculovirus expression vector system, MultiBac, to express PLAA (Bieniossek et al. 2008). Chemically competent E. coli DH10 EMBacY were transformed via heat shock with the pFL plasmid (Table 4.3) and plated on TB agar containing 50 µg/ml kanamycin, 10 µg/ml tetracycline, 7 µg/ml gentamycin, 40 µg/ml IPTG and 100 µg/ml X-Gal. The PLAA coding sequence was integrated into the bacmid via Tn7 transposition. Selection for a successful integration was done with a blue/white screen. Integration disrupts a lacZ gene so that colonies with successful integration remain white after 48h. Single positive clones were picked and grown in selective TB medium containing 50 µg/ml kanamycin, 10 µg/ml tetracycline and 7 µg/ml gentamycin. For purification of the bacmid, cells were lysed with the NucleoSpin® Plasmid kit (Macherey-Nagel). After centrifugation, the DNA in the supernatant was precipitated with 50% isopropanol at -20 °C over night and centrifuged. The pellet was washed with 70 % ethanol and resuspended gently in 40 µl sterile TE buffer.

S. frugiperda Sf9 cells (Invitrogen) were seeded and maintained in Sf900™ III serum free medium (Gibco) in suspension culture at 27 °C according to the supplier's

instructions. For transfection, Sf9 cells were seeded in 30 mm diameter wells (6 well plate, $1x10^6$ cells per well). FuGene HD transfection reagent (Promega) was used according to the manufactures instructions with 5 µl reagent and 20 µl bacmid DNA in 200 µl medium. The adherent cells were incubated for four days at 27 °C. Besides the recombinant protein PLAA, the bacmid codes for YFP under a late promoter. Therefore, after at least 72 h, transfection and viral production can be controlled with a fluorescent microscope. For the first virus amplification, $1x10^7$ cells were seeded into a 10 cm dish. The complete content of a 6 well was transferred to the 10 cm dish to infect the cells. The dish was incubated for four day at 27 °C. Virus generation V1 and V2 were done in 50 ml suspension culture. The cultures were incubated for four days between virus propagation. 2 ml of the supernatant was used to infect $5x10^7$ cells. V0 and V1 were stored with 5% FCS ate 4 °C in the dark. For the final expression, the complete supernatant of V2 was used to infect $1×10^6$ cells/ml in 1 l medium. The cells were incubated for four days at 27 °C in the dark at 115 rpm. Cells were harvested by 15 min centrifugation at 2300 x g, resuspended in cold PBS and centrifuged again for 10 min at 1000 x g. Cells from a 1 l expression culture were split into 3 parts before pelleting and the pellets stored at -80 °C. The remaining infected cells after each viral generation were used to monitor the expression of the protein with a His-pull down from the cell lysate.

For purification, a pellet was resuspended in 100 ml lysis buffer (50 mM HEPES pH 8.0, 150 mM KCl, 5 mM $MgCl_2$, 5 % Glycerol, 20 mM imidazole, 0.5 mM DTT, Roche complete EDTA-free protease inhibitor). Cells were lysed on ice via sonication with 3x20 s pulses with 30 s breaks (Bandelin Sonoplus, TT13). Lysed cells were centrifuged for 45 min at 35,000 x g. The supernatant was filtered through a 0.8 µm filter to remove abundant actin filaments and loaded onto a 5 ml HisTrap FF crude column (GE Healthcare) at ~2 ml/min. Next, the column was washed with 350 ml lysis buffer (without protease inhibitor) and eluted with 25 ml lysis buffer containing 300 mM imidazole on an ÄKTApurifier UPC10. The peak fraction were subjected to a buffer exchange to IEX buffer A (20 mM HEPES pH 7.2, 25 mM KCl, 5 mM $MgCl_2$, 5 % Glycerol) with Zeba™ Spin Desalting Columns, 7K MWCO (Thermo Scientific) and loaded onto a Mono Q 5/50 GL column (GE Healthcare). The protein was eluted with a gradient from 20 % to 80 % IEX B (as IEX A but 200 mM KCl) over 20 ml at 0.75 ml/min on an ÄKTApurifier UPC10 (GE Healthcare). The elution of protein was monitored with UV absorption at 280 nm. The peak fractions were pooled and concentrated with a 10 kDa cut-off centrifugal concentrator (Sartorius).

4.3 Protein concentration determination

The concentration of proteins was determined with UV absorption at 280 nm at a BioPhotometer D30 (Eppendorf) using extinction coefficients calculated with the expasy ProtParam web tool (Table 4.4). For p97 wild type, B1, A2 and B2, the extinction coefficient includes a correction for the bound ADP in D1 that causes a peak shift towards 260 nm. All given protein concentrations in this study refer to monomer concentrations.

Table 4.4 Extinction coefficients used in this study

protein	extinction coefficient ε ($M^{-1}cm^{-1}$)
p97 wt/B1/A2/B2	38277
p97 A1	35870
ND1L	23837
VPS4B	46410
UBXD1	29910
NSF	36900
Ub-GST	49850
PLAA	95800

CHMP1B 106-199 does not contain phenylalanines, tryptophans or cysteines. Therefore, a molar extinction coefficient could not be calculated. For protein concentration determination, the BCA assay (Interchim) with Lysozyme as a standard was used according to the manufactures instructions.

4.4 ATPase Assays

4.4.1 Malachite Green

The malachite Green assay was used for endpoint determination of the ATPase activity of wild type and mutant proteins and determination of IC_{50} values. 0.2 µM of ATPase were incubated with 2 mM ATP in reaction buffer (for p97 and NSF: 50 mM Hepes pH 7.4, 150 mM KCl, 2.5 mM $MgCl_2$, 15 % glycerol, 1 mM DTT, 0.01 % Triton X-100; for VPS4B: 20 mM Tris-HCl pH 7.4, 100 M KOAc, 5 mM $MgCl_2$) for 30 min (for p97 and NSF) or 10 min (for VPS4B) at 25 °C in 50 µl reaction volume. For determination of IC_{50} values, 1 µl of the compound was added to achieve the desired concentrations. The DMSO ratio was 2-3 %. The reaction was started by adding ATP and stopped by adding 100 µl BIOMOL Green reagent (Enzo Life Sciences). After color development, the absorption at 630 nm was measured with a SpectraMax Plus

384 (Molecular Devices) plate reader. A phosphate standard series was included on each ATPase reaction plate to quantitate the released phosphate. The data was analyzed with GraphPadPrism and fit to a dose-response curve with variable slope.

4.4.2 NADH coupled ATPase assay

For kinetic analysis, the NADH coupled ATPase assay was used to avoid product inhibition. The ATPase (0.25 µM p97 or 0.2 µM VP4B with 10 µM CHMP1B 106-199) was incubated with 4.8 µl Pyruvate Kinase/Lactic Dehydrogenase enzyme mix (~3.8/5.6 units) (Sigma-Aldrich), 6 mM phosphoenolpyruvate PEP and 1 mM nicotinamide adenine dinucleotide NADH. Furthermore, 2 µl of inhibitor or DMSO was added. The final volume of the ATPase mix was 40 µl in a 96 well plate. The ATP dilution series was prepared in 50 µl buffer. The same buffers as in for the malachite green assay were used. The plate was prewarmed to 37 °C and the reaction was started by adding 40 µl of the prepared ATP dilution to 40 µl ATPase mix. The decline in NADH absorbance at 340 nm was measured every 30 s for 30 min with the SpectraMax Plus 384 (Molecular Devices) plate reader. The extinction coefficient of NADH was calculated by using the absorption of the 0 s time point of the wells without ATP. Specific activity of the ATP was calculated with the decay rate of NADH (mol/min) that equals the rate of hydrolysis of ATP (mol/min). The data was analyzed with GraphPadPrism and fit to the Hill equation.

4.5 Anisotropy

For anisotropy measurements, a Cary Eclipse Fluorescence Spectrophotometer (Agilent) was used. To determine the nucleotide binding affinity of p97, a twofold dilution series of p97 with 20 nM of ATP-Bodipy (life technologies) 50 mM Hepes pH 7.4, 150 mM KCl, 2.5 mM $MgCl_2$, 15 % glycerol, 1 mM DTT, 0.01 % Triton X-100 was prepared. In further experiments, 1 µM ADP and or 20 µM I8 were added. The fluorescence signal was measured five times over five seconds and the mean used for curve fitting. For calculations of anisotropy, a G-factor of 1.7297 for ATP-Bodipy was determined beforehand. The data was analyzed with GraphPadPrism and fit to the one site total binding model. The anisotropy measurements of the rhodamine probe were conducted essentially the same way but with 100 nM of the probe. In this case, the G-factor was 1.9457.

4.6 CD-Spectroscopy

The influence of the multiple Alanine mutations in VPS4B was assessed with CD spectroscopy. The CD spectra of 0.2 g/l VPS4B wild type and mutants were measured in 50 mM KP_i buffer pH 7.4 between 190 nm and 260 nm (J-710, Jasco). Ten single scans were cumulated into a spectrum. The spectra of mutants were normalized to the wild type spectrum.

4.7 Analytical size exclusion chromatography

To investigate the multimeric status of p97, p97 was incubated with buffer (20 mM HEPES pH 7.2, 150 mM KCl, 5% glycerol, 5 mM $MgCl_2$, 0.01% Triton X-100) with 2.5 % DMSO or 20 µM I8, centrifuged for 10 min at 21,000 x g and loaded onto a Superose 6 PC 3.2/30 column connected to an ÄKTApurifier UPC10 (GE Healthcare). The degassed and filtered running buffer was supplemented with either DMSO or I8. The flow rate was set to 0.04 ml/min. The elution of protein was monitored by absorption at 280 nm.

4.8 Pull downs

For GST pulldown assays, proteins were mixed in 50 µl pull down buffer (20 mM Hepes pH 7.2, 150 mM KCl, 5% glycerol, 5 mM MgCl2, 2 mM ATP, 5 mM DTT, 0.01 % Triton X-100). For blocking, 1 g/l Lysozyme was added to the buffer. As bait, 15 µg Ub-GST was used. The ubiquitin has a G76V mutation that cannot be cleaved by DUBs from the GST tag. To minimize precipitation, p97 was first incubated with PLAA before adding YOD1 and UBXD1 at last. Samples were cleared by centrifugation at 17,000×g for 2 min before added to 10 µl bead slurry (Glutathione Sepharose 4B, GE Healthcare) and incubated rotating for up to 90 min at room temperature. The beads were washed three times with 80 µl buffer and eluted in 30 µl buffer containing 20 mM glutathione for 10 min at room temperature. 22 µl of eluates were analyzed by SDS-PAGE and stained with colloidal Coomassie.

4.9 Limited proteolysis

For limited proteolysis, 10 µM of p97, ND1L or VPS4B was mixed with 70 µM of inhibitor or DMSO on ice in 60 µl buffer (50 mM Hepes pH 7.4, 150 mM KCl, 2.5 mM $MgCl_2$, 15 % glycerol, 1 mM DTT, 0.01 % Triton X-100). For ND1L, a second reaction contained 2 mM ATPγS. For VPS4B, a second reaction contained 100 µM CHMP1B 106-199. To start the reaction, 7.5 ng/µl trypsin was added and incubated for up to two hours at 30 °C (p97, VPS4B) or 37 °C (ND1L). 10 µl Aliquots were taken at

different time points, supplemented with sample buffer and boiled for 5 min at 95 °C. Samples were analyzed by SDS-PAGE and stained with colloidal Coomassie.

4.10 SDS-PAGE

Protein samples from purification or pull downs were separated by size with standard SDS-PAGE (sodium dodecyl sulfate polyacrylamide gel electrophoresis) methods using a Tris/glycine/SDS running buffer (200 mM glycine, 25 mM Tris-HCl pH 8.8, 0.1 % SDS) and the Mini-PROTEAN Tetra Cell system (Bio-Rad). Samples were run at a constant current of 10 to 20 mA per gel. As markers, the broad range and SDS-PAGE Molecular Weight Standards (Bio-Rad) and PageRuler™ Prestained Protein Ladder (ThermoFisher Scientific) were used. Samples were boiled in sample buffer at 95 °C for 5 min before loading onto the gel. The gels were stained with colloidal Coomassie according to Dyballa, Metzger 2009.

References

Adell, Manuel Alonso Y.; Vogel, Georg F.; Pakdel, Mehrshad; Müller, Martin; Lindner, Herbert; Hess, Michael W.; Teis, David (2014): Coordinated binding of Vps4 to ESCRT-III drives membrane neck constriction during MVB vesicle formation. In *J Cell Biol* 205 (1), pp. 33–49. DOI: 10.1083/jcb.201310114.

Alonso Y Adell, Manuel; Migliano, Simona M.; Teis, David (2016): ESCRT-III and Vps4: a dynamic multipurpose tool for membrane budding and scission. In *The FEBS journal* 283 (18), pp. 3288–3302. DOI: 10.1111/febs.13688.

Alverez, Celeste; Arkin, Michelle R.; Bulfer, Stacie L.; Colombo, Raffaele; Kovaliov, Marina; LaPorte, Matthew G. et al. (2015): Structure-Activity Study of Bioisosteric Trifluoromethyl and Pentafluorosulfanyl Indole Inhibitors of the AAA ATPase p97. In *ACS medicinal chemistry letters* 6 (12), pp. 1225–1230. DOI: 10.1021/acsmedchemlett.5b00364.

Anderson, Daniel J.; Le Moigne, Ronan; Djakovic, Stevan; Kumar, Brajesh; Rice, Julie; Wong, Steve et al. (2015): Targeting the AAA ATPase p97 as an Approach to Treat Cancer through Disruption of Protein Homeostasis. In *Cancer cell* 28 (5), pp. 653–665. DOI: 10.1016/j.ccell.2015.10.002.

Asao, H.; Sasaki, Y.; Arita, T.; Tanaka, N.; Endo, K.; Kasai, H. et al. (1997): Hrs is associated with STAM, a signal-transducing adaptor molecule. Its suppressive effect on cytokine-induced cell growth. In *The Journal of biological chemistry* 272 (52), pp. 32785–32791.

Auld, Douglas S.; Farmen, Mark W.; Kahl, Steven D.; Kriauciunas, Aidas; McKnight, Kevin L.; Montrose, Chahrzad; Weidner, Jeffrey R. (2012): Receptor Binding Assays for HTS and Drug Discovery: Eli Lilly & Company and the National Center for Advancing Translational Sciences.

Auner, Holger W.; Moody, Anne Marie; Ward, Theresa H.; Kraus, Marianne; Milan, Enrico; May, Philippa et al. (2013): Combined inhibition of p97 and the proteasome causes lethal disruption of the secretory apparatus in multiple myeloma cells. In *PloS one* 8 (9), e74415. DOI: 10.1371/journal.pone.0074415.

Babst, Markus; Wendland, Beverly; Estepa, Eden J.; Emr, Scott D. (1998): The Vps4p AAA ATPase regulates membrane association of a Vps protein complex required for normal endosome function. In *The EMBO journal* 17 (11), pp. 2982–2993. DOI: 10.1093/emboj/17.11.2982.

Bache, Kristi G.; Raiborg, Camilla; Mehlum, Anja; Stenmark, Harald (2003): STAM and Hrs are subunits of a multivalent ubiquitin-binding complex on early endosomes. In *The Journal of biological chemistry* 278 (14), pp. 12513–12521. DOI: 10.1074/jbc.M210843200.

Banerjee, Soojay; Bartesaghi, Alberto; Merk, Alan; Rao, Prashant; Bulfer, Stacie L.; Yan, Yongzhao et al. (2016): 2.3 A resolution cryo-EM structure of human p97 and mechanism of allosteric inhibition. In *Science (New York, N.Y.)* 351 (6275), pp. 871–875. DOI: 10.1126/science.aad7974.

Barthelme, Dominik; Sauer, Robert T. (2012): Identification of the Cdc48*20S proteasome as an ancient AAA+ proteolytic machine. In *Science (New York, N.Y.)* 337 (6096), pp. 843–846. DOI: 10.1126/science.1224352.

Bauer, Renato A. (2015): Covalent inhibitors in drug discovery. From accidental discoveries to avoided liabilities and designed therapies. In *Drug Discovery Today* 20 (9), pp. 1061–1073. DOI: 10.1016/j.drudis.2015.05.005.

Bernardi, Kaleena M.; Williams, Jeffrey M.; Inoue, Takamasa; Schultz, Aric; Tsai, Billy (2013): A deubiquitinase negatively regulates retro-translocation of nonubiquitinated substrates. In *Molecular biology of the cell* 24 (22), pp. 3545–3556. DOI: 10.1091/mbc.E13-06-0332.

Beuron, Fabienne; Dreveny, Ingrid; Yuan, Xuemei; Pye, Valerie E.; McKeown, Ciaran; Briggs, Louise C. et al. (2006): Conformational changes in the AAA ATPase p97-p47 adaptor complex. In *The EMBO journal* 25 (9), pp. 1967–1976. DOI: 10.1038/sj.emboj.7601055.

Bieniossek, Christoph; Richmond, Timothy J.; Berger, Imre (2008): MultiBac: multigene baculovirus-based eukaryotic protein complex production. In *Current protocols in protein science* Chapter 5, Unit 5.20. DOI: 10.1002/0471140864.ps0520s51.

Blythe, Emily; Olson, Kristine; Chau, Vincent; Deshaies, Raymond (2017): Ubiquitin and ATP-dependent unfoldase activity of P97/VCP·NPLOC4·UFD1L1 is enhanced by a mutation that causes multisystem proteinopathy.

Bodnar, Nicholas O.; Rapoport, Tom A. (2017): Molecular Mechanism of Substrate Processing by the Cdc48 ATPase Complex. In *Cell* 169 (4), 722-735.e9. DOI: 10.1016/j.cell.2017.04.020.

Bordallo, J.; Plemper, R. K.; Finger, A.; Wolf, D. H. (1998): Der3p/Hrd1p is required for endoplasmic reticulum-associated degradation of misfolded lumenal and integral membrane proteins. In *Molecular biology of the cell* 9 (1), pp. 209–222.

Briggs, Louise C.; Baldwin, Geoff S.; Miyata, Non; Kondo, Hisao; Zhang, Xiaodong; Freemont, Paul S. (2008): Analysis of nucleotide binding to P97 reveals the properties of a tandem AAA hexameric ATPase. In *The Journal of biological chemistry* 283 (20), pp. 13745–13752. DOI: 10.1074/jbc.M709632200.

Bruderer, Roland M.; Brasseur, Catherine; Meyer, Hemmo H. (2004): The AAA ATPase p97/VCP interacts with its alternative co-factors, Ufd1-Npl4 and p47, through a common bipartite binding mechanism. In *The Journal of biological chemistry* 279 (48), pp. 49609–49616. DOI: 10.1074/jbc.M408695200.

Buchberger, Alexander; Schindelin, Hermann; Hanzelmann, Petra (2015): Control of p97 function by cofactor binding. In *FEBS letters* 589 (19 Pt A), pp. 2578–2589. DOI: 10.1016/j.febslet.2015.08.028.

Buchkovich, Nicholas J.; Henne, William Mike; Tang, Shaogeng; Emr, Scott D. (2013): Essential N-Terminal Insertion Motif Anchors the ESCRT-III Filament during MVB Vesicle Formation. In *Developmental cell* 27 (2), pp. 201–214. DOI: 10.1016/j.devcel.2013.09.009.

Bug, Monika; Meyer, Hemmo (2012): Expanding into new markets--VCP/p97 in endocytosis and autophagy. In *Journal of structural biology* 179 (2), pp. 78–82. DOI: 10.1016/j.jsb.2012.03.003.

Bulfer, Stacie L.; Chou, Tsui-Fen; Arkin, Michelle R. (2016): p97 Disease Mutations Modulate Nucleotide-Induced Conformation to Alter Protein-Protein Interactions. In *ACS chemical biology* 11 (8), pp. 2112–2116. DOI: 10.1021/acschembio.6b00350.

Caillat, Christophe; Macheboeuf, Pauline; Wu, Yuanfei; McCarthy, Andrew A.; Boeri-Erba, Elisabetta; Effantin, Gregory et al. (2015): Asymmetric ring structure of Vps4 required for ESCRT-III disassembly. In *Nature communications* 6. DOI: 10.1038/ncomms9781.

Chapman, Eli; Maksim, Nick; La Cruz, Fabian de; La Clair, James J. (2015): Inhibitors of the AAA+ chaperone p97. In *Molecules (Basel, Switzerland)* 20 (2), pp. 3027–3049. DOI: 10.3390/molecules20023027.

Chen, Junjun; Dexheimer, Thomas S.; Ai, Yongxing; Liang, Qin; Villamil, Mark A.; Inglese, James et al. (2011): Selective and cell-active inhibitors of the USP1/ UAF1 deubiquitinase complex reverse cisplatin resistance in non-small cell lung cancer cells. In *Chemistry & biology* 18 (11), pp. 1390–1400. DOI: 10.1016/j.chembiol.2011.08.014.

Chia, Wei Sheng; Chia, Diana Xueqi; Rao, Feng; Bar Nun, Shoshana; Geifman Shochat, Susana (2012): ATP binding to p97/VCP D1 domain regulates selective recruitment of adaptors to its proximal N-domain. In *PloS one* 7 (12), e50490. DOI: 10.1371/journal.pone.0050490.

Chou, Tsui-Fen; Brown, Steve J.; Minond, Dmitriy; Nordin, Brian E.; Li, Kelin; Jones, Amanda C. et al. (2011): Reversible inhibitor of p97, DBeQ, impairs both ubiquitin-dependent and autophagic protein clearance pathways. In *Proceedings of the National Academy of Sciences of the United States of America* 108 (12), pp. 4834–4839. DOI: 10.1073/pnas.1015312108.

Chou, Tsui-Fen; Bulfer, Stacie L.; Weihl, Conrad C.; Li, Kelin; Lis, Lev G.; Walters, Michael A. et al. (2014): Specific inhibition of p97/VCP ATPase and kinetic analysis demonstrate interaction between D1 and D2 ATPase domains. In *Journal of molecular biology* 426 (15), pp. 2886–2899. DOI: 10.1016/j.jmb.2014.05.022.

Chou, Tsui-Fen; Li, Kelin; Frankowski, Kevin J.; Schoenen, Frank J.; Deshaies, Raymond J. (2013): Structure-activity relationship study reveals ML240 and ML241 as potent and selective inhibitors of p97 ATPase. In *ChemMedChem* 8 (2), pp. 297–312. DOI: 10.1002/cmdc.201200520.

Christ, Liliane; Raiborg, Camilla; Wenzel, Eva M.; Campsteijn, Coen; Stenmark, Harald (2017): Cellular Functions and Molecular Mechanisms of the ESCRT Membrane-Scission Machinery. In *Trends in biochemical sciences* 42 (1), pp. 42–56. DOI: 10.1016/j.tibs.2016.08.016.

Clague, Michael J.; Coulson, Judy M.; Urbe, Sylvie (2012): Cellular functions of the DUBs. In *Journal of cell science* 125 (Pt 2), pp. 277–286. DOI: 10.1242/jcs.090985.

Clague, Michael J.; Heride, Claire; Urbé, Sylvie (2015): The demographics of the ubiquitin system. In *Trends in cell biology* 25 (7), pp. 417–426. DOI: 10.1016/j.tcb.2015.03.002.

Clague, Michael J.; Urbe, Sylvie (2010): Ubiquitin. Same molecule, different degradation pathways. In *Cell* 143 (5), pp. 682–685. DOI: 10.1016/j.cell.2010.11.012.

Dargemont, Catherine; Ossareh-Nazari, Batool (2012): Cdc48/p97, a key actor in the interplay between autophagy and ubiquitin/proteasome catabolic pathways. In *Biochimica et biophysica acta* 1823 (1), pp. 138–144. DOI: 10.1016/j.bbamcr.2011.07.011.

Davies, Brian A.; Babst, Markus; Katzmann, David J. (2011): Regulation of Vps4 during MVB Sorting and Cytokinesis. In *Traffic (Copenhagen, Denmark)* 12 (10), pp. 1298–1305. DOI: 10.1111/j.1600-0854.2011.01230.x.

Davies, Jason M.; Brunger, Axel T.; Weis, William I. (2008): Improved structures of full-length p97, an AAA ATPase: implications for mechanisms of nucleotide-dependent conformational change. In *Structure (London, England : 1993)* 16 (5), pp. 715–726. DOI: 10.1016/j.str.2008.02.010.

DeLaBarre, Byron; Brunger, Axel T. (2003): Complete structure of p97/valosin-containing protein reveals communication between nucleotide domains. In *Nature structural biology* 10 (10), pp. 856–863. DOI: 10.1038/nsb972.

DeLaBarre, Byron; Christianson, John C.; Kopito, Ron R.; Brunger, Axel T. (2006): Central pore residues mediate the p97/VCP activity required for ERAD. In *Molecular Cell* 22 (4), pp. 451–462. DOI: 10.1016/j.molcel.2006.03.036.

Dreveny, Ingrid; Kondo, Hisao; Uchiyama, Keiji; Shaw, Anthony; Zhang, Xiaodong; Freemont, Paul S. (2004): Structural basis of the interaction between the AAA ATPase p97/VCP and its adaptor protein p47. In *The EMBO journal* 23 (5), pp. 1030–1039. DOI: 10.1038/sj.emboj.7600139.

Dyballa, Nadine; Metzger, Sabine (2009): Fast and sensitive colloidal coomassie G-250 staining for proteins in polyacrylamide gels. In *Journal of visualized experiments : JoVE* (30). DOI: 10.3791/1431.

Erales, Jenny; Coffino, Philip (2014): Ubiquitin-independent proteasomal degradation. In *Biochimica et biophysica acta* 1843 (1), pp. 216–221. DOI: 10.1016/j.bbamcr.2013.05.008.

Ernst, Robert; Mueller, Britta; Ploegh, Hidde L.; Schlieker, Christian (2009): The otubain YOD1 is a deubiquitinating enzyme that associates with p97 to facilitate protein dislocation from the ER. In *Molecular Cell* 36 (1), pp. 28–38. DOI: 10.1016/j.molcel.2009.09.016.

Esaki, Masatoshi; Ogura, Teru (2010): ATP-bound form of the D1 AAA domain inhibits an essential function of Cdc48p/p97. In *Biochemistry and cell biology = Biochimie et biologie cellulaire* 88 (1), pp. 109–117. DOI: 10.1139/o09-116.

Ewens, Caroline A.; Panico, Silvia; Kloppsteck, Patrik; McKeown, Ciaran; Ebong, Ima-Obong; Robinson, Carol et al. (2014): The p97-FAF1 protein complex reveals a common mode of p97 adaptor binding. In *The Journal of biological chemistry* 289 (17), pp. 12077–12084. DOI: 10.1074/jbc.M114.559591.

Fang, Chen-Jie; Gui, Lin; Zhang, Xiaoyi; Moen, Derek R.; Li, Kelin; Frankowski, Kevin J. et al. (2015a): Evaluating p97 inhibitor analogues for their domain selectivity and potency against the p97-p47 complex. In *ChemMedChem* 10 (1), pp. 52–56. DOI: 10.1002/cmdc.201402420.

Fang, Lei; Hemion, Charles; Pinho Ferreira Bento, Ana C.; Bippes, Claudia C.; Flammer, Josef; Neutzner, Albert (2015b): Mitochondrial function in neuronal cells depends on p97/VCP/Cdc48-mediated quality control. In *Frontiers in cellular neuroscience* 9, p. 16. DOI: 10.3389/fncel.2015.00016.

Fang, Shengyun; Ferrone, Marco; Yang, Cuihong; Jensen, Jane P.; Tiwari, Swati; Weissman, Allan M. (2001): The tumor autocrine motility factor receptor, gp78, is a ubiquitin protein ligase implicated in degradation from the endoplasmic reticulum. In *PNAS* 98 (25), pp. 14422–14427. DOI: 10.1073/pnas.251401598.

Fernández-Sáiz, Vanesa; Buchberger, Alexander (2010): Imbalances in p97 co-factor interactions in human proteinopathy. In *EMBO reports* 11 (6), pp. 479–485. DOI: 10.1038/embor.2010.49.

Fiebiger, Edda; Hirsch, Christian; Vyas, Jatin M.; Gordon, Eva; Ploegh, Hidde L.; Tortorella, Domenico (2004): Dissection of the dislocation pathway for type I membrane proteins with a new small molecule inhibitor, eeyarestatin. In *Molecular biology of the cell* 15 (4), pp. 1635–1646. DOI: 10.1091/mbc.E03-07-0506.

Förster, Friedrich; Unverdorben, Pia; Śledź, Paweł; Baumeister, Wolfgang (2013): Unveiling the Long-Held Secrets of the 26S Proteasome. In *Structure* 21 (9), pp. 1551–1562. DOI: 10.1016/j.str.2013.08.010.

Fu, Qing-Shan; Zhou, Chen-Jie; Gao, Hong-Chang; Jiang, Ya-Jun; Zhou, Zi-Ren; Hong, Jing et al. (2009): Structural basis for ubiquitin recognition by a novel domain from human phospholipase A2-activating protein. In *Journal of Biological Chemistry* 284 (28), pp. 19043–19052. DOI: 10.1074/jbc.M109.009126.

Glinka, Tal; Alter, Joel; Braunstein, Ilana; Tzach, Lolita; Wei Sheng, Chia; Geifman, Susana et al. (2014): Signal-peptide-mediated translocation is regulated by a p97-AIRAPL complex. In *The Biochemical journal* 457 (2), pp. 253–261. DOI: 10.1042/BJ20130710.

Goh, Lai Kuan; Sorkin, Alexander (2013): Endocytosis of receptor tyrosine kinases. In *Cold Spring Harbor perspectives in biology* 5 (5), a017459. DOI: 10.1101/cshperspect.a017459.

Gonciarz, Malgorzata D.; Whitby, Frank G.; Eckert, Debra M.; Kieffer, Collin; Heroux, Annie; Sundquist, Wesley I.; Hill, Christopher P. (2008): Biochemical and structural studies of yeast Vps4 oligomerization. In *Journal of molecular biology* 384 (4), pp. 878–895. DOI: 10.1016/j.jmb.2008.09.066.

González-Bello, Concepción (2016): Designing Irreversible Inhibitors—Worth the Effort? In *ChemMedChem* 11 (1), pp. 22–30. DOI: 10.1002/cmdc.201500469.

Haines, Dale S.; Lee, J. Eugene; Beauparlant, Stephen L.; Kyle, Dane B.; Besten, Willem den; Sweredoski, Michael J. et al. (2012): Protein Interaction Profiling of the p97 Adaptor UBXD1 Points to a Role for the Complex in Modulating ERGIC-53 Trafficking. In *Mol Cell Proteomics* 11 (6), M111.016444. DOI: 10.1074/mcp.M111.016444.

Hampton, Randolph Y.; Sommer, Thomas (2012): Finding the will and the way of ERAD substrate retrotranslocation. In *Current Opinion in Cell Biology* 24 (4), pp. 460–466. DOI: 10.1016/j.ceb.2012.05.010.

Hanzelmann, Petra; Buchberger, Alexander; Schindelin, Hermann (2011): Hierarchical binding of cofactors to the AAA ATPase p97. In *Structure (London, England : 1993)* 19 (6), pp. 833–843. DOI: 10.1016/j.str.2011.03.018.

Hanzelmann, Petra; Schindelin, Hermann (2016): Characterization of an Additional Binding Surface on the p97 N-Terminal Domain Involved in Bipartite Cofactor Interactions. In *Structure (London, England : 1993)* 24 (1), pp. 140–147. DOI: 10.1016/j.str.2015.10.027.

Hänzelmann, Petra; Schindelin, Hermann (2017): The Interplay of Cofactor Interactions and Post-translational Modifications in the Regulation of the AAA+ ATPase p97. In *Front. Mol. Biosci.* 4, p. 21. DOI: 10.3389/fmolb.2017.00021.

Her, Nam-Gu; Toth, Julia I.; Ma, Chen-Ting; Wei, Yang; Motamedchaboki, Khatereh; Sergienko, Eduard; Petroski, Matthew D. (2016): p97 Composition Changes Caused by Allosteric Inhibition Are Suppressed by an On-Target Mechanism that Increases the Enzyme's ATPase Activity. In *Cell chemical biology* 23 (4), pp. 517–528. DOI: 10.1016/j.chembiol.2016.03.012.

Huang, Chengdong; Li, Guangtao; Lennarz, William J. (2012): Dynamic flexibility of the ATPase p97 is important for its interprotomer motion transmission. In *Proceedings of the National Academy of Sciences of the United States of America* 109 (25), pp. 9792–9797. DOI: 10.1073/pnas.1205853109.

Huotari, Jatta; Helenius, Ari (2011): Endosome maturation. In *The EMBO journal* 30 (17), pp. 3481–3500. DOI: 10.1038/emboj.2011.286.

Inobe, Tomonao; Fishbain, Susan; Prakash, Sumit; Matouschek, Andreas (2011): Defining the geometry of the two-component proteasome degron. In *Nature chemical biology* 7 (3), pp. 161–167. DOI: 10.1038/nchembio.521.

Inobe, Tomonao; Matouschek, Andreas (2014): Paradigms of protein degradation by the proteasome. In *Current opinion in structural biology* 24, pp. 156–164. DOI: 10.1016/j.sbi.2014.02.002.

Inoue, Michio; Kamikubo, Hironari; Kataoka, Mikio; Kato, Ryuichi; Yoshimori, Tamotsu; Wakatsuki, Soichi; Kawasaki, Masato (2008): Nucleotide-dependent conformational changes and assembly of the AAA ATPase SKD1/VPS4B. In *Traffic (Copenhagen, Denmark)* 9 (12), pp. 2180–2189. DOI: 10.1111/j.1600-0854.2008.00831.x.

Isaacson, Rivka L.; Pye, Valerie E.; Simpson, Peter; Meyer, Hemmo H.; Zhang, Xiaodong; Freemont, Paul S.; Matthews, Steve (2007): Detailed structural insights into the p97-Npl4-Ufd1 interface. In *The Journal of biological chemistry* 282 (29), pp. 21361–21369. DOI: 10.1074/jbc.M610069200.

Kang, J.; Wang, L.; Cai, F.; Rampe, D. (2000): High affinity blockade of the HERG cardiac K(+) channel by the neuroleptic pimozide. In *European journal of pharmacology* 392 (3), pp. 137–140.

Kang, Wonchull; Yang, Jin Kuk (2011): Crystal structure of human FAF1 UBX domain reveals a novel FcisP touch-turn motif in p97/VCP-binding region. In *Biochemical and biophysical research communications* 407 (3), pp. 531–534. DOI: 10.1016/j.bbrc.2011.03.052.

Kern, Maximilian; Fernandez-Saiz, Vanesa; Schafer, Zasie; Buchberger, Alexander (2009): UBXD1 binds p97 through two independent binding sites. In *Biochemical and biophysical research communications* 380 (2), pp. 303–307. DOI: 10.1016/j.bbrc.2009.01.076.

Kieffer, Collin; Skalicky, Jack J.; Morita, Eiji; Domenico, Ivana de; Ward, Diane M.; Kaplan, Jerry; Sundquist, Wesley I. (2008): Two Distinct Modes of ESCRT-III Recognition Are Required for VPS4 Functions in Lysosomal Protein Targeting and HIV-1 Budding. In *Developmental cell* 15 (1), pp. 62–73. DOI: 10.1016/j.devcel.2008.05.014.

Kirchner, Philipp; Bug, Monika; Meyer, Hemmo (2013): Ubiquitination of the N-terminal region of caveolin-1 regulates endosomal sorting by the VCP/p97 AAA-ATPase. In *Journal of Biological Chemistry* 288 (10), pp. 7363–7372. DOI: 10.1074/jbc.M112.429076.

Kish-Trier, Erik; Hill, Christopher P. (2013): Structural biology of the proteasome. In *Annual review of biophysics* 42, pp. 29–49. DOI: 10.1146/annurev-biophys-083012-130417.

Kisselev, A. F.; Goldberg, A. L. (2001): Proteasome inhibitors. From research tools to drug candidates. In *Chemistry & biology* 8 (8), pp. 739–758.

Kleiger, Gary; Mayor, Thibault (2014): Perilous journey. A tour of the ubiquitin–proteasome system. In *Trends in cell biology* 24 (6), pp. 352–359. DOI: 10.1016/j.tcb.2013.12.003.

Komander, David; Clague, Michael J.; Urbé, Sylvie (2009): Breaking the chains. Structure and function of the deubiquitinases. In *Nature Reviews Molecular Cell Biology* 10 (8), pp. 550–563. DOI: 10.1038/nrm2731.

Komander, David; Rape, Michael (2012): The ubiquitin code. In *Annual review of biochemistry* 81, pp. 203–229. DOI: 10.1146/annurev-biochem-060310-170328.

Kostelansky, Michael S.; Schluter, Cayetana; Tam, Yuen Yi C.; Lee, Sangho; Ghirlando, Rodolfo; Beach, Bridgette et al. (2007): Molecular architecture and functional model of the complete yeast ESCRT-I heterotetramer. In *Cell* 129 (3), pp. 485–498. DOI: 10.1016/j.cell.2007.03.016.

Kozelka, Jiri (2017): Lone pair-pi interactions in biological systems: occurrence, function, and physical origin. In *European biophysics journal : EBJ. DOI:* 10.1007/s00249-017-1210-1.

Landsberg, Michael John; Vajjhala, Parimala Rao; Rothnagel, Rosalba; Munn, Alan Leslie; Hankamer, Ben (2009): Three-Dimensional Structure of AAA ATPase Vps4. Advancing Structural Insights into the Mechanisms of Endosomal Sorting and Enveloped Virus Budding. In *Structure* 17 (3), pp. 427–437. DOI: 10.1016/j.str.2008.12.020.

Lee, Min Jae; Lee, Byung-Hoon; Hanna, John; King, Randall W.; Finley, Daniel (2011): Trimming of Ubiquitin Chains by Proteasome-associated Deubiquitinating Enzymes. In *Mol Cell Proteomics* 10 (5), R110.003871. DOI: 10.1074/mcp.R110.003871.

Li, Ju-Mei; Wu, Hongyu; Zhang, Wenzheng; Blackburn, Michael R.; Jin, Jianping (2014): The p97-UFD1L-NPL4 Protein Complex Mediates Cytokine-Induced IκBα Proteolysis. In *Mol. Cell. Biol.* 34 (3), pp. 335–347. DOI: 10.1128/MCB.01190-13.

Li, Zhaofei; Blissard, Gary W. (2012): Cellular VPS4 Is Required for Efficient Entry and Egress of Budded Virions of Autographa californica Multiple Nucleopolyhedrovirus. In *J. Virol.* 86 (1), pp. 459–472. DOI: 10.1128/JVI.06049-11.

Lin, H. Helen; Li, Xu; Chen, Jo-Lin; Sun, Xiuzhu; Cooper, Fariba Norouziyan; Chen, Yun-Ru et al. (2012): Identification of an AAA ATPase VPS4B-dependent pathway that modulates epidermal growth factor receptor abundance and signaling during hypoxia. In *Molecular and cellular biology* 32 (6), pp. 1124–1138. DOI: 10.1128/MCB.06053-11.

Luo, Ji; Solimini, Nicole L.; Elledge, Stephen J. (2009): Principles of cancer therapy: oncogene and non-oncogene addiction. In *Cell* 136 (5), pp. 823–837. DOI: 10.1016/j.cell.2009.02.024.

Madsen, Louise; Andersen, Katrine M.; Prag, Soren; Moos, Torben; Semple, Colin A.; Seeger, Michael; Hartmann-Petersen, Rasmus (2008): Ubxd1 is a novel co-factor of the human p97 ATPase. In *The international journal of biochemistry & cell biology* 40 (12), pp. 2927–2942. DOI: 10.1016/j.biocel.2008.06.008.

Magnaghi, Paola; D'Alessio, Roberto; Valsasina, Barbara; Avanzi, Nilla; Rizzi, Simona; Asa, Daniela et al. (2013): Covalent and allosteric inhibitors of the ATPase

VCP/p97 induce cancer cell death. In *Nature chemical biology* 9 (9), pp. 548–556. DOI: 10.1038/nchembio.1313.

Magori, Shimpei; Citovsky, Vitaly (2011): Hijacking of the Host SCF Ubiquitin Ligase Machinery by Plant Pathogens. In *Frontiers in plant science* 2, p. 87. DOI: 10.3389/fpls.2011.00087.

Mattissek, Claudia; Teis, David (2014): The role of the endosomal sorting complexes required for transport (ESCRT) in tumorigenesis. In *Molecular Membrane Biology* 31 (4), pp. 111–119. DOI: 10.3109/09687688.2014.894210.

Meerang, Mayura; Ritz, Danilo; Paliwal, Shreya; Garajova, Zuzana; Bosshard, Matthias; Mailand, Niels et al. (2011): The ubiquitin-selective segregase VCP/p97 orchestrates the response to DNA double-strand breaks. In *Nature cell biology* 13 (11), pp. 1376–1382. DOI: 10.1038/ncb2367.

Merrill, Samuel A.; Hanson, Phyllis I. (2010): Activation of human VPS4A by ESCRT-III proteins reveals ability of substrates to relieve enzyme autoinhibition. In *The Journal of biological chemistry* 285 (46), pp. 35428–35438. DOI: 10.1074/jbc.M110.126318.

Messick, Troy Eugene; Russell, Nathaniel Scott; Iwata, Ayaka Jennifer; Sarachan, Kathryn Lorenz; Shiekhattar, Ramin; Shanks, John R. et al. (2008): Structural basis for ubiquitin recognition by the Otu1 ovarian tumor domain protein. In *The Journal of biological chemistry* 283 (16), pp. 11038–11049. DOI: 10.1074/jbc.M704398200.

Mevissen, Tycho E. T.; Hospenthal, Manuela K.; Geurink, Paul P.; Elliott, Paul R.; Akutsu, Masato; Arnaudo, Nadia et al. (2013): OTU deubiquitinases reveal mechanisms of linkage specificity and enable ubiquitin chain restriction analysis. In *Cell* 154 (1), pp. 169–184. DOI: 10.1016/j.cell.2013.05.046.

Meyer, Hemmo; Bug, Monika; Bremer, Sebastian (2012): Emerging functions of the VCP/p97 AAA-ATPase in the ubiquitin system. In *Nature cell biology* 14 (2), pp. 117–123. DOI: 10.1038/ncb2407.

Meyer, Hemmo; Weihl, Conrad C. (2014): The VCP/p97 system at a glance: connecting cellular function to disease pathogenesis. In *Journal of cell science* 127 (Pt 18), pp. 3877–3883. DOI: 10.1242/jcs.093831.

Monroe, Nicole; Han, Han; Gonciarz, Malgorzata D.; Eckert, Debra M.; Karren, Mary Anne; Whitby, Frank G. et al. (2014): The oligomeric state of the active Vps4 AAA

ATPase. In *Journal of molecular biology* 426 (3), pp. 510–525. DOI: 10.1016/j.jmb.2013.09.043.

Monroe, Nicole; Hill, Christopher P. (2016): Meiotic Clade AAA ATPases: Protein Polymer Disassembly Machines. In *Journal of molecular biology* 428 (9 Pt B), pp. 1897–1911. DOI: 10.1016/j.jmb.2015.11.004.

Murata, Shigeo; Yashiroda, Hideki; Tanaka, Keiji (2009): Molecular mechanisms of proteasome assembly. In *Nature Reviews Molecular Cell Biology* 10 (2), pp. 104–115. DOI: 10.1038/nrm2630.

Muscat, Richard; Sampson, David; Willner, Paul (1990): Dopaminergic mechanism of imipramine action in an animal model of depression. In *Biological Psychiatry* 28 (3), pp. 223–230. DOI: 10.1016/0006-3223(90)90577-O.

Na, Hyuntae; Song, Guang (2016): Predicting the functional motions of p97 using symmetric normal modes. In *Proteins* 84 (12), pp. 1823–1835. DOI: 10.1002/prot.25164.

Nakatsukasa, Kunio; Brodsky, Jeffrey L. (2008): The Recognition and Retrotranslocation of Misfolded Proteins from the Endoplasmic Reticulum. In *Traffic (Copenhagen, Denmark)* 9 (6), pp. 861–870. DOI: 10.1111/j.1600-0854.2008.00729.x.

Ndoja, Ada; Cohen, Robert E.; Yao, Tingting (2014): Ubiquitin signals proteolysis-independent stripping of transcription factors. In *Molecular Cell* 53 (6), pp. 893–903. DOI: 10.1016/j.molcel.2014.02.002.

Nishikawa, Shuh-ichi; Fewell, Sheara W.; Kato, Yoshihito; Brodsky, Jeffrey L.; Endo, Toshiya (2001): Molecular Chaperones in the Yeast Endoplasmic Reticulum Maintain the Solubility of Proteins for Retrotranslocation and Degradation. In *The Journal of cell biology* 153 (5), pp. 1061–1070.

Niwa, Hajime; Ewens, Caroline A.; Tsang, Chun; Yeung, Heidi O.; Zhang, Xiaodong; Freemont, Paul S. (2012): The role of the N-domain in the ATPase activity of the mammalian AAA ATPase p97/VCP. In *The Journal of biological chemistry* 287 (11), pp. 8561–8570. DOI: 10.1074/jbc.M111.302778.

Noguchi, Masakatsu; Takata, Takahiro; Kimura, Yoko; Manno, Atsushi; Murakami, Katsuhiro; Koike, Masaaki et al. (2005): ATPase activity of p97/valosin-containing protein is regulated by oxidative modification of the evolutionally conserved cysteine

522 residue in Walker A motif. In *The Journal of biological chemistry* 280 (50), pp. 41332–41341. DOI: 10.1074/jbc.M509700200.

Noi, Kentaro; Yamamoto, Daisuke; Nishikori, Shingo; Arita-Morioka, Ken-ichi; Kato, Takayuki; Ando, Toshio; Ogura, Teru (2013): High-speed atomic force microscopic observation of ATP-dependent rotation of the AAA+ chaperone p97. In *Structure (London, England : 1993)* 21 (11), pp. 1992–2002. DOI: 10.1016/j.str.2013.08.017.

Papadopoulos, Chrisovalantis; Kirchner, Philipp; Bug, Monika; Grum, Daniel; Koerver, Lisa; Schulze, Nina et al. (2017): VCP/p97 cooperates with YOD1, UBXD1 and PLAA to drive clearance of ruptured lysosomes by autophagy. In *The EMBO journal* 36 (2), pp. 135–150. DOI: 10.15252/embj.201695148.

Pasqual, Giulia; Rojek, Jillian M.; Masin, Mark; Chatton, Jean-Yves; Kunz, Stefan (2011): Old World Arenaviruses Enter the Host Cell via the Multivesicular Body and Depend on the Endosomal Sorting Complex Required for Transport. In *PLOS Pathogens* 7 (9), e1002232. DOI: 10.1371/journal.ppat.1002232.

Peters, J. M.; Walsh, M. J.; Franke, W. W. (1990): An abundant and ubiquitous homo-oligomeric ring-shaped ATPase particle related to the putative vesicle fusion proteins Sec18p and NSF. In *The EMBO journal* 9 (6), pp. 1757–1767.

Pineda-Molina, Estela; Belrhali, Hassan; Piefer, Andrew J.; Akula, Indira; Bates, Paul; Weissenhorn, Winfried (2006): The crystal structure of the C-terminal domain of Vps28 reveals a conserved surface required for Vps20 recruitment. In *Traffic (Copenhagen, Denmark)* 7 (8), pp. 1007–1016. DOI: 10.1111/j.1600-0854.2006.00440.x.

Purser, Sophie; Moore, Peter R.; Swallow, Steve; Gouverneur, Véronique (2008): Fluorine in medicinal chemistry. In *Chem. Soc. Rev.* 37 (2), pp. 320–330. DOI: 10.1039/B610213C.

Qiu, Liyan; Pashkova, Natasha; Walker, John R.; Winistorfer, Stanley; Allali-Hassani, Abdellah; Akutsu, Masato et al. (2010): Structure and function of the PLAA/Ufd3-p97/Cdc48 complex. In *The Journal of biological chemistry* 285 (1), pp. 365–372. DOI: 10.1074/jbc.M109.044685.

Raiborg, C.; Bremnes, B.; Mehlum, A.; Gillooly, D. J.; D'Arrigo, A.; Stang, E.; Stenmark, H. (2001): FYVE and coiled-coil domains determine the specific localisation of Hrs to early endosomes. In *Journal of cell science* 114 (Pt 12), pp. 2255–2263.

Ramadan, Kristijan; Bruderer, Roland; Spiga, Fabio M.; Popp, Oliver; Baur, Tina; Gotta, Monica; Meyer, Hemmo H. (2007): Cdc48/p97 promotes reformation of the nucleus by extracting the kinase Aurora B from chromatin. In *Nature* 450 (7173), pp. 1258–1262. DOI: 10.1038/nature06388.

Ren, J.; Pashkova, N.; Winistorfer, S.; Piper, R. C. (2008): DOA1/UFD3 Plays a Role in Sorting Ubiquitinated Membrane Proteins into Multivesicular Bodies. In *Journal of Biological Chemistry* 283 (31), pp. 21599–21611. DOI: 10.1074/jbc.M802982200.

Riemer, Anne; Dobrynin, Grzegorz; Dressler, Alina; Bremer, Sebastian; Soni, Aashish; Iliakis, George; Meyer, Hemmo (2014): The p97-Ufd1-Npl4 ATPase complex ensures robustness of the G2/M checkpoint by facilitating CDC25A degradation. In *Cell cycle (Georgetown, Tex.)* 13 (6), pp. 919–927. DOI: 10.4161/cc.27779.

Ritz, Danilo; Vuk, Maja; Kirchner, Philipp; Bug, Monika; Schutz, Sabina; Hayer, Arnold et al. (2011): Endolysosomal sorting of ubiquitylated caveolin-1 is regulated by VCP and UBXD1 and impaired by VCP disease mutations. In *Nature cell biology* 13 (9), pp. 1116–1123. DOI: 10.1038/ncb2301.

Rothballer, Andrea; Tzvetkov, Nikolay; Zwickl, Peter (2007): Mutations in p97/VCP induce unfolding activity. In *FEBS letters* 581 (6), pp. 1197–1201. DOI: 10.1016/j.febslet.2007.02.031.

Ryu, Je-Kyung; Jahn, Reinhard; Yoon, Tae-Young (2016): Review. Progresses in understanding N-ethylmaleimide sensitive factor (NSF) mediated disassembly of SNARE complexes. In *Biopolymers* 105 (8), pp. 518–531. DOI: 10.1002/bip.22854.

Ryu, Je-Kyung; Min, Duyoung; Rah, Sang-Hyun; Kim, Soo Jin; Park, Yongsoo; Kim, Haesoo et al. (2015): Spring-loaded unraveling of a single SNARE complex by NSF in one round of ATP turnover. In *Science (New York, N.Y.)* 347 (6229), pp. 1485–1489. DOI: 10.1126/science.aaa5267.

Scheuring, S.; Rohricht, R. A.; Schoning-Burkhardt, B.; Beyer, A.; Muller, S.; Abts, H. F.; Kohrer, K. (2001): Mammalian cells express two VPS4 proteins both of which are involved in intracellular protein trafficking. In *Journal of molecular biology* 312 (3), pp. 469–480. DOI: 10.1006/jmbi.2001.4917.

Schöneberg, Johannes; Lee, Il-Hyung; Iwasa, Janet H.; Hurley, James H. (2017): Reverse-topology membrane scission by the ESCRT proteins. In *Nature Reviews Molecular Cell Biology* 18 (1), pp. 5–17. DOI: 10.1038/nrm.2016.121.

Schuetz, Anne K.; Kay, Lewis E. (2016): A Dynamic molecular basis for malfunction in disease mutants of p97/VCP. In *eLife* 5. DOI: 10.7554/eLife.20143.

Schuller, Jan M.; Beck, Florian; Lossl, Philip; Heck, Albert J. R.; Forster, Friedrich (2016): Nucleotide-dependent conformational changes of the AAA+ ATPase p97 revisited. In *FEBS letters* 590 (5), pp. 595–604. DOI: 10.1002/1873-3468.12091.

Scott, Anna; Chung, Hyo-Young; Gonciarz-Swiatek, Malgorzata; Hill, Gina C.; Whitby, Frank G.; Gaspar, Jason et al. (2005a): Structural and mechanistic studies of VPS4 proteins. In *The EMBO journal* 24 (20), pp. 3658–3669. DOI: 10.1038/sj.emboj.7600818.

Scott, Anna; Gaspar, Jason; Stuchell-Brereton, Melissa D.; Alam, Steven L.; Skalicky, Jack J.; Sundquist, Wesley I. (2005b): Structure and ESCRT-III protein interactions of the MIT domain of human VPS4A. In *PNAS* 102 (39), pp. 13813–13818. DOI: 10.1073/pnas.0502165102.

Shtanko, Olena; Nikitina, Raisa A.; Altuntas, Cengiz Z.; Chepurnov, Alexander A.; Davey, Robert A. (2014): Crimean-Congo hemorrhagic fever virus entry into host cells occurs through the multivesicular body and requires ESCRT regulators. In *PLoS pathogens* 10 (9), e1004390. DOI: 10.1371/journal.ppat.1004390.

Slagsvold, Thomas; Aasland, Rein; Hirano, Satoshi; Bache, Kristi G.; Raiborg, Camilla; Trambaiolo, Daniel et al. (2005): Eap45 in mammalian ESCRT-II binds ubiquitin via a phosphoinositide-interacting GLUE domain. In *The Journal of biological chemistry* 280 (20), pp. 19600–19606. DOI: 10.1074/jbc.M501510200.

Stolz, Alexandra; Hilt, Wolfgang; Buchberger, Alexander; Wolf, Dieter H. (2011): Cdc48: a power machine in protein degradation. In *Trends in biochemical sciences* 36 (10), pp. 515–523. DOI: 10.1016/j.tibs.2011.06.001.

Suzuki, Michitaka; Otsuka, Toshihiko; Ohsaki, Yuki; Cheng, Jinglei; Taniguchi, Takako; Hashimoto, Hisashi et al. (2012): Derlin-1 and UBXD8 are engaged in dislocation and degradation of lipidated ApoB-100 at lipid droplets. In *Molecular biology of the cell* 23 (5), pp. 800–810. DOI: 10.1091/mbc.E11-11-0950.

Swatek, Kirby N.; Komander, David (2016): Ubiquitin modifications. In *Cell Research* 26 (4), pp. 399–422. DOI: 10.1038/cr.2016.39.

Tang, Wai Kwan; Di Xia (2013): Altered intersubunit communication is the molecular basis for functional defects of pathogenic p97 mutants. In *The Journal of biological chemistry* 288 (51), pp. 36624–36635. DOI: 10.1074/jbc.M113.488924.

Tang, Wai Kwan; Di Xia (2016): Mutations in the Human AAA+ Chaperone p97 and Related Diseases. In *Frontiers in molecular biosciences* 3, p. 79. DOI: 10.3389/fmolb.2016.00079.

Tang, Wai Kwan; Li, Dongyang; Li, Chou-chi; Esser, Lothar; Dai, Renming; Guo, Liang; Di Xia (2010): A novel ATP-dependent conformation in p97 N-D1 fragment revealed by crystal structures of disease-related mutants. In *The EMBO journal* 29 (13), pp. 2217–2229. DOI: 10.1038/emboj.2010.104.

Tao, Shasha; Tillotson, Joseph; Wijeratne, E. M. Kithsiri; Xu, Ya-ming; Kang, MinJin; Wu, Tongde et al. (2015): Withaferin A Analogs That Target the AAA+ Chaperone p97. In *ACS chemical biology* 10 (8), pp. 1916–1924. DOI: 10.1021/acschembio.5b00367.

Taylor, Eric B.; Rutter, Jared (2011): Mitochondrial quality control by the ubiquitin-proteasome system. In *Biochemical Society transactions* 39 (5), pp. 1509–1513. DOI: 10.1042/BST0391509.

Thrower, Julia S.; Hoffman, Laura; Rechsteiner, Martin; Pickart, Cecile M. (2000): Recognition of the polyubiquitin proteolytic signal. In *The EMBO journal* 19 (1), pp. 94–102. DOI: 10.1093/emboj/19.1.94.

Trusch, Franziska; Matena, Anja; Vuk, Maja; Koerver, Lisa; Knaevelsrud, Helene; Freemont, Paul S. et al. (2015): The N-terminal Region of the Ubiquitin Regulatory X (UBX) Domain-containing Protein 1 (UBXD1) Modulates Interdomain Communication within the Valosin-containing Protein p97. In *The Journal of biological chemistry* 290 (49), pp. 29414–29427. DOI: 10.1074/jbc.M115.680686.

van den Boom, Johannes; Wolf, Markus; Weimann, Lena; Schulze, Nina; Li, Fanghua; Kaschani, Farnusch et al. (2016): VCP/p97 Extracts Sterically Trapped Ku70/80 Rings from DNA in Double-Strand Break Repair. In *Molecular Cell* 64 (1), pp. 189–198. DOI: 10.1016/j.molcel.2016.08.037.

Vekaria, Pratikkumar Harsukhbhai; Home, Trisha; Weir, Scott; Schoenen, Frank J.; Rao, Rekha (2016): Targeting p97 to Disrupt Protein Homeostasis in Cancer. In *Frontiers in oncology* 6, p. 181. DOI: 10.3389/fonc.2016.00181.

Verma, Rati; Oania, Robert S.; Kolawa, Natalie J.; Deshaies, Raymond J. (2013): Cdc48/p97 promotes degradation of aberrant nascent polypeptides bound to the ribosome. In *eLife* 2, e00308. DOI: 10.7554/eLife.00308.

Votteler, Jörg; Sundquist, Wesley I. (2013): Virus Budding and the ESCRT Pathway. In *Cell host & microbe* 14 (3). DOI: 10.1016/j.chom.2013.08.012.

Wang, Qing; Song, Changcheng; Li, Chou-Chi H. (2003): Hexamerization of p97-VCP is promoted by ATP binding to the D1 domain and required for ATPase and biological activities. In *Biochemical and biophysical research communications* 300 (2), pp. 253–260. DOI: 10.1016/S0006-291X(02)02840-1.

Wang, Qiuyan; Li, Lianyun; Ye, Yihong (2008): Inhibition of p97-dependent protein degradation by Eeyarestatin I. In *The Journal of biological chemistry* 283 (12), pp. 7445–7454. DOI: 10.1074/jbc.M708347200.

Wang, Su-Jane (2002): Inhibition of glutamate release by fluspirilene in cerebrocortical nerve terminals (synaptosomes). In *Synapse (New York, N.Y.)* 44 (1), pp. 36–41. DOI: 10.1002/syn.10053.

Wang, Xiaoli; Herr, Roger A.; Chua, Wei-Jen; Lybarger, Lonnie; Wiertz, Emmanuel J. H. J.; Hansen, Ted H. (2007): Ubiquitination of serine, threonine, or lysine residues on the cytoplasmic tail can induce ERAD of MHC-I by viral E3 ligase mK3. In *The Journal of cell biology* 177 (4), pp. 613–624. DOI: 10.1083/jcb.200611063.

Watkinson, R. E.; Tam, J. C. H.; Vaysburd, M. J.; James, L. C. (2013): Simultaneous neutralization and innate immune detection of a replicating virus by TRIM21. In *Journal of virology* 87 (13), pp. 7309–7313. DOI: 10.1128/JVI.00647-13.

Weiss, William A.; Taylor, Stephen S.; Shokat, Kevan M. (2007): Recognizing and exploiting differences between RNAi and small-molecule inhibitors. In *Nature chemical biology* 3 (12), pp. 739–744. DOI: 10.1038/nchembio1207-739.

Williams, Roger L.; Urbe, Sylvie (2007): The emerging shape of the ESCRT machinery. In *Nature reviews. Molecular cell biology* 8 (5), pp. 355–368. DOI: 10.1038/nrm2162.

Wolf, Dieter H.; Stolz, Alexandra (2012): The Cdc48 machine in endoplasmic reticulum associated protein degradation. In *Biochimica et biophysica acta* 1823 (1), pp. 117–124. DOI: 10.1016/j.bbamcr.2011.09.002.

Wu, Xi; Li, Lanlan; Jiang, Hui (2016): Doa1 targets ubiquitinated substrates for mitochondria-associated degradation. In *J Cell Biol* 213 (1), pp. 49–63. DOI: 10.1083/jcb.201510098.

Xu, Ping; Duong, Duc M.; Seyfried, Nicholas T.; Cheng, Dongmei; Xie, Yang; Robert, Jessica et al. (2009): Quantitative Proteomics Reveals the Function of Unconventional Ubiquitin Chains in Proteasomal Degradation. In *Cell* 137 (1), pp. 133–145. DOI: 10.1016/j.cell.2009.01.041.

Yang, Bei; Stjepanovic, Goran; Shen, Qingtao; Martin, Andreas; Hurley, James H. (2015): Vps4 disassembles an ESCRT-III filament by global unfolding and processive translocation. In *Nature structural & molecular biology* 22 (6), pp. 492–498. DOI: 10.1038/nsmb.3015.

Yang, Dong; Hurley, James H. (2010): Structural role of the Vps4-Vta1 interface in ESCRT-III recycling. In *Structure (London, England : 1993)* 18 (8), pp. 976–984. DOI: 10.1016/j.str.2010.04.014.

Ye, Yihong; Meyer, Hemmo H.; Rapoport, Tom A. (2001): The AAA ATPase Cdc48/p97 and its partners transport proteins from the ER into the cytosol. In *Nature* 414 (6864), pp. 652–656. DOI: 10.1038/414652a.

Ye, Yihong; Meyer, Hemmo H.; Rapoport, Tom A. (2003): Function of the p97-Ufd1-Npl4 complex in retrotranslocation from the ER to the cytosol: dual recognition of nonubiquitinated polypeptide segments and polyubiquitin chains. In *The Journal of cell biology* 162 (1), pp. 71–84. DOI: 10.1083/jcb.200302169.

Ye, Yihong; Rape, Michael (2009): Building ubiquitin chains. E2 enzymes at work. In *Nature Reviews Molecular Cell Biology* 10 (11), pp. 755–764. DOI: 10.1038/nrm2780.

Yeung, Heidi O.; Forster, Andreas; Bebeacua, Cecilia; Niwa, Hajime; Ewens, Caroline; McKeown, Ciaran et al. (2014): Inter-ring rotations of AAA ATPase p97 revealed by electron cryomicroscopy. In *Open biology* 4, p. 130142. DOI: 10.1098/rsob.130142.

Yeung, Heidi O.; Kloppsteck, Patrik; Niwa, Hajime; Isaacson, Rivka L.; Matthews, Steve; Zhang, Xiaodong; Freemont, Paul S. (2008): Insights into adaptor binding to the AAA protein p97. In *Biochemical Society transactions* 36 (Pt 1), pp. 62–67. DOI: 10.1042/BST0360062.

Yorikawa, Chiharu; Shibata, Hideki; Waguri, Satoshi; Hatta, Kazumi; Horii, Mio; Katoh, Keiichi et al. (2005): Human CHMP6, a myristoylated ESCRT-III protein, interacts directly with an ESCRT-II component EAP20 and regulates endosomal cargo sorting. In *The Biochemical journal* 387 (Pt 1), pp. 17–26. DOI: 10.1042/BJ20041227.

Zhang, Ting; Mishra, Prashant; Hay, Bruce A.; Chan, David; Guo, Ming (2017): Valosin-containing protein (VCP/p97) inhibitors relieve Mitofusin-dependent mitochondrial defects due to VCP disease mutants. In *eLife* 6. DOI: 10.7554/eLife.17834.

Zhang, Ting; Ye, Yihong (2014): The Final Moments of Misfolded Proteins en Route to the Proteasome. In *DNA and Cell Biology* 33 (8), pp. 477–483. DOI: 10.1089/dna.2014.2452.

Zhang, Xiaoyi; Gui, Lin; Zhang, Xiaoyan; Bulfer, Stacie L.; Sanghez, Valentina; Wong, Daniel E. et al. (2015): Altered cofactor regulation with disease-associated p97/VCP mutations. In *Proceedings of the National Academy of Sciences of the United States of America* 112 (14), E1705-14. DOI: 10.1073/pnas.1418820112.

Zhao, Gang; Zhou, Xiaoke; Wang, Liqun; Li, Guangtao; Schindelin, Hermann; Lennarz, William J. (2007): Studies on peptide:N-glycanase-p97 interaction suggest that p97 phosphorylation modulates endoplasmic reticulum-associated degradation. In *Proceedings of the National Academy of Sciences of the United States of America* 104 (21), pp. 8785–8790. DOI: 10.1073/pnas.0702966104.

Zhong, Xiaoyan; Pittman, Randall N. (2006): Ataxin-3 binds VCP/p97 and regulates retrotranslocation of ERAD substrates. In *Human molecular genetics* 15 (16), pp. 2409–2420. DOI: 10.1093/hmg/ddl164.

Zhong, Xiaoyan; Shen, Yuxian; Ballar, Petek; Apostolou, Andria; Agami, Reuven; Fang, Shengyun (2004): AAA ATPase p97/valosin-containing protein interacts with gp78, a ubiquitin ligase for endoplasmic reticulum-associated degradation. In *The Journal of biological chemistry* 279 (44), pp. 45676–45684. DOI: 10.1074/jbc.M409034200.

Zhou, Han-Jie; Wang, Jinhai; Yao, Bing; Wong, Steve; Djakovic, Stevan; Kumar, Brajesh et al. (2015): Discovery of a First-in-Class, Potent, Selective, and Orally Bioavailable Inhibitor of the p97 AAA ATPase (CB-5083). In *Journal of medicinal chemistry* 58 (24), pp. 9480–9497. DOI: 10.1021/acs.jmedchem.5b01346.

Abbreviations

ADP	adenosine 5′-diphosphate
AIRAPL	arsenite-inducible RNA-associated protein-like protein
AMSH	associated molecule with the SH3 domain of STAM
ATP	adenosine 5′-triphosphate
ATPγS	adenosine-5’-(3-thio)-triphosphate
CD	circular dichroism
CDC	cell division cycle
CHMP	charged multivesicular body protein
CHOP	CCAAT/enhancer-binding protein homologous protein
CMT	Charcot-Marie-Tooth disease
cryo-EM	cryo-electron microscopy
Da	dalton
DBeQ	N2,N4-dibenzylquinazoline-2,4-diamine
DMSO	dimethyl sulfoxide
DNA	deoxyribonucleic acid
dNTP	deoxynucleosid triphospate
DOA1	degradation of alpha 1
DTT	dithiothreitol
DUB	deubiquitinase
EAP45	ELL associated protein
EDTA	ethylenediaminetetraacetic acid
EerI	eeyarestatin I
EGFR	epidermal growth factor receptor
ER	endoplasmic reticulum
ERAD	endoplasmic reticulum associated degradation
ESCRT	endosomal sorting complex required for transport
FAF1	FAS-associated factor 1
FALS	familial amyotrophic lateral sclerosis
FCS	fetal calf serum
FD	frontotemporal dementia
GFP	green fluorescent protein
GST	glutathione S-transferase
gp78	glycoprotein 78
HECT	homologous to E6-AP carboxyl terminus
HEPES	(4-(2-hydroxyethyl)-1-piperazineethanesulfonic acid)
HIV	human immunodeficiency virus
Hrd1	HMG-coA Reductase Degradation 1

HRS	hepatocyte growth factor (HGF)-regulated Tyr-kinase substrate
IBM	inclusion body myopathy
IBMPFD	inclusion body myopathy associated with Paget's disease of the bone and frontotemporal dementia
IC	inhibitory concentration
IEX	ion exchange cromatography
ILV	intraluminal vesicle
ISS	intersubunit signaling motif
IST1	increased salt tolerance 1
IκBα	nuclear factor of kappa light polypeptide gene enhancer in B-cells inhibitor, alpha
JAMM	JAB1/MPN/MOV34
MIM	MIT interaction motif
MIT	microtubule interacting and transport
MSP1	multisystem proteinopathy 1
MTS	3-(4,5-dimethylthiazol-2-yl)-5-(3-carboxymethoxyphenyl)-2-(4-sulfophenyl)-2H-tetrazolium)
MVB	multivesicular body
MVE	multivesicular endosome
MWCO	molecular weight cut off
NADH	nicotinamide adenine dinucleotide (reduced)
NEM	N-Ethylmaleimide
NMR	nuclear magnetic resonance
NPL4	nuclear protein localization protein 4
NSF	N-ethylmaleimide-sensitive factor
ODD	oxygen-dependent degradation domain
OTU	ovarian tumor proteases
PAGE	polyacrylamide gel electrophoresis
PBS	phosphate buffered saline
PCR	polymerase chain reaction
PEP	phosphoenolpyruvate
PFU	PLAA family ubiquitin binding
PI3P	phosphatidylinositol 3-phosphate
PIM	PUB interacting motif
PLAA	phospholipase A_2 activating protein
PMSF	phenylmethane sulfonyl fluoride
PUB	PNGase/UBA or UBX containing proteins
PUL	PLAP, Ufd3p, and Lub1p
RBR	RING between RING
RING	really interesting new gene

Rpn	regulatory particle non-ATPase
Rpt	regulatory particle triple-A
SDS	sodium dodecyl sulfate
SEC	size exclusion chromatography
Sec61	secretory 61
STAM	signal transducing adaptor molecule
TAR	trans-activation response
TB	terrific broth
TDP-43	TAR DNA-binding protein 43
TSG101	tumor susceptibility gene 101
Ub	ubiquitin
UBA	ubiquitin-associated
UBA	ubiquitin-associated
UbL	ubiquitin-like
UBX	ubiquitin regulatory X
UBXD1	ubiquitin regulatory X domain 1
UBX-L	ubiquitin regulatory X-like
UCH	ubiquitin C-terminal hydrolases
UFD1	ubiquitin fusion degradation protein 1
UIM	ubiquitin-interacting motif
UPR	unfolded protein response
UPS	ubiquitin-proteasome system
USP	ubiquitin-specific protease
UV	ultra violet
VAT	VCP-like ATPase from *Thermoplasma acidophilum*
VBM	VCP-binding motif
VCP	valosin containing protein
VIM	VCP-interacting motif
VPS	vacuolar protein sorting-associated protein
VSL	Vta1/SBP-1/Lip5
YFP	yellow fluorescent protein
YOD1	ubiquitin thioesterase OTU1
ZnF	zinc finger

Acknowledgments

First, I want to thank Hemmo for advice and guidance, valuable insights, and letting me work my way through this project

I thank Markus for the mentoring, the optimism, and new perspectives. Also a special thank you to members of the AG Kaiser: To Jan for all the synthesis and help with chemistry and to Farnusch for the mass spectrometry.

I owe the whole AG Bayer thanks for sharing knowledge, cuvettes, reagents, time and importantly, for your former lab members. I thank the ZMB members in all the different groups for support, smoothies, and overall fun. I thank the CRC1093 for the amazing time and science we had.

A big thank you goes to all the current and former members in the lab, especially those that were somehow recruited to the inhibitor project, for the help and a great atmosphere during and after work. Special thanks go to the Rose of Hope and the office crew. Also thank you to my subgroup, because without you I'm nothing.

And I thank my family and friends outside the lab, for being with me while having no idea what I did.

It was a blast from start to end.

Curriculum vitae

Der Lebenslauf ist in der Online-Version aus Gründen des Datenschutzes nicht enthalten

Der Lebenslauf ist in der Online-Version aus Gründen des Datenschutzes nicht enthalten

Affidavits/ Erklärungen

Erklärung

Hiermit erkläre ich, gem. § 7 Abs. (2) d) + f) der Promotionsordnung der Fakultät für Biologie zur Erlangung des Dr. rer. nat., dass ich die vorliegende Dissertation selbständig verfasst und mich keiner anderen als der angegebenen Hilfsmittel bedient, bei der Abfassung der Dissertation nur die angegebenen Hilfsmittel benutzt und alle wörtlich oder inhaltlich übernommenen Stellen als solche gekennzeichnet habe.

Essen, den _____ _____

Unterschrift des/r Doktoranden/in

Erklärung

Hiermit erkläre ich, gem. § 7 Abs. (2) e) + g) der Promotionsordnung der Fakultät für Biologie zur Erlangung des Dr. rer. nat., dass ich keine anderen Promotionen bzw. Promotionsversuche in der Vergangenheit durchgeführt habe und dass diese Arbeit von keiner anderen Fakultät/Fachbereich abgelehnt worden ist.

Essen, den _____ _____

Unterschrift des/r Doktoranden/in

Erklärung

Hiermit erkläre ich, gem. § 6 Abs. (2) g) der Promotionsordnung der Fakultät für Biologie zur Erlangung der Dr. rer. nat., dass ich das Arbeitsgebiet, dem das Thema „Analysis of a novel allosteric inhibitor of the AAA+ ATPase p97 and its mechanism“ zuzuordnen ist, in Forschung und Lehre vertrete und den Antrag von Robert Pöhler befürworte und die Betreuung auch im Falle eines Weggangs, wenn nicht wichtige Gründe dem entgegenstehen, weiterführen werde.

Essen, den _____ _____

Unterschrift eines Mitglieds der Universität Duisburg-Essen